

# POLITECNICO DI TORINO

**Corso di Laurea Magistrale  
in Ingegneria Energetica e Nucleare**

**Tesi di Laurea Magistrale**

## **Li-ion battery pack cooling system for a hybrid railway: time-dependent analysis and optimization**



**Relatore**

Prof. Massimo Santarelli

**Candidato:**

Fabio Nasca

**Co-relatore**

Ing. Arpit Maheshwari

**Tutor Aziendale**

Ing. Andrea Tosetto

ANNO ACCADEMICO 2017/2018



# Index

Abstract .....	1
1. Introduction.....	2
2. Hybrid Electric Vehicles (HEVs) .....	4
2.1 Configurations and Classification.....	5
3. Electrochemical Energy Storage Systems (EESs) .....	9
3.1 Classification of EES systems.....	9
4. Batteries .....	20
4.1 Working principle of electro-chemical cells.....	20
4.2 Batteries Classification and Operating parameters .....	26
4.3 Li-ion battery: State of Art .....	28
4.3.1 Charge configuration.....	34
4.3.2 Discharge configuration .....	35
4.3.3 Geometries .....	37
4.3.4 Pros&Cons of Li-ion battery .....	43
4.3.5 How to compose a battery pack .....	44
5. Thermal issues and BTMS .....	46
5.1 Thermal fluxes management .....	46
5.2 Optimal operating conditions .....	48
5.3 Battery Thermal Management System (BTMS) .....	50
5.4 Types of cooling systems.....	52
5.4.1 Air cooling/heating.....	53
5.4.2 Liquid cooling/heating .....	55
5.4.3 Phase Change Material (PCM) .....	57
5.4.4 Heat Pipe .....	60
5.4.5 Heat pipe assisted PCM.....	61
6. Case Study .....	63
6.1 Hybrid railway description .....	63
6.2 The model: A Liquid-Cooled Lithium-ion Battery Pack .....	67
6.2.1 Geometry.....	67
6.2.2 Materials.....	69
6.2.3 Physics of the problem .....	70
6.2.4 Boundary Conditions (BCs).....	72
6.2.5 Mesh .....	74
6.2.6 Simulation results and Optimization .....	75

6.2.6.1	Volumetric Flow Rate ( $\dot{V}_{fin}$ ) .....	80
6.2.6.2	Coolant Inlet Temperature ( $T_{inlet}$ ) .....	86
6.2.6.3	Square section channel edge ( $l_1$ ) .....	88
6.2.7	Water-cooling coupled with Phase Change Material (PCM) .....	92
6.2.8	The development of nanofluids .....	96
7.	Conclusions .....	99
	Bibliography .....	101

# Abstract

Nowadays, the development and use of electric and hybrid vehicles are assuming a significant role in the transport sector due to the rapid and sudden changes in climate caused by gas emissions into the atmosphere beyond the allowable limits. As a result, the concept of a sustainable development becomes fundamental and ‘zero-emission’ technologies are constantly evolving and improving.

The first part of this thesis, carried out in collaboration with *Blue-Group Engineering and Design* company and thanks to my supervisor *Massimo Santarelli* and its assistant *Arpit Maheswari*, concerns a brief description of hybrid vehicles configurations followed by a review of various types of Electrochemical Energy Storage systems (EESs). We will then focus on the classification of the batteries and on their working principles, examining in depth the state of art of Lithium ion chemistries.

Entering into the thesis work, the following chapters deal with the critical thermal issues during battery operations, its optimal operating conditions and the importance of having a performant battery thermal management system (BTMS) to keep the device within the best thermal range of functioning. BTMS systems are classified and outlined in detail.

The design part concerns the sizing of a Li-ion battery pack applied to a railway, whose characteristics have been provided by *Blue Group*, and the analysis and subsequent optimization of a specific liquid cooling system. The battery pack-BTMS model has been created on COMSOL Multiphysics software to simulate its thermal behaviour during a discharge process through a time-dependent study. Different coolants are examined in order to point out which of them is the most suitable and effective. The objective is to pick out the optimal values of the control parameters chosen for this study such that to minimize battery pack average temperature, maintaining it into the desired thermal range, and to reach an uniform temperature distribution over the pack. Finally, the liquid-cooled Li-ion battery pack is coupled with a Phase Change Material (PCM) to highlight the overall thermal enhancement, while the last case study for future developments is conducted using a nanofluid.

# 1. Introduction

Since late of 20th century, the environmental pollution and energy crisis have become two global issues: the end of 2015 and the beginning of 2016 were characterized by widespread and persistent critical situations of atmospheric pollution in most Italian and European metropolitan areas. Transportation sector is one of the major contributors; the growing number of vehicles circulating in the world is the main cause of the increase of carbon dioxide emissions and of the rising exploitation of fossil fuel resources. The dependence on oil brings with it geopolitical and economic problems and requires the implementation of energy policies that reduce the use of fossil fuels and diversify the employed resources.

The outcome of COP21 in December 2015 in Paris and the signing of the agreement achieved by 175 countries in New York in April constitute a significant, even if not resolute, acknowledgment of the urgency of an epochal turning point. Therefore, in Paris the insufficient security level guaranteed by the 2°C threshold was noted, where an increase in the average temperature of this entity would determine a strong impact in terms of extreme weather events.

Every effort should be made to limit the increase in global mean temperature to 1.5°C. In order to adopt consistent measures, Europe should indeed reduce by 2030 own emissions by at least 62% compared to 1990 levels. In 2014, the use of fossil fuels resulted in the emission into the atmosphere of 35.9 Gt of CO<sub>2</sub>, about 60% more than what was emitted in 1990. In 1990, Europe and USA issued 42.5% of the total, while China and India contributed for the 14%. In 2014 the percentages are approximately 25% and 34%, respectively. In this regard, it is appropriate to consider the fact that estimates of global CO<sub>2</sub> emissions can be processed and presented on the basis of a territorial perspective (such as those shown in the following graph):

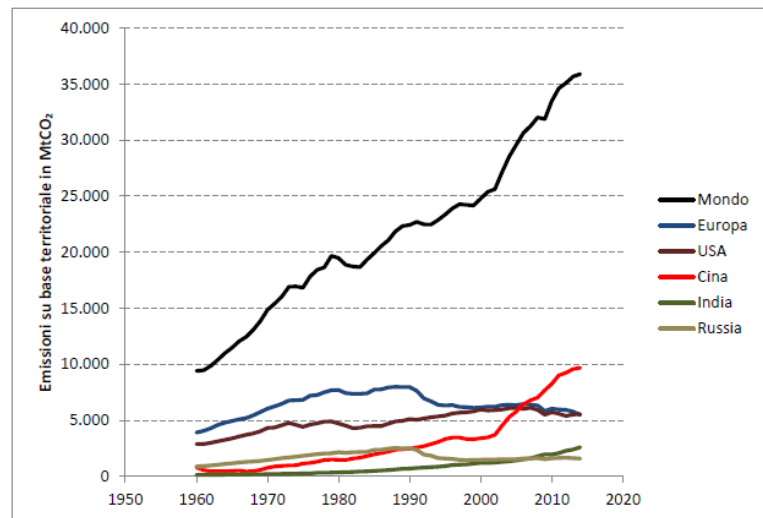


**FIGURE 1. CO<sub>2</sub> Anthropogenic emissions on territorial basis [1]**

According to the latest report of the *International Energy Agency* and *International Union of Railways*, which returns calculations on 2012 data, the 23.1% of the world CO<sub>2</sub> emissions from fuel combustion is attributable to the transport sector. The statistical compendium on transportation published annually by the *European Commission* quantifies a total of 4544 Mt of GHG (*Greenhouse Gas*) issued by the 28 members states in 2012, of which 1173 Mt attributable to the transport sector (approximately 26%). The trend of total and transports estimated GHG emissions and the percentages from 1990 to 2012 attributable to transport sector over the total emissions in Italy and UE are presented in the following figures [2]:

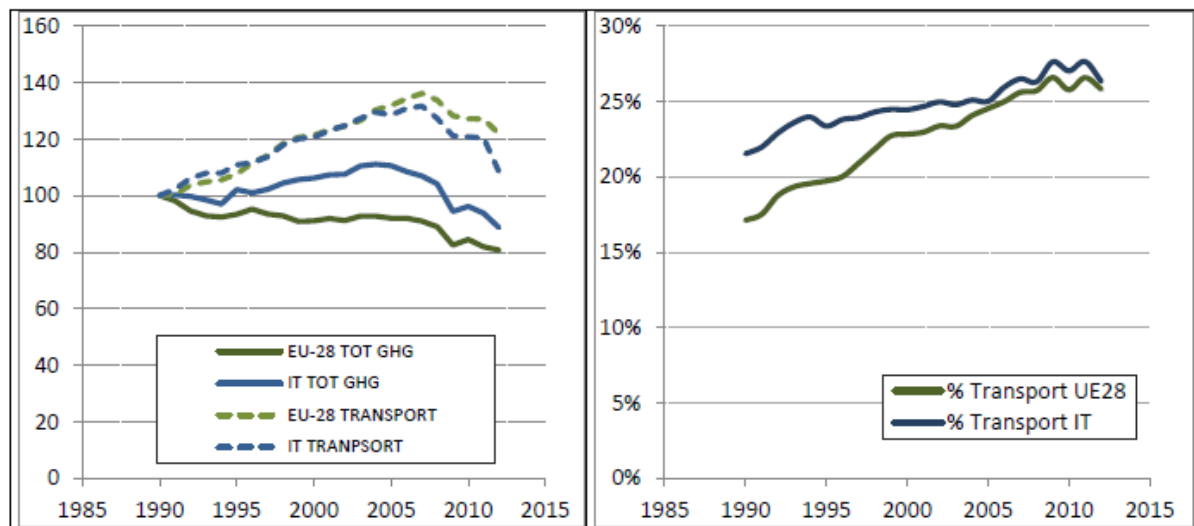


**FIGURE 2. (LEFT) GHG total and sectorial emissions in UE and Italy (indices on basis 1990=100). (RIGHT) GHG Percentages emissions due to transports over the total emissions [3].**

In this respect, Hybrid Electric Vehicles (HEVs) constitute an important solution: their growing popularity is caused by the present energy economy that is based on fossil fuels and includes the continuous increase in the demand for oil, depletion of non-renewable energy resources, and dependency on supplies from politically unstable regions. These challenges (together with the present growth in CO<sub>2</sub> emissions) lead to continuous growing fuel prices and environmental taxes. The application of the hybrid technology gives an opportunity to decrease the petrol consumptions and to decrease the CO<sub>2</sub> emissions as in the HEVs the internal combustion engine (ICE) can be downsized to operate in optimal conditions. However, it is not possible to achieve without an energy storage system (ESS), which is necessary for an energy recuperation and a power peak compensation. The lithium ion (Li-ion) battery is considered to be the preferred choice for energy storage device because of its high specific power, acceptable energy density and low self-discharge rate. [4]

## 2. Hybrid Electric Vehicles (HEVs)

Vehicles in which two or more forms of energy storage coexist, in order to generate mechanical energy, are called hybrid vehicles. They represent a possible solution immediately achievable to:

- improve vehicle performance to reduce fuel consumption and lower CO<sub>2</sub> emissions;
- reduce polluting emissions in urban areas;
- reduce dependence on fossil energy sources.

More specifically, a hybrid propulsion vehicle is equipped with two or more components which work in synergy with each other by combining a conventional internal combustion engine with an electric propulsion system. It is a type of technology which indulges both mechanical drive train and electric vehicle. A mechanical drive is composed by the fuel tank (it contains fuels like petrol or diesel), the combustion engine, the gear box and the transmission branch to the wheels. An electric drive consists of the battery, electric motor and power electronics to control the entire system. The main advantage of hybrid vehicles is the elimination of the defects in starting from an arrest, subjected to the physical laws of inertia. In the vehicle with coupled endothermic engine starting in electric, the two engines are suitable to coexist; the internal combustion engine transforms the chemical energy of the fuel (of considerable energy density) with an acceptable efficiency, in particular in some operating points (at low speed the electric



is more efficient, at high the endothermic). Instead, the electric motor converts with a greater efficiency an energy available on board in smaller quantities. Each electric machine is able itself to work in traction and generation and therefore each hybrid vehicle tries to exploit the ability to “brake” in slowdowns, generating energy otherwise dissipated in form of heat during brakes. In particular, Regenerative Braking is an energy recovery mechanism which slows down a vehicle by converting its kinetic energy into electrical one, which can be used immediately or stored until needed in batteries. Another advantage is the possibility, even at high speeds for short distances, to support the endothermic engine in acceleration phase.

## 2.1 Configurations and Classification

There are two main schemes for the integration of a thermal engine and an electric machine: series hybrid and parallel hybrid. The combination of the two gives rise to the mixed hybrid.

- **Series Hybrid**

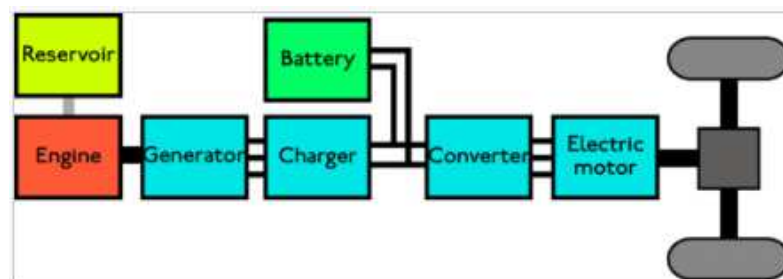


FIGURE 3. SERIES HYBRID CONFIGURATION [5]

This technology is very similar to that employed in diesel-electric locomotives. In this type the internal combustion engine is not connected to the driven wheels and can be operated mostly in the maximum efficiency region; it has the task of generating the current in order to power the electric engine that transform it into motion, while the energy in surplus is used to recharge the batteries. Sometimes, when a large quantity of energy is required, it is drawn from both the heat engine and the batteries.

Since electric motors are able to operate on a vast range of rotational speed, this structure allows to remove or reduce the need for a complex transmission. For this reason, it would allow the use of more efficient turbine engines instead of alternatives, since the efficiency of alternative internal combustion engines changes with the number of revolutions, whereas in the hybrid

series systems the revolutions of the thermal engine are set to always obtain the maximum efficiency (not having to undergo either accelerations or decelerations). The major shortcomings of the series configuration are the high power installed in each component and the request of a generator; in fact, the energy from the internal combustion engine is converted twice before to drive the wheels. [6] Series Hybrids are the most efficient for vehicles requiring continuous braking and restarting such as urban means, buses and taxis.

- **Parallel Hybrid**

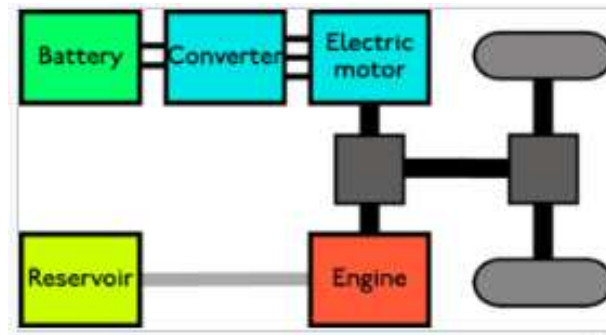


FIGURE 4. PARALLEL HYBRID CONFIGURATION [5]

It is considered more suitable for vehicles in the automotive and road transport sectors. In this case the two motors (thermal and electrical) are powered in independent ways transmitting energy to the same motor shaft. There is direct mechanical connection between the hybrid power unit and the wheels, whereby both motors (electric and thermal) provide torque to the wheels. In addition, this layout has an electric traction motor and can recovery a share of the braking energy in order to charge the batteries (regenerative braking) or help internal combustion engine during acceleration conditions. A particularity lies in the fact that start, acceleration and braking insist on the electrical part, thus helping to decrease the consumption of the hybrid engine. There are several configurations depending on the structure of the mechanical combination between the internal combustion engine and the electrical motor.

- **Series-Parallel Hybrid**

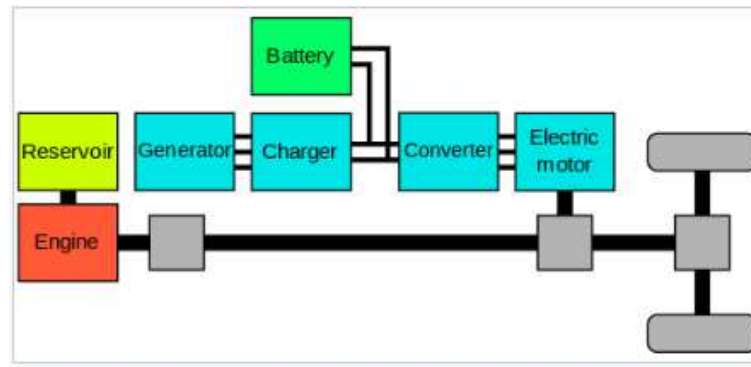


FIGURE 5. SERIES-PARALLEL HYBRID CONFIGURATION [5]

Mixed Hybrid are characterized by a mechanical node, as in parallel, and by an electrical node, as in series. The two layouts are merged together in order to have both advantages.

Depending on the degree of hybridization (power of the electric propulsion with respect to the total installed power) and the capacity of the hybrid propulsion system to store electricity, various levels of hybridization (characterized by a growing distance in pure electric mode and by an increasing degree of hybridization) can be defined:

- **Micro-hybrid**

The electric part (the 12 Volt lead-acid battery and the starter motor of 2-3 kW) allows the Stop and Start function of the thermal engine. In practice, the engine switches off when it is not needed and then it turns on automatically when accelerator or the clutch pedal are pressed. The advantages with respect to a traditional car are a partial refill of the battery through the alternator taking advantage of the dispersed energy in deceleration phase and reduced consumption by 5%.

- **Mild-Hybrid**

The electrical system is composed of electric motors of 10-15 kW powered by NiMH (nickel-metal hydride) or Lithium batteries from 42 to 150Volts. The thermal engine, in addition to taking advantage of the Stop and Start function, it is assisted by the electric ones in acceleration phase. Every time the hybrid car decelerates the energy, otherwise dispersed, is recovered and used to recharge the batteries.

- **Full-Hybrid**

Full-Hybrid cars are the only ones able to travel in electric only mode thanks to electric motors and more powerful batteries. This feature can be exploited mainly in the city and for this reason full-hybrid cars enjoy state incentives and can circulate freely in cities with traffic restrictions. Currently, the routes travelled with only electric traction are very small, generally no more than a few kilometer, due to the limited capacity of normal batteries. All builders are performing test on prototypes powered by lithium batteries with the advantage of having a greater autonomy but the disadvantage of being too much expensive for immediate use on standard vehicles.

	<b>Micro</b>	<b>Mild</b>	<b>Full</b>
<b>Power (kW)</b>	2.5	10-20	30-50
<b>Voltage (V)</b>	12	100-200	200-300
<b>Energy Saving (%)</b>	5-10	20-30	30-50
<b>Price increase (%)</b>	3	20-30	30-40

### 3. Electrochemical Energy Storage Systems (EESs)

The fundamental challenge for clean energy vehicles to be commercialised is energy storage. The main challenge associated with renewable energy generation is the intermittency of the renewable source of power. Because of this, back-up generation sources fuelled by fossil fuels are required.

One solution to the problem is the utilisation of electrical energy storage systems (EESs) to store the excess renewable energy and then reusing this energy when the renewable energy source is insufficient to meet the demand.

#### 3.1 Classification of EES systems

A widely-used approach for classifying EES systems is the determination in relation to the form of energy used. They are classified into mechanical, electrochemical, chemical, electrical and thermal energy storage systems.

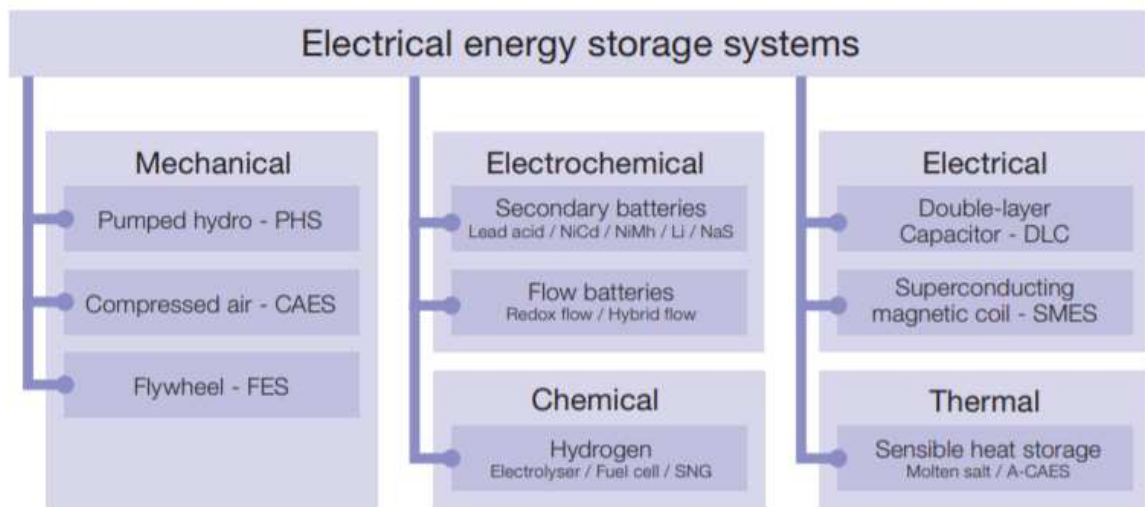


FIGURE 6. CLASSIFICATION OF ELECTRICAL ENERGY STORAGE SYSTEMS IN RELATION TO ENERGY FORM [6]

- **Mechanical energy storage systems**

The most common are:

- Pumped Hydro Storage (PHS)

Conventional PHS systems use two water reservoirs at different elevations to pump water during off-peak hours from the lower to the upper reservoir (charging phase). When required,

water flows back from the upper to the lower reservoir, powered a turbine with a generator to produce electricity (discharging phase).

- Compressed air energy storage (CAES)

CAES plants are largely equivalent to pumped-hydro power plants in terms of their applications, output and storage capacity. But, instead of pumping water from a lower to an upper pond during periods of excess power, in a CAES plant, ambient air is compressed and stored under pressure in an underground cavern. When electricity is required, the pressurized air is heated and expanded in an expansion turbine driving a generator for power production.

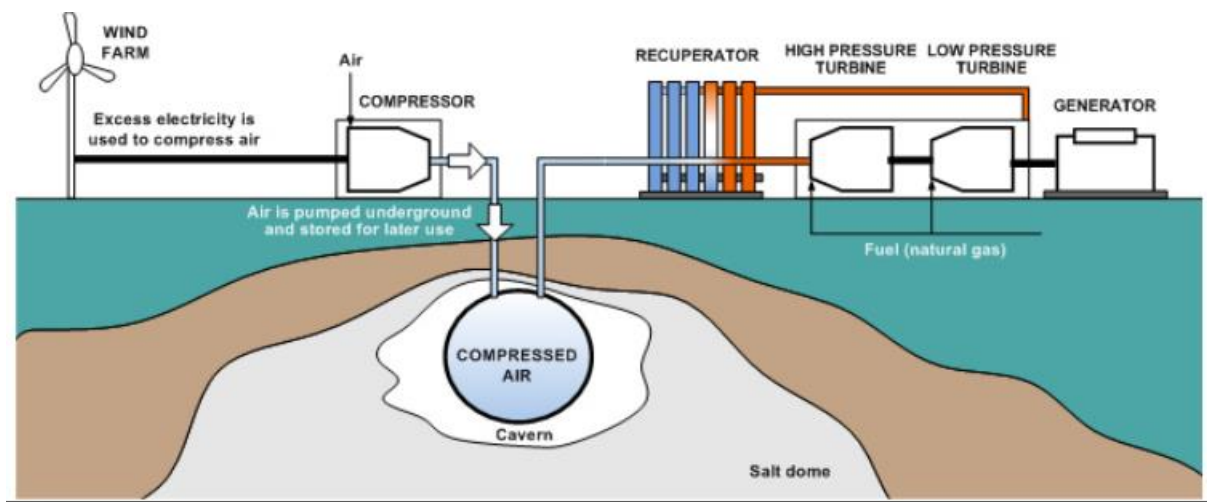


FIGURE 7. CAES SCHEME (COMPRESSED AIR ENERGY STORAGE) [7]

- Flywheel (FES)

In flywheel energy storage, rotational energy is stored in an accelerated rotor, a massive rotating cylinder. It contains a spinning mass in its centre that is driven by a motor; when energy is need, the spinning force drives a device similar to a turbine to produce electricity, slowing the rate of rotation. A flywheel is recharged by using the motor to increase its rotational speed once again. The main features of flywheels are the excellent cycle stability and a long life, little maintenance, high power density and the use of environmentally inert material. However, flywheels have a high level of self-discharge due to air resistance and bearing losses and suffer from low current efficiency.

- **Electrochemical energy storage systems**

On its most basic level, a battery is a device consisting of one or more electrochemical cells that convert stored chemical energy into electrical energy. Each cell contains a positive terminal, or cathode, and a negative terminal, or anode. Electrolytes allow ions to move between the electrodes and terminals, which allows current to flow out of the battery to perform work. Advances in technology and materials have greatly increased the reliability and output of modern battery systems. Continued innovation has created new technologies like electrochemical capacitors that can be charged and discharged simultaneously and instantly, and provide an almost unlimited operational lifespan.

Most of them are technologically mature for practical use. First, five secondary (rechargeable) battery types are listed: lead acid, NiCd, NiMH, Li-ion and NaS. Then follow two groups of flow battery.

- Lead acid battery

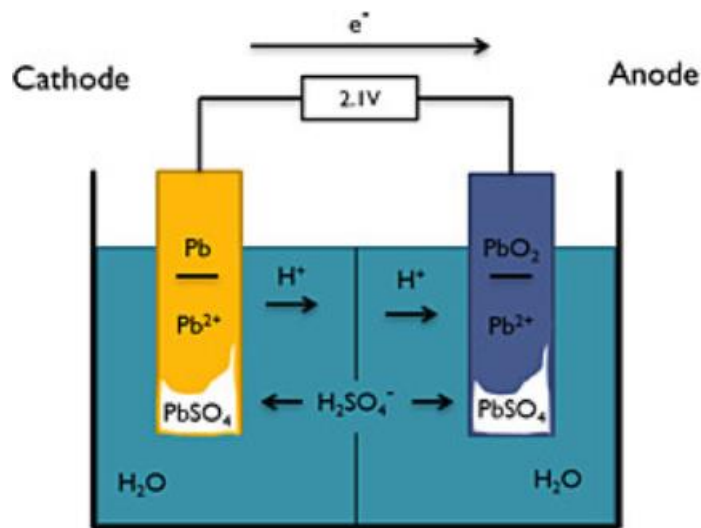


FIGURE 8. LEAD-ACID BATTERY [8]

In the fully charged state, the negative plate consists of lead and the positive one lead dioxide, with the electrolyte of concentrated sulfuric acid. In the discharge state both the positive and negative plates become lead sulphate ( $\text{PbSO}_4$ ), and the electrolyte loses much of its dissolved sulfuric acid and becomes primarily water. This battery is used in both mobile and stationary applications. One disadvantage of lead acid batteries is usable capacity decrease when high

power is discharged. Advantages are a good cost/performance ratio, easy recyclability and a simple charge technology. [9]

- Nickel-Cadmium

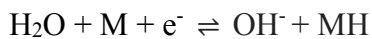
Compared to lead acid batteries, nickel-based have a higher power density, a slightly greater energy density and the number of cycle is higher. Thank to these features, NiCd batteries have a major capacity and are used in electric vehicles. From a technical point of view, NiCd batteries are very successful battery product because they are the only batteries able to perform well even at low temperatures in the range from -20°C to -40°C. However, because of the toxicity of cadmium, these batteries are presently used only for stationary applications in Europe and have been prohibited for consumers use.

- Nickel-Metal Hydride



FIGURE 9. NIMH BATTERIES

The negative electrode reaction occurring in a NiMH cell is:



On the positive electrode, NiO(OH) nickel oxyhydroxide, is formed:



NiMH cells have an alkaline electrolyte, usually potassium hydroxide. The positive electrode is nickel hydroxide and the negative electrode is hydrogen ions stored in a metal-hydride



structure that is the electrode. NiMH were developed initially to replace NiCd batteries. Indeed, NiMH batteries have all the properties of NiCd batteries, with the exception of the maximum nominal capacity (still lower). Furthermore, NiMH batteries have much higher energy densities.

- Li-ion



FIGURE 10. A LI-ION BATTERY TYPE AND FUNCTIONING

The term “lithium-ion” refers not to a single electrochemical couple but to a wide array of different chemistries, all of which are characterized by the transfer of lithium ions between the electrodes during the charge and discharge reactions. Li-ion cells do not contain metallic lithium; rather, the ions are intercalated into the structure of other materials, such as lithiated metal oxides or phosphates in the cathode and carbon (typically graphite) or lithium titanate in the anode.

Li-ion battery is currently one of the most popular types for laptops and cell phones, as well as some electric and hybrid electric vehicle, with one of the best weight/power ratios, no memory effect and a slow loss of charge when not in use. These batteries can be dangerous if used improperly and in any case, unless they are treated with care, they are assumed to have a shorter service life than other types of batteries (an entire chapter will be dedicated on lithium-ion battery later).

- Sodium-Sulphur

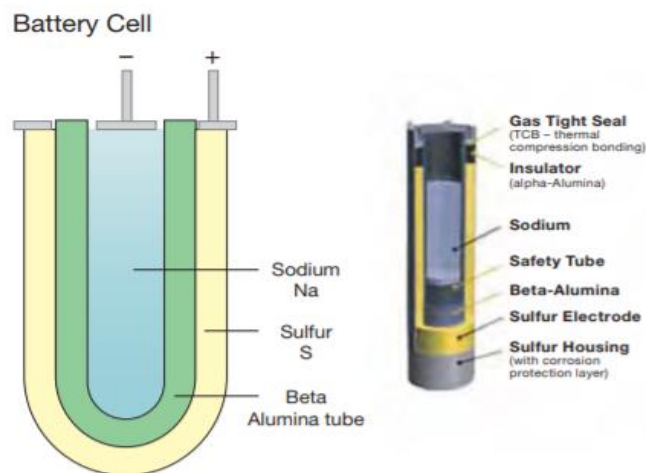


FIGURE 11. NAS BATTERY [6]

Sodium Sulphur batteries consist of liquid (molten) sulphur at the positive electrode and liquid (molten) sodium at the negative electrode; the active materials are separated by a solid beta alumina ceramic electrolyte. This ceramic allows only positively charged sodium-ions to pass through. The battery temperature is kept between 300°C and 350°C to maintain the electrodes molten. During discharge electrons are stripped off the sodium metal leading to formation of the sodium-ions that then move through the electrolyte to the positive electrode compartment. The electrons that are stripped off the sodium metal move through the circuit and then back into the battery at the positive electrode, where they are taken up by the molten sulphur to form polysulfide. The positively charged sodium-ions moving into the positive electrode compartment balance the electron charge flow. During charge this process is reversed.

- **Flow Batteries**

In conventional secondary batteries, the energy is charged and discharged in the active masses of the electrodes. A flow battery is also a rechargeable battery, but the energy is stored in one or more electroactive species which are dissolved in liquid electrolytes. The electrolytes are stored externally in tanks and pumped through the electrochemical cell that converts chemical energy directly to electricity and vice versa. One of the biggest advantages of flow batteries is that they can be almost instantly recharged by replacing the electrolyte liquid, while simultaneously recovering the spent material for re-energization.

- Redox flow

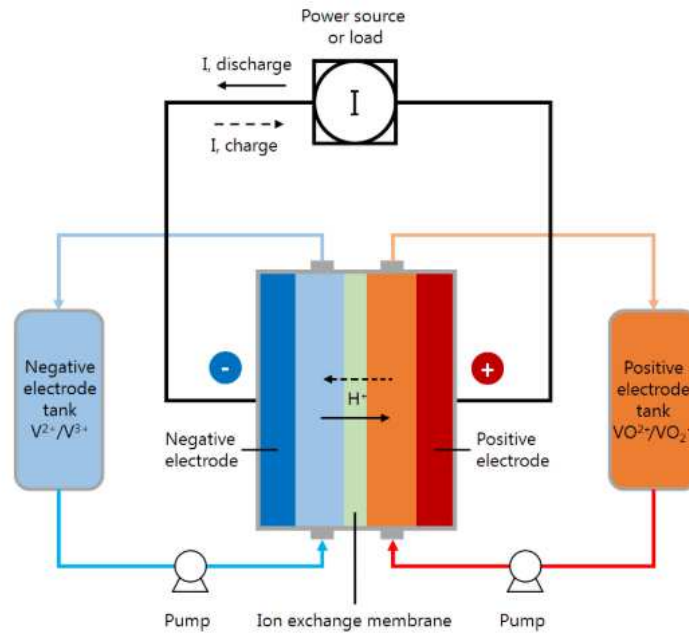


FIGURE 12. VANADIUM REDOX FLOW BATTERY [10]

Redox flow batteries (RFB) represent one class of electrochemical energy storage devices. The name “redox” refers to chemical reduction and oxidation reactions employed in the RFB to store energy in liquid electrolyte solutions which flow through a battery of electrochemical cells during charge and discharge. During discharge, an electron is released via an oxidation reaction from a high chemical potential state on the negative or anode side of the battery. The electron moves through an external circuit to do useful work. Finally, the electron is accepted via a reduction reaction at a lower chemical potential state on the positive or cathode side of the battery. The direction of the current and the chemical reactions are reversed during charging.

Theoretically a RFB can be “recharged” within a few minutes by pumping out the discharged electrolyte and replacing it with recharged electrolyte. That is why redox flow batteries are under discussion for mobile applications. However, up to now the energy density of the electrolytes has been too low for electric vehicles.

- Hybrid flow

In a hybrid flow battery (HFB) one of the active masses is internally stored within the electrochemical cell, whereas the other remains in the liquid electrolyte and is stored externally in a tank. Therefore, hybrid flow cells combine features of conventional secondary batteries and redox flow batteries: the capacity of the battery depends on the size of the electrochemical

cell. Typical examples of a HFB are the Zn-Ce and the Zn-Br systems. In both cases the anolyte consists of an acid solution of  $\text{Zn}^{2+}$  ions. During charging Zn is deposited at the electrode and at discharging  $\text{Zn}^{2+}$  goes back into solution. As membrane, a microporous polyolefin material is used; most of the electrodes are carbon-plastic composites.

- **Chemical energy storage systems**

The main purpose of such a chemical energy storage system is to use “excess” electricity to produce hydrogen via water electrolysis. Once hydrogen is produced different ways are available for using it as an energy carrier, either as pure hydrogen or as SNG. Although the overall efficiency of hydrogen and SNG is low compared to storage technologies such as PHS and Li-ion, chemical energy storage is the only concept which allows storage of large amounts of energy (up to the TWh range) and for greater periods of time – even as seasonal storage. Another advantage of hydrogen and SNG is that these universal energy carriers can be used in different sectors, such as transport, mobility, heating and the chemical industry.

- Hydrogen storage systems

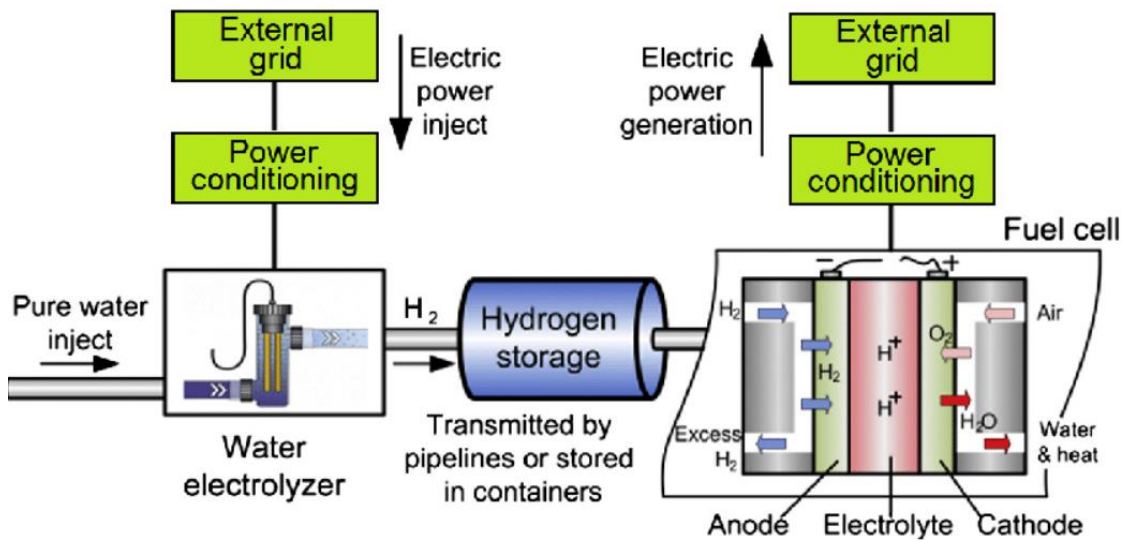


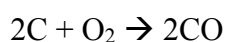
FIGURE 13. TOPOLOGY OF HYDROGEN STORAGE SYSTEM [11]

A typical hydrogen storage system consists of an electrolyzer, a hydrogen storage tank and a fuel cell. Electrolyzers (that could be a SOEC or PEMEC or AEC) are exploited to produce chemicals with economic/thermodynamic value: it is an electrochemical converter which splits water with the help of electricity into hydrogen and oxygen by an endothermic process. Then, resulted hydrogen is stored under pressure in tanks; to generate electricity, both gases flow into

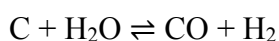
the fuel cell where an electrochemical reaction which is the reverse of water splitting takes place: H<sub>2</sub> and O<sub>2</sub> react and produce water, heat is released and electricity is generated. Different approaches exist to storing the hydrogen, either as a gas under high pressure, a liquid at very low temperature, adsorbed on metal hydrides or chemically bonded in complex hydrides.

- Synthetic natural gas (SNG)

Synthetic natural gas is a type of gas created from coal that serves as a substitute for natural gas and is suitable for transmission in natural gas pipelines. Synthetic natural gas is created through a thermo-chemical conversion. The first step in this conversion is the *gasification* of the solid carbon source, whether it be coal or biomass (which would create Bio-SNG), with steam or oxygen. Here the coal is burned with a limited supply of oxygen or air and the main product is carbon dioxide:



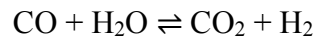
To reduce the amount of nitrogen in this gas, modern gas plants use pure oxygen for combustion. If steam is added to this pure oxygen, then a water gas reaction occurs instead of the traditional combustion:



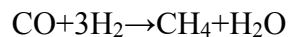
These processes drive off some of the volatile material, and the product is known as a producer gas. Generally, this occurs in a gasifier which feeds coal into a high pressure, high temperature vessel and distributes steam or oxygen evenly while removing ash to gasify the coal. This producer gas is a mixture containing H<sub>2</sub>, CO, CO<sub>2</sub>, H<sub>2</sub>O, and CH<sub>4</sub> along with *other* hydrocarbons and some impurities. The exact composition of this gas depends on the type of reactor used, operating conditions, and other processes during the gasification process. This gas also contains impurities such as oils, tars and ammonia which must be removed - although ammonia levels are lower if the water gas reaction takes place.

To purify this gas, it must undergo gas cleaning and gas conditioning. During gas cleaning, impurities such as ammonia and sulphur are removed from the producer gas whereas in gas conditioning is the process by which parts of the producer gas are converted so that the final composition of the gas is suitable for its use. What is left after this cleaning and conditioning is useful synthesis gas (carbon monoxide and hydrogen) plus some methane, and carbon dioxide.

To finish making the synthetic natural gas, the syngas must undergo *water gas shift reactions and methanation*. The water gas shift reaction combines carbon monoxide with steam to create carbon dioxide and hydrogen in the following reaction:



This reaction requires a metal catalyst to occur. Since the end "goal" of this gas is to obtain methane (the main component of natural gas) some of the carbon monoxide is retained, so the reaction does not go through to completion. At this point, the carbon dioxide is separated out using a type of scrubbing and only the final methanation step remains. During methanation, carbon monoxide reacts with the hydrogen that was created with the help of a nickel catalyst to create methane and steam in the following reaction: [9]



As in the case of hydrogen, the SNG produced can be stored in pressure tanks, underground, or fed directly into the gas grid.

- **Electrical storage systems**

- Double-layer capacitors (DLC)

This special type of capacitor has properties that are about halfway between regular capacitors and rechargeable (secondary) batteries. While a battery stores an electrical charge through a chemical reaction, DLC stores charge by means of an electric double layer formed by ions adhering to the surface of an activated carbon electrode. Whereas charging a rechargeable battery requires several hours, an electric double layer capacitor can be charged in a matter of seconds. Furthermore, the number of charge cycles for a battery is limited, but the electric double layer capacitor in principle has no such limitation.

- Superconducting magnetic energy storage (SMES)

Superconducting magnetic energy storage (SMES) systems work according to an electrodynamic principle. The energy is stored in the magnetic field created by the flow of direct current in a superconducting coil, which is kept below its superconducting critical temperature.

The main advantage of SMES is the very quick response time: the requested power is available almost instantaneously. Moreover, the system is characterized by its high overall round-trip efficiency (85% - 90%) and the very high power output which can be provided for a short period of time.

- **Thermal storage systems**

Thermal energy storage technologies allow us to temporarily reserve energy produced in the form of heat or cold for use at a different time.

Take for example modern solar thermal power plants, which produce all of their energy when the sun is shining during the day. The excess energy produced during peak sunlight is often stored in these facilities - in the form of molten salt or other materials - and can be used into the evening to generate steam to drive a turbine to produce electricity. Alternatively, a facility can use 'off-peak' electricity rates which are lower at night to produce ice, which can be incorporated into a building's cooling system to lower demand for energy during the day. Thermal energy storage is an effective resource at capturing and storing energy on a temporary basis to be used at a later time.

Thermal storage can be subdivided into different technologies:

- *sensible heat storage*: the storage medium may be a liquid such as water or thermo-oil, or a solid such as concrete or the ground. Thermal energy is stored solely through a change of temperature of the storage medium. The capacity of a storage system is defined by the specific heat capacity and the mass of the medium used;
- *latent heat storage*: is accomplished by using phase change materials (PCMs, such as organic paraffins or inorganic salt hydrates) as a storage media. Latent heat is the energy exchanged during a phase change; it is also called “hidden” heat, because there is no change of temperature during energy transfer. The advantage of latent heat storage is its capacity to store large amounts of energy in a small volume and with a minimal temperature change, which allows efficient heat transfer;
- *sorption (adsorption, absorption) storage systems* work as thermo-chemical heat pumps under vacuum conditions and have a more complex design. Heat from a high-temperature source heats up an adsorbent (e.g. silica gel or zeolite), and vapour (working fluid, e.g. water) is desorbed from this adsorbent and condensed in a condenser at low temperatures. The heat of condensation is withdrawn from the system. The dried adsorbent and the separated working fluid can be stored as long as desired. During the discharging process the working fluid takes

up low-temperature heat in an evaporator. Subsequently, the vapour of the working fluid adsorbs on the adsorbent and heat of adsorption is released at high temperatures.

## 4. Batteries

Batteries are closed electro-chemical cells able to convert chemical energy directly in electricity. Reaction is fed by molecules contained directly into the structures of the electrodes, so the materials of electrodes participate to the reaction (there is no feeding from outside. They can work both in direct and inverse operation: a battery can be operated as a fuel cell, to produce power (direct functioning) or as an electrolyzer, to restore the chemical potential of reactants (inverse functioning). When placed in condition of “closed external circuit”, oxidation-reduction (redox) reactions occur spontaneously inside it; the flow of electrons produced by these reactions is intercepted thanks to the particular structure of the batteries and used to power electrical devices. One of the main advantages of this form of energy is that it is not subject to limits of thermodynamic efficiency of the Carnot cycle. Therefore, very high efficiencies (close to 100%) are possible.

### 4.1 Working principle of electro-chemical cells

The cell is composed of three main components: anode, cathode and electrolyte layer.

- *Anode*: electrode where the reaction of oxidation occurs (reaction in which there is a delivery of free electrons). Conventionally, in charge phase the anode is assumed the positive electrode, in discharge the negative one.
- *Electrolyte*: layer which physically separates anode and cathode. It should be characterized by a very low molecular diffusivity, a very low capability to conduct  $e^-$  and a very high ions conductivity.
- *Cathode*: electrode where the reaction of reduction occurs (reaction in which there is a gain of free electrons). Conventionally, in charge phase the anode is assumed the negative electrode, in discharge the positive one.

Even if there is no contact between the two reactants of the two electrodes (thanks to electrolyte layer) the reaction however occurs because ions (oxidized form of anodic reactant through oxidation) can travel across the electrolyte and electrons can travel in an external circuit (since



they cannot pass across the electrolyte, they will follow an alternative path). In such a process, a charge separation occurs generating electrical fields on both electrodes. Therefore, a voltage difference  $\Delta V$  between electrodes is created. By closing the external circuit, the equilibrium at electrodes is broken and a current  $I$  is generated by  $e^-$  flux. Finally, the presence of a current  $I$  flowing across a voltage gradient will generate electrical power:  $W_{el} = \Delta V * I$ .

A very simple scheme of an electro-chemical cell is shown in the following:

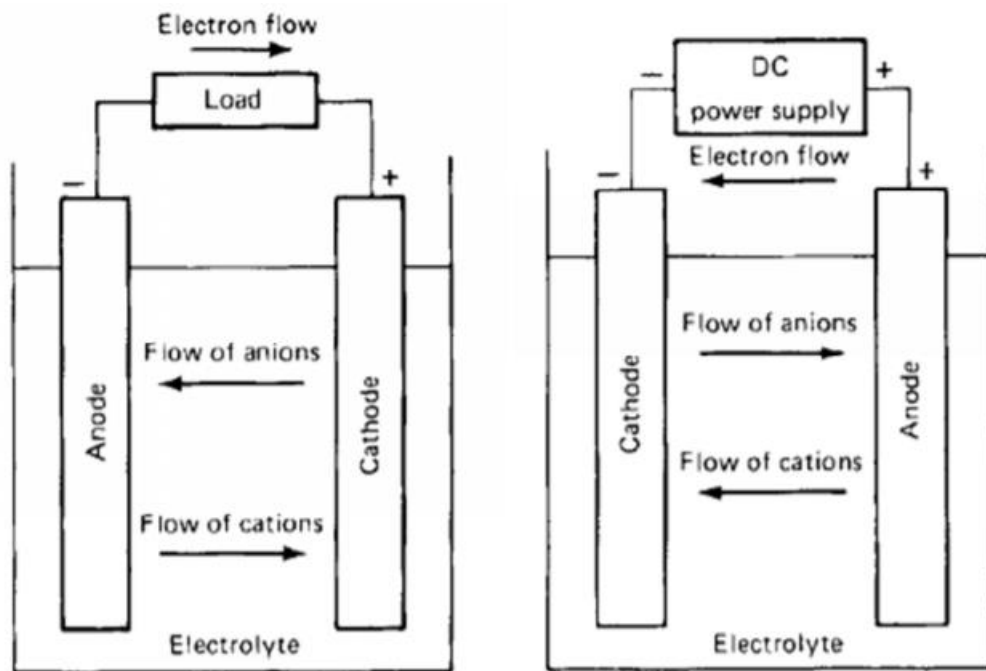


FIGURE 14. (LEFT) DISCHARGE AND (RIGHT) CHARGE PROCESS

A *galvanic cell* is an electro-chemical cell in which the disequilibrium of reactants in terms of Gibbs free energy (a state function representing free energy in iso-thermobaric transformations that determines the spontaneity of a reaction) is directly transformed into electrical power ( $\Delta G \rightarrow W_{el}$ ).

An *electrolytic cell* is an electro-chemical cell in which a not spontaneous reaction (with  $\Delta G > 0$ ) is driven by electrical power (electrical energy is converted to chemical energy associated to a chemical element/compound,  $W_{el} \rightarrow \Delta G$ ).

*Faraday law* gives the relationship between molar flow rate of species reacting at electrodes ( $N_R$ ) and the current flowing in the external circuit ( $I$ ):

$$N_R = \frac{I}{z_R * F}$$

where  $F$  is the Faraday constant (equal to  $96487 \frac{C}{mol}$ ) and  $z_R$  is the charge number of specie.

The only situation in which the cell is working in reversible condition is when the circuit is open, since no transport phenomena occur and, as a consequence, there is no generation of entropy. The voltage measured across the cell in this situation is called *OCV (Open Circuit Voltage)* and the law that governs it is the Nernst Equation:

generic reaction  $\rightarrow v_a A + v_b B \rightarrow v_c C + v_d D$

$$OCV = -\frac{\Delta G(T, P)}{z_R * F} = -\frac{\Delta G(T, P_0)}{z_R * F} + \frac{\bar{R} * T}{z_R * F} * \ln \frac{[A]^{v_a} [B]^{v_b}}{[C]^{v_c} [D]^{v_d}}$$

where  $[A]$ ,  $[B]$ ,  $[C]$ ,  $[D]$  are the reactants and products concentrations. Nernst equation can be written also in terms of partial pressures:

$$OCV = -\frac{\Delta G(T, P_0)}{z_R * F} + \frac{\bar{R} * T}{z_R * F} \frac{\prod_i^n (\frac{P_i}{P_0})^{v_i}}{\prod_i^m (\frac{P_i}{P_0})^{v_i}}$$

OCV is potential drop in case of ideal conditions, which corresponds to open circuit conditions ( $I = 0$ ). When the circuit is closed, a current  $I$  (different from zero) starts flowing in the external circuit breaking the chemical equilibriums which were taking place at the electrodes. In this case, the system is no more in ideal conditions, but it is operating in real ones and the potential drop across the cell will be always lower/higher (for a Galvanic/Electrolytic cell) than OCV. The differences between real and ideal functioning arise because of the occurring of mass and charge transport phenomena which characterize the real behaviour of the system.

The relationship between the potential drop across the cell and the intensity of the current flowing in the cell varies from cell to cell and it's called *polarization curve*:  $V_c = V_c(I)$ .

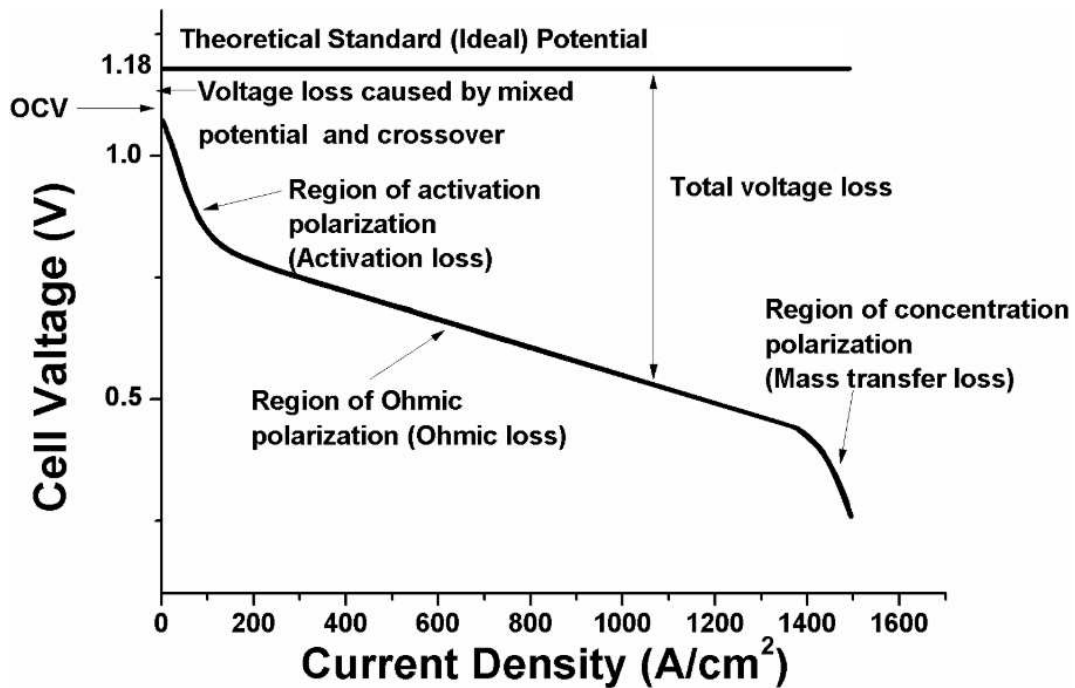
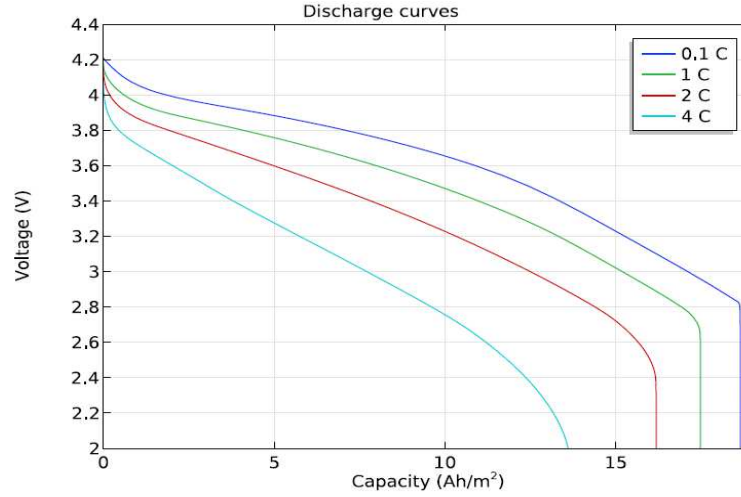


FIGURE 15. POLARIZATION CURVE, DISCHARGE PHASE

Considering a discharge phase,  $V_c$  decreases when  $I$  rise up because of irreversibilities associated to the following transport phenomena:

- *charge transfer*: related to kinetic behaviour of electro-chemical reaction both at anode and at cathode. More specifically, it is a kinetic process related to the activation of the reactions occurring separately at the two electrodes; each of the half electro-chemical reaction has an own given behaviour that is strictly related to the rate of reaction. The activation overvoltage is the voltage drop spent in order to activate the electro-chemical reaction, by increasing its rate of reaction;
- *charge conduction*: related to ion conduction in the electrolyte and electrons in electrodes and external circuit. Most of ohmic voltage drop (it is the product of the current density by the area specific resistance ASR) is associated to ion conduction across the electrolyte layer. In order to reduce ohmic overvoltage, the thickness of the electrolyte layer should be as low as possible ensuring at the same time that the same layer is thick enough to avoid electrons and molecules transport (thus avoiding short-circuiting occurring);
- *mass transfer*: related to molecules diffusion through the electrodes pores. Physically, diffusion phenomena will not directly drive a potential drop, but rather it will drive a reactant concentration reduction which, in turn, will drive a potential drop through a Nernstian effect.

Voltage profiles vary changing the discharge current. The discharge current values are expressed as a function of the battery capacity,  $X \cdot C$  where  $C$  is the nominal capacity of the battery and  $X$  is a multiplicative factor. For example, a battery with a capacity of 50Ah and a discharge curve with a current equal to  $2C$ , has a discharge current equal to 100A. The higher is the discharge current, the lower will be the voltage at the ends of the battery.



**FIGURE 16. VOLTAGE VARIATION WITH C-RATE**

The cell voltage will not only be affected by the entity of applied current (transport) but also by the state of charge/discharge (SOC/SOD parameters equal to 0 when battery is completely discharged/charged and equal to 1 when battery is completely charged/discharged), which in turn is determined by the amount of substance in the anode structure (i.e. in Lithium-ion battery, as the SOD grows, the disequilibrium in terms of  $\Delta G$  between anode and cathode will decrease because of the variation of Lithium quantity in the anode). Logically, if the discharge current increases the battery is discharged in less time because more power is required. However, discharge current causes a rising in the working temperature which in turn affects the voltage at the cell terminals. For this reason, it is important to cool the battery so that to try to contain the working temperature inside the allowable range. This must be done especially in those applications tending to discharge the battery completely, because at the end of the discharge phase, the temperature increases more rapidly.

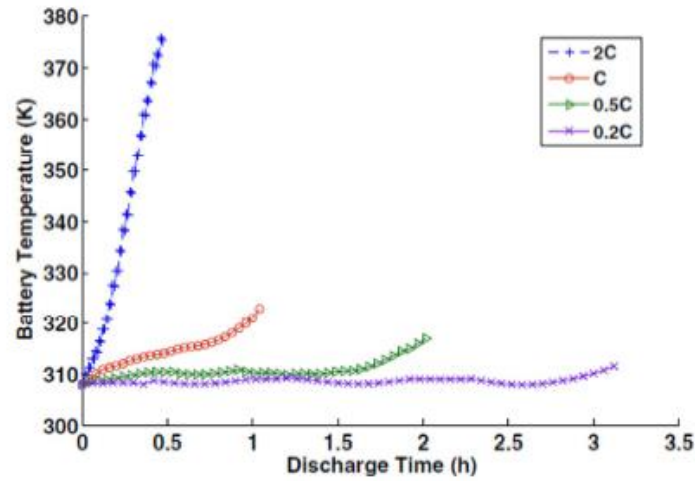


FIGURE 17. TEMPERATURE TREND DURING DISCHARGE AT DIFFERENT C-RATE

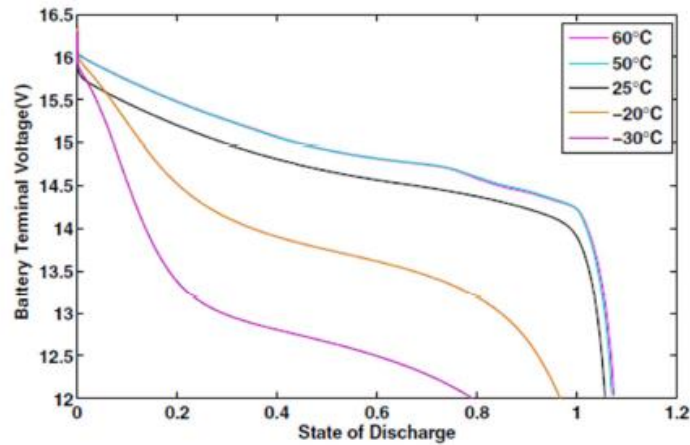


FIGURE 18. VOLTAGE IN FUNCTION OF SOD (STATE OF DISCHARGE) AT DIFFERENT TEMPERATURES

However, the topic of the temperature is quite delicate than just described, because a battery (i.e. Li-ion batteries) could have problems not only at high but also at low temperatures. If battery is working at low temperature, the speed with which chemical reactions occur is smaller and therefore the carrying capacity of the current is reduced, thus decreasing the energy extractable from the cell. In addition, prolonged exposure to low temperatures, below the allowed temperature, can lead to irreversible capacity losses.

## 4.2 Batteries Classification and Operating parameters

A first general classification of the batteries is the following:

*Primary batteries*: they can be used only once because reactants are consumed during discharge process. They can't be refilled and must be throw away when they have exhausted their energy.

*Secondary batteries*: they can be reused because reactions producing electricity during discharge process are reversed in the charging one. The battery charge is restored by flowing through the system a current opposed to that produced in the discharge.

The characteristics that distinguish the electric energy storage systems on-board vehicle are:

- *Efficiency*: it is a measure of how much energy is effectively given by the battery after it has been charged;
- *Capacity*: it represents the amount of charge needed to deliver an ampere of current for 1 hour, or 3600 coulombs [Ah]. For this reason, it is mainly used to measure the time in which a battery will run out (i.e. a 1Ah battery continuously delivering 1A will discharge in an hour, delivering instead 500 mA will discharge in 2 hours). In addition, for rechargeable batteries, it is used to estimate the charging time (e.g. to fully charge a 1Ah battery with constant current of 500 mA it will take 2 hours).

Note the capacity of the batter, it can go back to the value of the discharge current (or charge). For example, if a battery has a capacity of 500 mAh, a discharge at 2C-rate means a current of 1A, while a charge at C/10 rate means a current of 50mA.

- *Energy density*: amount of energy that can be delivered per unit of volume  $\left[\frac{Wh}{m^3}\right]$ . Vehicle batteries can't be too much bulky and voluminous;
- *Specific energy*: amount of energy that can be delivered per unit of mass  $\left[\frac{Wh}{kg}\right]$ ;
- *Specific power or density power*: power per unit of weight  $\left[\frac{W}{kg}\right]$  or per unit of volume  $\left[\frac{W}{m^3}\right]$ ;
- *Lifespan*: all the batteries gradually degrade as they come used. The number of allowable cycles determine the average life of a battery. Life of an accumulator indicates the number of time it can be discharged and then charged before its performance in terms of theoretical capacity comes down below a certain prefixed limit (generally at 75%-80% of the initial value);
- *Self-discharge*: if the accumulator remains unused for a long time, it undergoes a gradual reduction in charge. This is due to several factors, such as chemical phenomena

inside the battery, actual corrosion and impurities between electrode and electrolyte, defects in insulation between anode and cathode and too fast recharges. The self-discharge speed depends a lot on the outdoor temperature;

- *Cost*: it depends on both the materials used and the average battery life. An expensive battery can be acceptable if it lasts a long time. On the other hand, one can accept having to change a battery often if it is relatively cheap.

A *Ragone plot* is a plot used for performance comparison of various battery types. On such a chart the values of specific energy (in  $\left[\frac{Wh}{kg}\right]$ ) are plotted versus specific power (in  $\left[\frac{W}{kg}\right]$ ). Both axes are logarithmic, which allows comparing performance of very different devices (for example, extremely high and extremely low power).

Conceptually, the horizontal axis describes how much energy is available, while the vertical axis shows how quickly that energy can be delivered, otherwise known as power, per unit mass. A point in a Ragone plot thus represents the amount of time during which the energy (per mass) on the X-axis can be delivered at the power (per mass) on the Y-axis, and that time (in hours) is given as the ratio between the energy and the power densities. Consequently, the iso-curves in a Ragone plot are straight lines with unity slope.

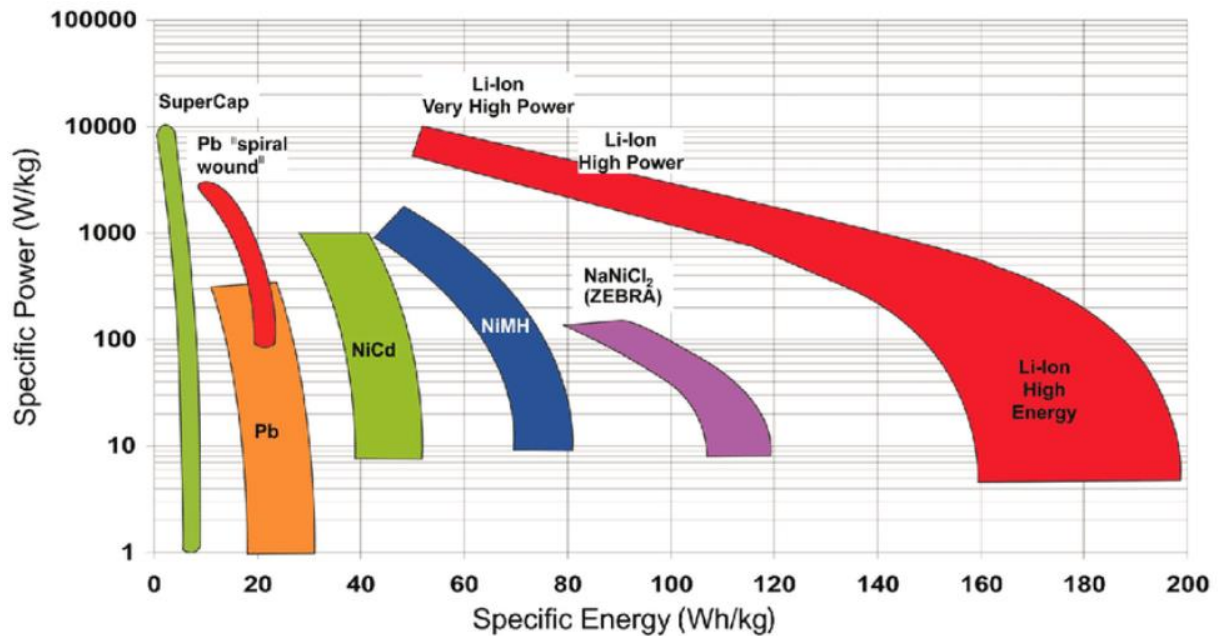


FIGURE 19. RAGONE PLOT [12]

	NiCd	NiMH	Piombo acido	Li-ioni	Li- polimeri	Na-NiCl <sub>2</sub>
Densità energetica (Wh/Kg)	45-80	60-120	30-50	110-160	100-130	120
Numero cicli (fino all'80% della capacità iniziale )	500	1000-1200	200-300	500-1000	1200-1500	1000
Tempo di ricarica	1h	2-4h	8-16h	2-4h	2-4h	4-8h
Autoscarica (per mese a T ambiente)	20,00%	30,00%	5,00%	10,00%	10,00%	14% al giorno per mantenere la temperatur a
Temperatura di utilizzo	-40 + 60°C	-20 +60° C	-20 +60° C	-5 +60° C	0 +60°C	300°C

FIGURE 20. DIFFERENT BATTERIES CHARACTERISTICS

### 4.3 Li-ion battery: State of Art

Lithium batteries are one of the most performing among the various types of batteries on the market. The reason for this fact can be understood by observing the periodic table of the elements: lithium is the lightest alkaline metal, and the less electronegative in nature. This makes it an excellent donor of electrons, which results in a high reduction potential (a measure of a chemical species to acquire electrons to be reduced). So, combined with a very electronegative material is able to develop a high d.d.p. among the two electrodes. The low molecular weight also causes its density to be relatively low. Together, these two aspects make lithium batteries among the devices marketed with higher energy density.

Lithium batteries are divided into two main categories: Lithium-Metallic and Lithium-Ion. Initially the first lithium batteries were all lithium metal; however, they suffered from serious safety problems related to the high reactivity of lithium itself. Lithium-ion cells do not contain the element in metallic form in neither of the two electrodes, but only chemical species able to bind with lithium ions, thus ensuring greater safety with the same specific energy.



The operating mechanism of Li-ion batteries is based on the migration of lithium ions which are cyclically extracted and introduced into a host matrix (the so-called “intercalation electrode”) during the charge and discharge processes. Redox reactions of the host matrix occur parallel to the ion migration, causing the external flow of electrons.

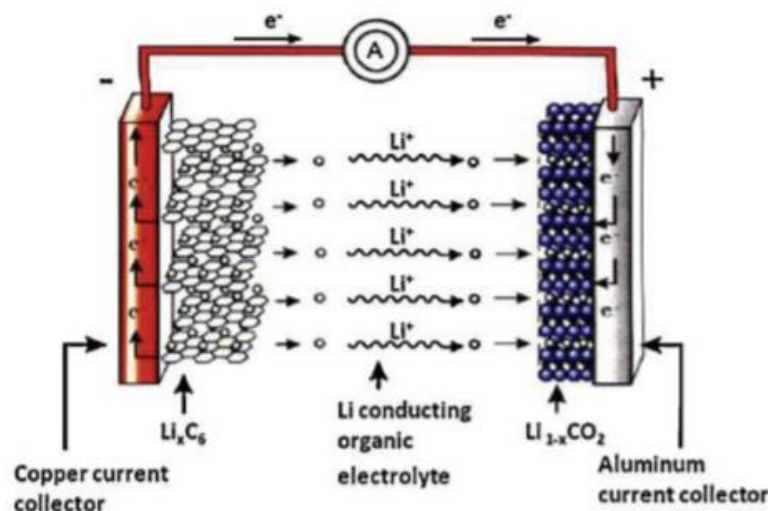


FIGURE 21. FUNCTIONING MECHANISM OF LI-ION BATTERIES

Lithium batteries use a variety of electrode and electrolytic materials, giving rise to a large number of electrochemical couples. The choice of anodic and cathodic materials and of electrolyte determines working voltage and affects the specific energy of the single cell.

- *Cathodic materials*

Currently, the most promising materials for cathode construction are Manganese (Mn), Nickel (Ni), Cobalt (Co) and Titanium (Ti), which have a crystalline structure open enough with channels and spaces inside which lithium ions are inserted, but less reliability and safety than Iron Phosphate.

- **Lithium Manganese Oxide (LiMn<sub>2</sub>O<sub>4</sub> o LMO)**

Li-ion with Manganese spinel improves ion flow on the electrode, which results in lower internal resistance (thus enabling fast charging and high-current discharging) and improved current handling. A further advantage of spinel is high thermal stability and enhanced safety, but the cycle and calendar life are limited and specific energy is more moderate than cobalt one.

Design flexibility allows engineers to maximize the battery for either life span, specific power and specific energy.

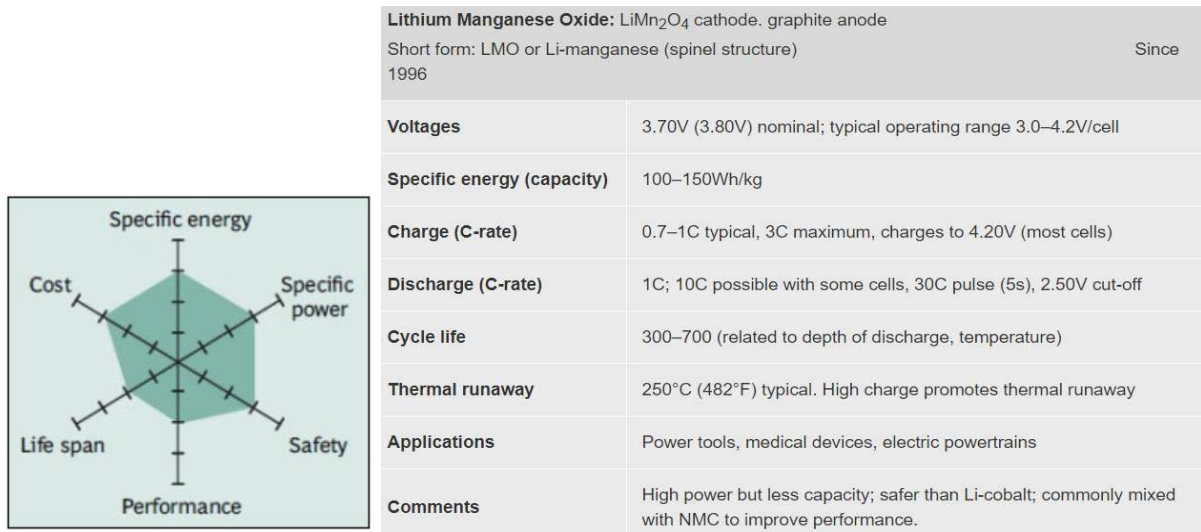
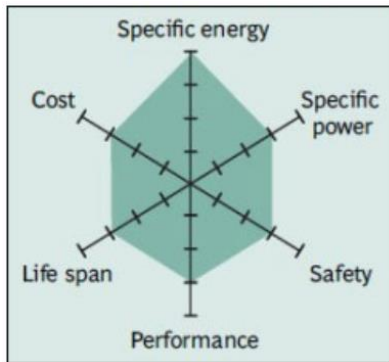


FIGURE 22. LMO CATHODE [13]

- **Lithium Nickel Manganese Cobalt Oxide ( $\text{LiNiMnCoO}_2$  or NMC)**

One of the most successful Li-ion systems. They can be flexible to serve as Energy cells (made for maximum capacity to provide long runtimes) or Power cells (has moderate capacity but excellent load capabilities). The secret of NMC lies in combining nickel and manganese: the former is known for its high specific energy but poor stability, the latter has the benefit of forming a spinel structure to achieve low internal resistance but offers a low specific energy. Combining them enhances each other strengths. NMC is the battery of choice for power tools, e-bikes and other electric powertrains; the cathode combination is typically one-third nickel, one-third manganese and one-third cobalt. Nickel-based systems have higher energy density, lower cost and longer cycle life than the cobalt-based cells but they have a slightly lower voltage.

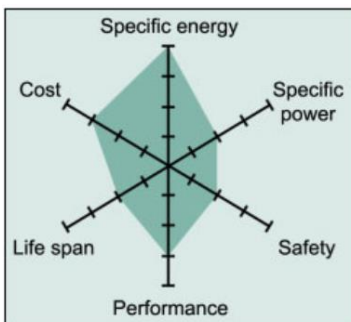


<b>Lithium Nickel Manganese Cobalt Oxide:</b> LiNiMnCoO <sub>2</sub> . cathode, graphite anode Short form: NMC (NCM, CMN, CNM, MNC, MCN similar with different metal combinations) Since 2008	
<b>Voltages</b>	3.60V, 3.70V nominal; typical operating range 3.0–4.2V/cell, or higher
<b>Specific energy (capacity)</b>	150–220Wh/kg
<b>Charge (C-rate)</b>	0.7–1C, charges to 4.20V, some go to 4.30V; 3h charge typical. Charge current above 1C shortens battery life.
<b>Discharge (C-rate)</b>	1C; 2C possible on some cells; 2.50V cut-off
<b>Cycle life</b>	1000–2000 (related to depth of discharge, temperature)
<b>Thermal runaway</b>	210°C (410°F) typical. High charge promotes thermal runaway
<b>Cost</b>	~\$420 per kWh (Source: RWTH, Aachen)
<b>Applications</b>	E-bikes, medical devices, EVs, industrial
<b>Comments</b>	Provides high capacity and high power. Serves as Hybrid Cell. Favorite chemistry for many uses; market share is increasing.

FIGURE 23. LiNiMnCoO<sub>2</sub> CATHODE [13]

- **Lithium Cobalt Oxide (LiCoO<sub>2</sub>)**

Its high specific energy makes Li-cobalt the favorite choice for mobile phones, laptops and digital cameras. The battery consists of a cobalt oxide cathode and a graphite anode. The cathode has a layered structure; lithium ions move from the anode to the cathode during discharge process. The flow reverses on charge. The drawback of Li-cobalt is a relatively short life span, low thermal stability and limited specific power.



<b>Lithium Cobalt Oxide:</b> LiCoO <sub>2</sub> cathode (~60% Co), graphite anode Short form: LCO or Li-cobalt. Since 1991	
<b>Voltages</b>	3.60V nominal; typical operating range 3.0–4.2V/cell
<b>Specific energy (capacity)</b>	150–200Wh/kg. Specialty cells provide up to 240Wh/kg.
<b>Charge (C-rate)</b>	0.7–1C, charges to 4.20V (most cells); 3h charge typical. Charge current above 1C shortens battery life.
<b>Discharge (C-rate)</b>	1C; 2.50V cut off. Discharge current above 1C shortens battery life.
<b>Cycle life</b>	500–1000, related to depth of discharge, load, temperature
<b>Thermal runaway</b>	150°C (302°F). Full charge promotes thermal runaway
<b>Applications</b>	Mobile phones, tablets, laptops, cameras
<b>Comments</b>	Very high specific energy, limited specific power. Cobalt is expensive. Serves as Energy Cell. Market share has stabilized.

FIGURE 24. LiCoO<sub>2</sub> CATHODE [13]

- *Anodic materials*

- **Graphite ( $\text{Li}_x\text{C}_6$ )**

It is widely used for the anode. Graphite presents a layered structure, with planes of atoms arranged in hexagonal structures strongly linked together, while the various plans are bound together weakly. Since lithium ions are weaklier bounded to the graphite than to the metallic oxides, their displacement towards the cathode during discharge is energetically promoted. During charge this tendency is reversed.

- **Lithium Titanate ( $\text{Li}_4\text{Ti}_5\text{O}_{12}$  o LTO)**

Li-titanate replaces the graphite in the anode of a typical lithium-ion battery and the material forms into a spinel structure. The cathode can be LMO or NMC. It has a nominal cell voltage of 2.4V, can be fast charged and delivers a high discharge current of 10C. Li-titanate is safe, has excellent low-temperature discharge characteristics and obtains a capacity of 80% at  $-30^\circ\text{C}$ . LTO has advantages over the conventional cobalt-blended Li-ion with graphite anode by attaining zero-strain property, no SEI (Solide Electrolyte Interface) film formation and no lithium plating when fast charging and charging at low temperature. Thermal stability under high temperature is also better than other Li-ion systems; however, this battery type is expensive. Typical uses are electric powertrains. The following figure illustrates the characteristics of LTO battery:

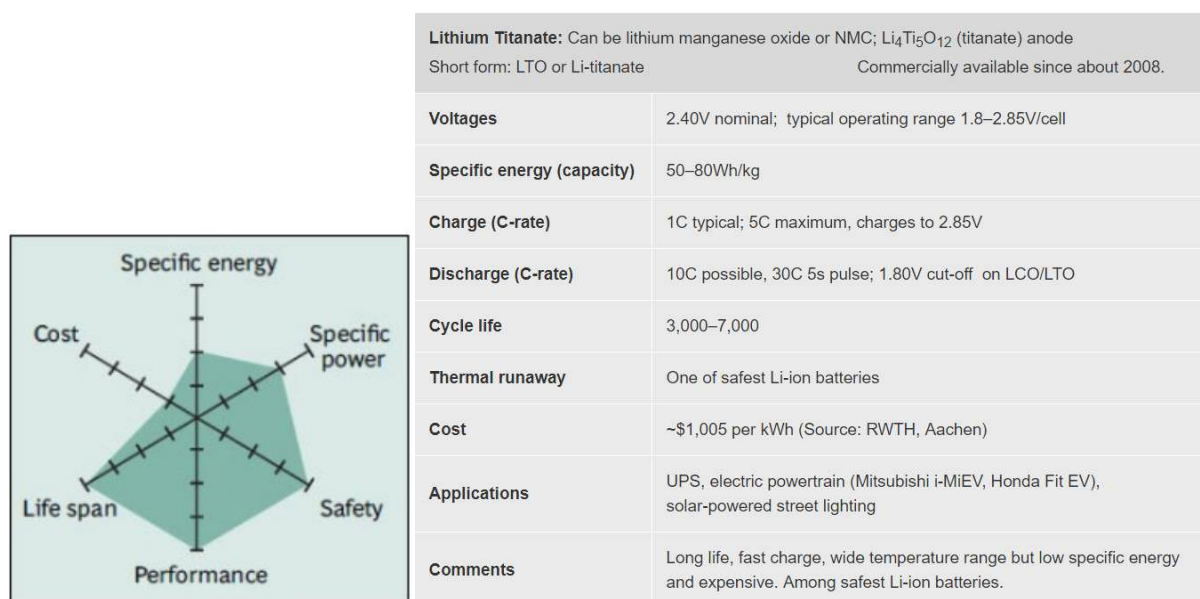


FIGURE 25. LTO-ANODE [13]

The next figure compares the specific energy of the battery types mentioned until now: while Li-aluminum (Lithium Nickel Cobalt Aluminum Oxide or in short form NCA) enjoys the highest specific energy, even if manganese (LMO) and phosphate (LFP) are superior in terms of specific power and thermal stability. LTO may have low capacity but this chemistry outlives most other batteries regarding life span and also has the best performance at cold temperature. Moving towards the electric powertrain, safety and cycle life will gain dominance over capacity. [13]

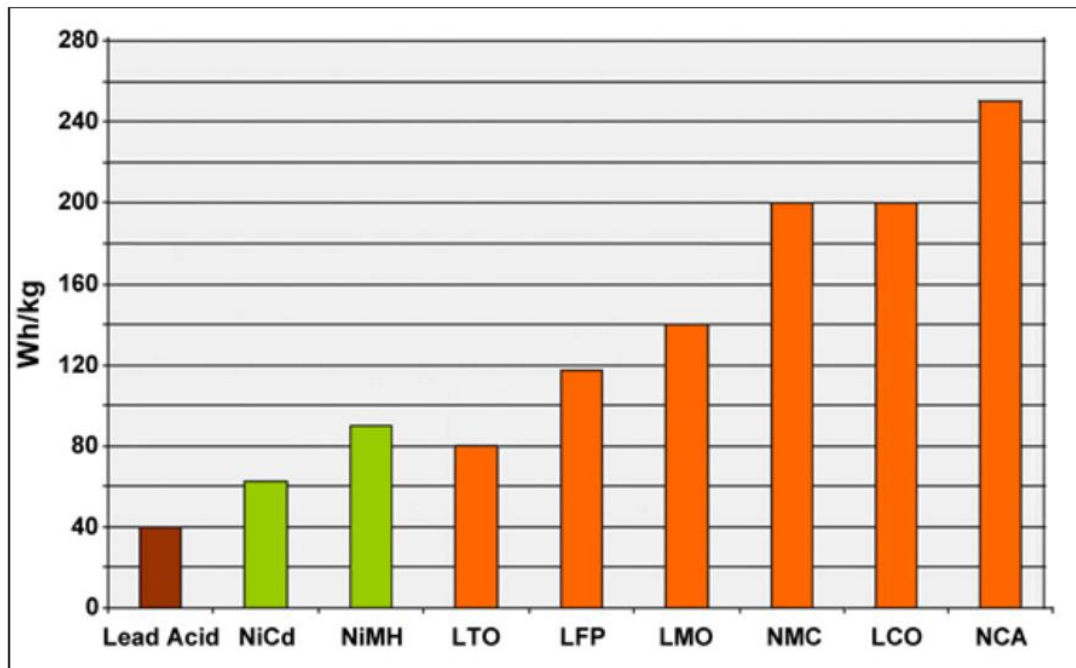


FIGURE 26. BATTERY SPECIFIC ENERGY COMPARISON [13]

- *Electrolyte*

• **Electrolyte in liquid solution**

The electrolyte is often a lithium salt solution (usually  $\text{LiPF}_6$ ) dissolved in a non-aqueous organic solvent, able to dissolve the lithium salt and transporting current via Li-ions. The separators are usually microporous membranes made of polyethylene or polypropylene. Due to the low conductivity of organic electrolytes, adequate cell or battery power can be obtained only with electrodes and separators that are much thinner than those used in batteries with aqueous electrolytes.  $\text{LiPF}_6$  also exploits the inertness of hexafluorophosphate anion toward strong reducing agents such as lithium metal.

- **Solid polymer (polyethylene (CH<sub>2</sub>)<sub>n</sub>) + liquid Li salts**

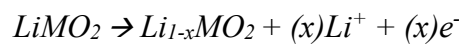
The main feature that differentiates them is that the lithium salt electrolyte is not contained in an organic solvent, as in the widely used lithium ion design, but is inserted in a solid polymer composite. The polymer electrolyte replaces the traditional one porous separator, which is soaked with the electrolyte. The project of dry polymer offers simplifications regarding construction, robustness, safety and geometry with thin thickness; unfortunately, the dry polymer guarantees low conductivity due to high internal resistance.

#### 4.3.1 Charge configuration

In all lithium batteries, during redox reactions associated with the processes of charge and discharge, lithium ions migrate from an electrode to another reversibly. When cell is totally discharged, all the present lithium is contained in the cathode, except the amount in the salts constituting the electrolyte.

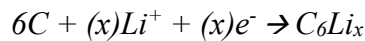
During charging process, lithium ion is extracted from the oxide metallic component of the cathode and transferred to the anode, while electrons migrate from the cathode to the anode through the external circuit and the cathodic metal is then oxidized. At the anode, the charging process determines the entrapment of the lithium ion, which reduces to lithium in the graphite matrix by acquiring electrons coming from the external circuit. Specifically, during this phase the following reactions take place:

- At anode side, oxidation:

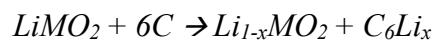


where  $M$  is a generic metal and its choice affects the thermodynamic behaviour of the cell, while  $x$  is the number of sites in which Li-ions can be intercalated in cathode structure.

- At cathode side, reduction:



The total reaction occurring in charging configuration is:



As the circuit is closed, the lithium concentration in the anode structure will vary involving a consequent modification of  $\Delta g_{anode-cathode}$ . In particular,  $\Delta G$  will grow until it reacts the value associated to the full charge state.

The charging process of a lithium ion battery, for a cell composed by a lithium cobalt oxide  $\text{LiCoO}_2$  cathode and an anode in graphite and electrolyte in liquid state, is presented in the following figure:

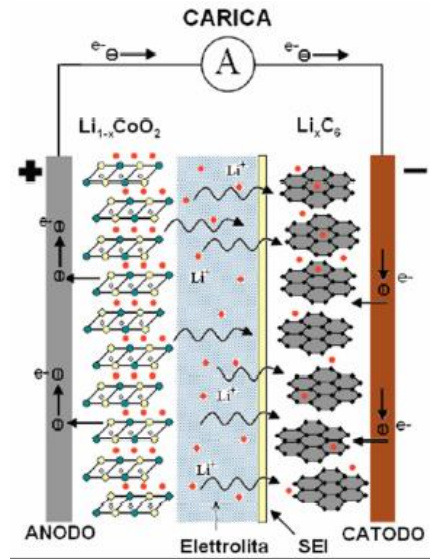
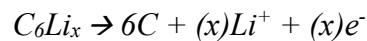


FIGURE 27. LI-ION BATTERY CHARGE CONFIGURATION

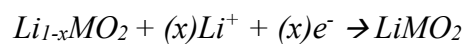
#### 4.3.2 Discharge configuration

Here the functioning is inverted with respect to the discharge configuration. During the discharge, the lithium intercalated in the graphite matrix oxidizes releasing the electrons outside, while Li-ions migrate through the electrolyte to the cathode which reduces. Practically, the following reactions occur:

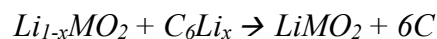
- At anodic side, oxidation:



- At cathodic side, reduction:



The total reaction occurring in charging configuration is:





In a charged battery in open circuit conditions, the lithium atoms intercalated in the anode structure are in equilibrium with the Li-ions in the electrolyte layer. As the circuit get closed, this equilibrium is broken, and Li-ions start travelling from anode to cathode, involving the discharge phase. Lithium atoms are extracted from the anode structure: first atoms near electrolyte layer are extracted: as the discharge goes on, all the atoms are withdrawn until even those furthest away undergo de-intercalation. Contemporary, Li-ions travels across the electrolyte layer and start being intercalated in the cathode structure. The first occupied sites are those neighbours the electrolyte layer and then intercalation goes on until even the furthest sites are occupied.  $\Delta g_{anode-cathode}$  will be modified, and it will decrease until it is no more able to drive battery operation.

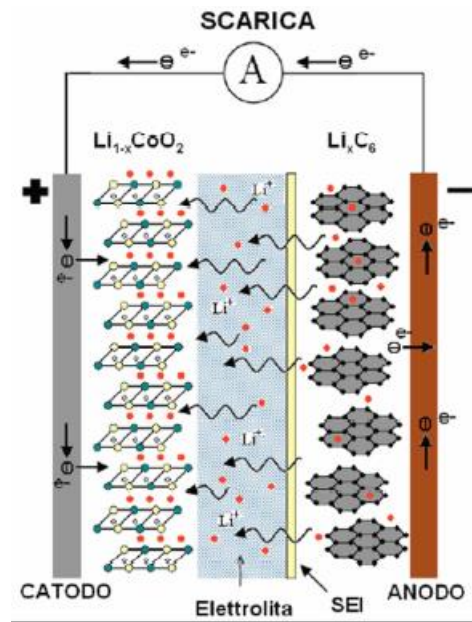


FIGURE 28. LI-ION BATTERY DISCHARGE CONFIGURATION



### 4.3.3 Geometries

#### Cylindrical Cell



FIGURE 29. 18650 CYLINDRICAL CELL

The cylindrical cell constitutes one of the most widely used packaging styles for primary and secondary batteries. The advantages are ease of manufacture and good mechanical stability. The metallic cylinder measure 18mm in diameter and 65mm the length. The larger 26650 cell measures 26mm in diameter. The 18650 remains one of the most popular cell packages.

The battery material domain consists of:

- wound sheets of active cell material (positive electrode, separator, negative electrode in sequence), 65 mm high and radius of 9 mm;
- a mandrel (nylon isolator around which the battery cell sheets are wound, 2 mm radius);
- cylindrical battery connector on top of the battery (steel);
- a tubular cylinder canister to withstand high internal pressures without deforming.

Most cylindrical cells also feature a pressure relief mechanism, and the simplest design utilizes a membrane seal that ruptures under high pressure. The figure below shows a cross section of a cylindrical cell:

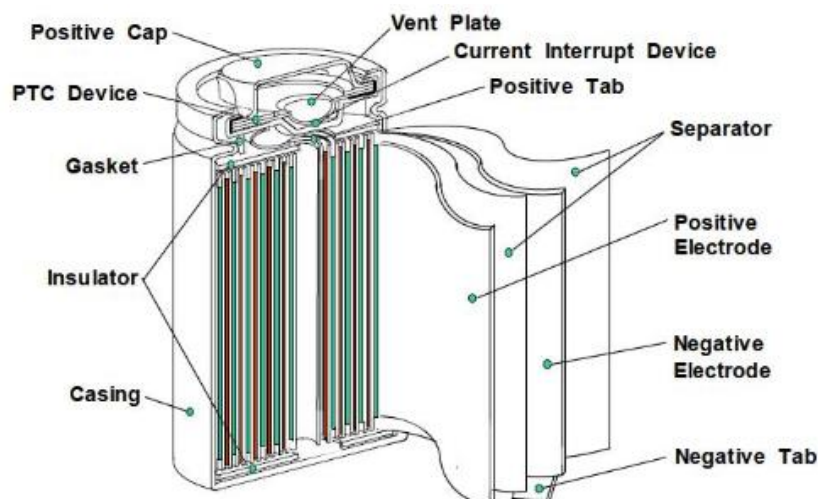


FIGURE 30. INTERNAL STRUCTURE OF CYLINDRICAL CELL [14]

Typical applications for the cylindrical cell are power tools, medical instruments, laptops and e-bikes. To allow variations within a given size, manufacturers use partial cell lengths, such as half and three-quarter formats, and nickel-cadmium provides the largest variety of cell choices.

The 18650 could well be the most optimized cell; it offers one of the lowest *costs per Wh* and has good reliability records. As consumers move to the flat designs in smart phones and tablets, the demand for the 18650 is fading; the Tesla electric vehicles also use this cell format for now. As of end of 2016, the battery industry fears battery shortages to meet the growing demand for electric vehicles.

The demand for the 18650 would have peaked in 2011 had it not been for new demands in military, medical and drones, including the Tesla electric car. The switch to a flat-design in consumer products and larger format for the electric powertrain will eventually saturate the 18650.

There are other cylindrical Li-ion formats with dimensions of 20700, 21700 and 22700. Meanwhile, Tesla, Panasonic and Samsung have decided on the 21700 for easy of manufacturing, optimal capacity and other benefits. While the 18650 has a volume of  $66\text{cm}^3$  with a capacity of around 3000mAh, the  $97\text{cm}^3$  volume of the 21700 is said to produce a capacity of up to 6000mAh, essentially doubling the capacity with a 50% increase in volume. The larger 26650 cell with a diameter of 26mm does not enjoy the same popularity as the 18650. [15]

Even though the cylindrical cell does not fully utilize the space by creating air cavities on side-by-side placement, the 18650 has a higher energy density than a prismatic/pouch Li-ion cell. The 3Ah 18650 delivers 248Ah/kg, whereas a modern pouch cell has about 140Ah/kg. The higher energy density of the cylindrical cell compensates for its less ideal stacking abilities and the empty space can always be used for cooling to improve thermal management.

Cell disintegration cannot always be prevented but propagation can. Cylindrical cells are often spaced apart to stop propagation should one cell take off. Spacing also helps in the thermal management. In addition, a cylindrical design does not change size.

### **Button Cell**

The button cell, also known as coin cell, enabled compact design in portable devices. It is a small single cell battery shaped as a squat cylinder typically 5 to 25 *mm* in diameter and 1 to 6

mm high. A metal can form the bottom body and positive terminal of the cell, while an insulated top cap is the negative terminal. The figure below illustrates the button cells with a cross section.

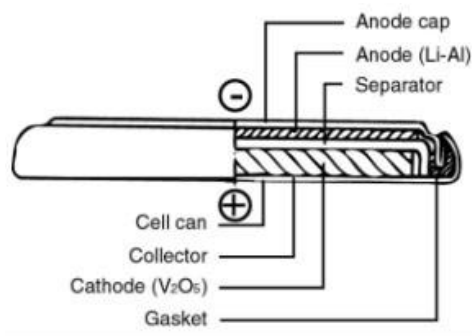


**FIGURE 31. INTERNAL STRUCTURE OF BUTTON CELL**

Higher voltages were achieved by stacking the cells into a tube. Cordless telephones, medical devices and security wands at airports used these batteries.

A drawback of the button cell is swelling if charged too rapidly. Button cells have no safety vent and can only be charged at a 10- to 16-hour charge; however, newer designs claim rapid charge capability.

Cell of different chemical composition made in the same size are mechanically interchangeable. However, the composition can affect service life and voltage stability: using the wrong cell may lead to short life or improper operation. Sometimes, different cells of the same type and size and specified capacity are optimised for different loads by using different electrolytes, so that one may have longer service life than the other if supplying a relatively high current. Common anode materials are zinc (nominal voltage of 1.5V) or lithium (nominal voltage of 3V); common cathode materials are manganese dioxide, silver oxide, carbon monofluoride.



## Prismatic Cell



FIGURE 32. PRISMATIC CELLS [16]

Introduced in the early 1990s, the modern prismatic cell satisfies the demand for thinner sizes. Wrapped in elegant packages, prismatic cells make optimal use of space by using a layered approach, improving space utilization and allowing flexible design. Prismatic cell designs are an excellent way to reduce weight, thanks to an optimal exploitation of space, and cost as well as optimize packaging efficiency at the battery level. The following figure shows the prismatic cell:

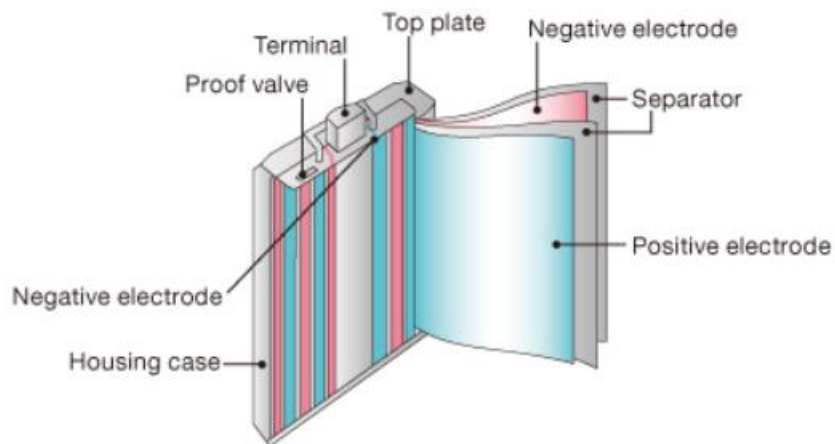


FIGURE 33. INTERNAL STRUCTURE OF PRISMATIC CELL [17]

However, they can be more expensive to manufacture, less efficient in thermal management and have a shorter cycle life than the cylindrical design. These cells are predominantly found

in mobile phones, tablets and low-profile laptops ranging from 800mAh to 4,000mAh. No universal format exists and each manufacturer designs its own.

Prismatic cells are also available in large formats. Packaged in welded aluminum housings, the cells deliver capacities of 20–50Ah and are primarily used for electric powertrains in hybrid and electric vehicles. They are contained in a rectangular can; the electrodes are either stacked or in the form of a flattened spiral. [18]

### **Pouch Cell**

In 1995, the pouch cell surprised the battery world with a radical new design making the best use of space. Rather than using a metallic cylinder and glass-to-metal electrical feed-through for insulation, conductive foil-tabs were welded to the electrodes and sealed to the pouch carry the positive and negative terminals to the outside.



**FIGURE34. POUCH CELL [19]**

The pouch cell makes most efficient use of space and achieves 90–95 percent packaging efficiency, the highest among battery packs. Eliminating the metal enclosure reduces weight, but the cell needs support and allowance to expand in the battery compartment. The pouch packs are used in consumer, military and automotive applications. No standardized pouch cells exist. The pouch cell offers a simple, flexible and lightweight solution to battery design. Exposure to high humidity and hot temperature can shorten service life.

Pouch cells have high energy density suitable for both high- and medium-power ranges, supply up to 9000 full cycles at 100%DoD up to 20 years calendar life (depending on the operating conditions). [20]

Although easily stackable, provision must be made for swelling. While smaller pouch packs can grow 8–10 percent over 500 cycles, large cells may expand to that size in 5,000 cycles. It is best not to stack pouch cells on top of each other but to lay them flat, side by side or allow extra space in between them. Avoid sharp edges that can stress the pouch cells as they expand.

Extreme swelling is a concern. Users of pouch packs have reported up to 3 percent swelling incidents and the pressure created can crack the battery cover. Figure below shows a swollen pouch cell.



FIGURE 35. SWOLLEN POUCH CELL [14]

Technology improved and prismatic and pouch cells have the potential for greater capacity than the cylindrical format. Large flat packs serve electric powertrains and Energy Storage System (ESS) with good results. The cost per kWh in the prismatic/pouch cell is still higher than with the 18650 cell but this is changing.

Summarizing, each format has pros and cons:

- **Cylindrical cell** has high specific energy, good mechanical stability and lends itself to automated manufacturing. Cell design allows added safety features that are not possible with other formats [21]; it cycles well, offers a long calendar life and is low cost, but it has less than ideal packaging density. The cylindrical cell is commonly used for portable applications.
- **Prismatic cell** is encased in aluminium or steel for stability. Jelly-rolled or stacked, the cell is space-efficient but can be costlier to manufacture than the cylindrical cell. Modern prismatic cells are used in the electric powertrain and energy storage systems.
- **Pouch cell** uses laminated architecture in a bag. It is light and cost-effective but exposure to humidity and high temperature can shorten life. Swelling of 8–10 percent over 500 cycles must be considered with some cell designs. Large cells work best with light loading and moderate charge times. The pouch cell is growing in popularity and serves similar applications to the prismatic cell.

#### 4.3.4 Pros&Cons of Li-ion battery

##### Advantages

- Li-ion batteries can be designed in a wide range of shapes and sizes to efficiently fill the available space in the devices in which they are located;
- these batteries are much lighter because lithium has the lowest weight among alkaline metals;
- lithium ions battery has a very high energy density (up to  $500 \left[ \frac{Wh}{l} \right]$ ) and specific energy (up to  $200 \left[ \frac{Wh}{kg} \right]$ ) which makes them important in weight-volume sensitive applications;
- has the greatest electrochemical potential; voltage per single cell between 2.5-4.2V;
- load characteristics are good;
- long lifespan (over 1000 cycles);
- functioning within a wide temperature range;
- high rate capability (until to 5C-rate)
- negligible self-discharge (about 5% in a month);
- Li-ion batteries don't suffer the memory effect

##### Disadvantages

- Elevate costs;
- Li-ion battery presents a progressive degradation even if not used: it has a fixed shelf life from the time of manufacture, regardless of the number of charge/discharge cycles [22];
- a single Li-ion element should never be discharged under a certain voltage to avoid irreversible damages. As a result, all systems using Li-ion elements are equipped with a circuit that turns off the device when the battery is discharged below the threshold [23];
- the chemistry of Li-ion batteries is not totally safe: it can explode if overheated or over-charged as it develops hydrogen inside the casing. For this reason, it requires several mandatory safety systems;
- Li-ion batteries can easily break, catch fire or explode when exposed to high temperatures or direct sunlight. Shorting a Li-ion battery can cause fires and explosions.

### 4.3.5 How to compose a battery pack

A Li-ion battery pack consists of various components: the elementary cells, a container, an electronic supervision and control systems called BMS (Battery Management Systems), fuses, terminals and connection cables, a cooling system, a data communication system.



**FIGURE 35. COMPONENTS OF A BATTERY PACK [24]**

*Connection cables:* made of copper, can be flexible cables or rigid plates. They connect all the cells;

*Signal cables:* used to carry voltage, current and temperature measurement from each cell to the BMS;

*Main and secondary modules of the BMS:* they are the electronics of the package. They check

the security, the knowledge of the residual charge, the performance optimization;

*Traction current cables:* large copper cables. They bring the current from the battery to the electric drive (inverter and motor);

*Vehicle communication interface:* information coming from the battery are entered in the vehicle CAN communication system. The typical information sent are the amount of charge available, expected autonomy, temperature, various alarms;

*Current meter:* instrument for the measurements and control of the supply of current:

*Insulation meter:* instrument checking electrical safety;

*Main relay:* it is an automatic and safety switch; it separates the battery from the rest of the vehicle [24].

Linking the elements properly, suitable battery packages can be built for a wide range of applications, from low power and low capacity up to high power and high capacity for electric and hybrid vehicles.

Connecting the elements in series (+ with -), voltage is increased: the total is the sum of the voltages of each element. Connecting the elements (+ with +, - with -) the resulting capacity is the sum of the capacities of each element.



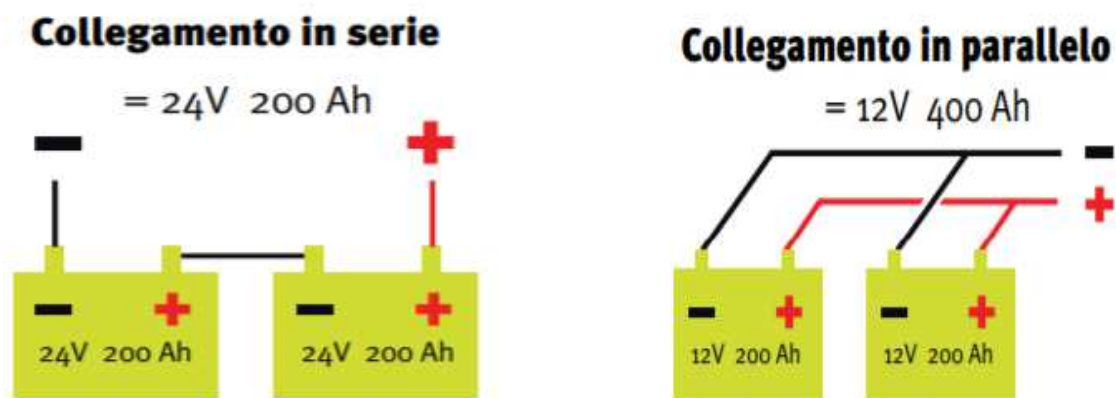


FIGURE 36. (LEFT) SERIES CONNECTION. (RIGHT) PARALLEL CONNECTION [24]

## 5. Thermal issues and BTMS

Many thermal fluxes are exchanged during charge/discharge cell processes. More precisely, these heat fluxes are the “collateral effect” of the occurrence of the reaction itself and over-voltages: charge transfer, charge conduction and mass transport will generate heat and, contemporarily, the effect of reaction thermodynamics will generate an exothermic or endothermic heat flux (depending on the working regime of the cell).

### 5.1 Thermal fluxes management

In *galvanic cells* ( $\Delta g_{reaction} < 0$  and so  $\Delta s < 0$ ) there are only heat generating phenomena. Therefore, it will always be characterized by an exothermic behaviour:

$$|\Phi_{th}| = |\Phi_{react}| + |\Phi_{irr}|$$

$\Phi_{react}$  is the amount of heat coming from the reaction; exploiting the Faraday law, it is equal to the product of  $q_{react} = T * \Delta s_{react} \left[ \frac{J}{mol} \right]$  and the molar flow rate of the specie reacting  $N_R = \frac{I}{z_R * F}$ :

$$|\Phi_{react}| = - \frac{I}{z_R * F} * T * \Delta s_{react} [W] \text{ with } \Phi_{react} < 0 \text{ (exothermic)}$$

$\Phi_{irr} < 0$  is the heat produced by transport phenomena; it is equal to:

$$|\Phi_{irr}| = I * \sum n_j$$

where  $n_j$  are the overpotentials that may take place in the cell. Combining these two equations,  $\Phi_{th}$  final expression can be obtained:

$$|\Phi_{th}| = \left( - \frac{\Delta h_{react}}{z_R * F} - V_c \right) * I$$

Definitively, the quantity  $\left( - \frac{\Delta h_{react}}{z_R * F} - V_c \right)$  constitutes the losses that convert the chemical energy into thermal energy rather than electrical one; these losses are due to irreversibilities

generation during the occurrence of the reaction and to irreversibilities which take place because of transport phenomena. The produced thermal power increase more than linearly with  $I$ , because at larger value of the current cell voltage is larger too.

In case of *electrolytic cells* ( $\Delta g_{reaction} > 0$  and so  $\Delta s > 0$ ) there will be absorption of a heat flux  $T * \Delta s_{react}$ . This cell can work with an endothermic or exothermic behaviour depending on the entity of the thermal fluxes. If  $|\Phi_{react}| < |\Phi_{irr}|$  it will be an exothermic behaviour, otherwise endothermic.

$$|\Phi_{th}| = |\Phi_{react}| - |\Phi_{irr}|$$

The heat flux produced by thermodynamic irreversibilities is:

$$|\Phi_{react}| = \frac{T * \Delta s_{react}}{z_R * F}, \Phi_{react} > 0 \text{ because } \Delta s_{react} > 0$$

Heat flux due to transport phenomena irreversibilities is the same of galvanic cells:

$$|\Phi_{irr}| = I * \Sigma n_j$$

By putting together both these equations:

$$\Phi_{th} = \left( \frac{\Delta h_{react}}{z_R * F} - V_c \right) * I$$

- if  $\frac{\Delta h_{react}}{z_R * F} > V_c \rightarrow \Phi_{th} > 0 \rightarrow$  endothermic behaviour, reaction needs heat to be supplied;
- if  $\frac{\Delta h_{react}}{z_R * F} = V_c \rightarrow \Phi_{th} = 0 \rightarrow$  thermoneutral voltage of the cell (thermoneutral behaviour);
- if  $\frac{\Delta h_{react}}{z_R * F} < V_c \rightarrow \Phi_{th} < 0 \rightarrow$  exothermic behaviour (reaction needs heat to be removed).

## 5.2 Optimal operating conditions

Battery performances are strictly dependent on the functioning temperatures of the module and on the temperature distribution not only within the entire module but also in each single cell composing the module itself. So, temperatures greatly affect not only performances, but also lifespan of the batteries and a thermal control must be used to guarantee uniform temperature of the pack, an optimal duration of it and to enhance lifecycle cost and safety. Indeed, when thermal runaway occurs, at the electrodes and electrolyte exothermic decomposition reaction lead to increase cell temperature causing serious damages and lifetime reduction of the whole system [25].

As seen in the previous chapters, various chemical and electrochemical reactions take place during charge/discharge phases; especially, at high C-rates it could be generated more heat than normal case. The generated heat depends on the structure of the cell, state of charge/discharge profile, chemistry, etc. and increasing the size of the battery pack and, consequently, the number of cells could cause several imbalance problems [26]. Either low ( $<15^{\circ}\text{C}$ ) or high temperature ( $>50^{\circ}\text{C}$ ) will progressively reduce the cycle life. Pesaran pointed out that batteries have a relatively large range of optimal operability generally between  $15^{\circ}\text{C} - 40^{\circ}\text{C}$  [27] and the temperature difference should be maximum  $5^{\circ}\text{C}$  between to modules [28] so that to have small changes in order to achieve a proper balance between performance and lifetime. In the following figure, it is seen that the power of a Li-ion battery reaches the worst value at high and low temperatures and, in addition, the peak is reached in the range of  $20^{\circ}\text{C} - 40^{\circ}\text{C}$  [29]:

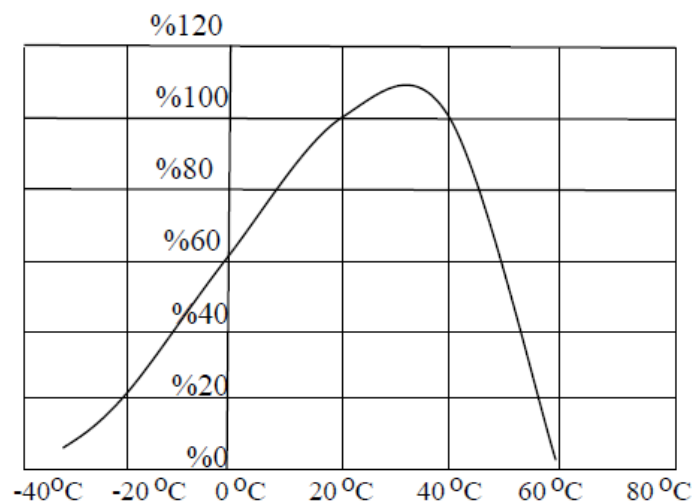


FIGURE 37. LI-ION BATTERY POWER VS TEMPERATURE

Ladrech also provided a temperature band for lithium-ion batteries dividing it into 4 sections namely decline of battery capacity and pulse performance ( $0 - 10^{\circ}\text{C}$ ), optimal range ( $20-30^{\circ}\text{C}$ ), faster self-discharge ( $30-40^{\circ}\text{C}$ ) and irreversible reactions and short-circuit ( $40-60^{\circ}\text{C}$ ) [30]. According to Sato, charging efficiency and life cycle can be dramatically reduced above a temperature of  $50^{\circ}\text{C}$  [31]; Khateeb showed that thermal runaway of the Li-ion cells starts at the temperature range  $70 - 100^{\circ}\text{C}$  compromising battery safety [32]. Definitely, putting together all these studies, the working temperature for lithium ion batteries should be kept below  $40^{\circ}\text{C}$  and above  $15^{\circ}\text{C}$ .

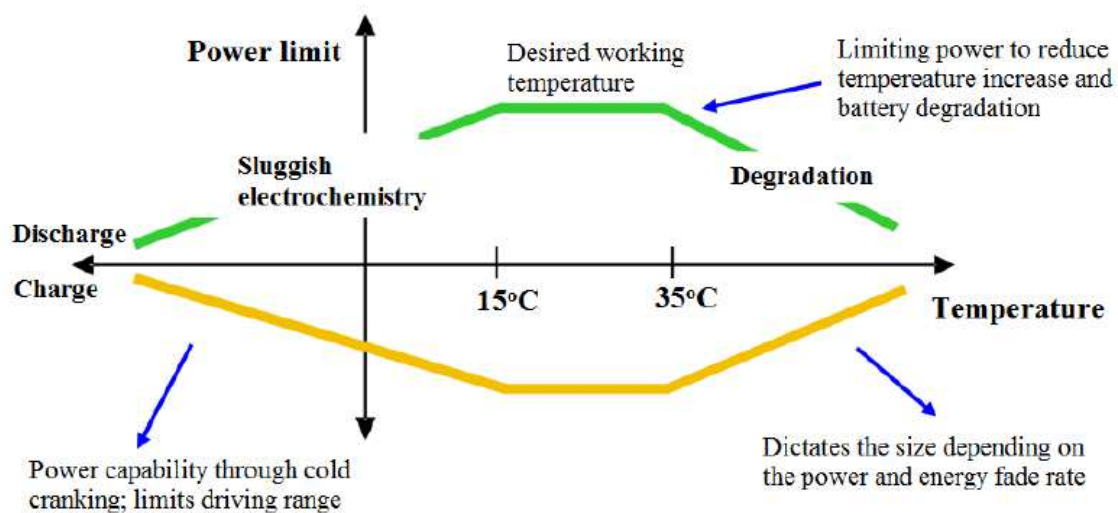


FIGURE 38. POWER LIMITS VS BATTERY TEMPERATURE

Temperature affects batteries in 5 important ways [33]:

- it can disrupt electrochemical operation principle;
- it extends efficient charging and depending on this, extend charging time;
- it reduces energy efficiency;
- it puts at risk safety and reliability;
- it shortens lifespan and require maintenance [33]

Two main problems are linked to the temperature values: charge and discharge phases are characterized by an increasing of the temperature level beyond allowable limits and uneven temperature distribution among cells and modules attributes to a localised deterioration [34]. Moreover, environmental condition is a parameter mainly affecting good battery performances:

most scientific studies have found that functioning and energy storage are significantly reduced at temperatures as low as  $-10^{\circ}\text{C}$ , other studies, it was noted that li-ion batteries are very performant and highly efficient in energy storage but their performance is noticeably reduced at  $-30^{\circ}\text{C}$  [35]. In that case, battery needs to be heated up quickly.

### 5.3 Battery Thermal Management System (BTMS)

Battery thermal management is critical in achieving performance and extended life of batteries in electric and hybrid vehicles under real driving conditions. [36] Thus, BTMS plays a fundamental role handling different functions according with external ambient temperature and operating modes. Designing a battery thermal management system for a given application means to answer a series of important questions such as: “What are the permissible working temperatures?”, “How much heat must be removed from a cell and how quickly?”, “What kind of transfer fluid is necessary?”, “What about costs?”. Then, it is necessary to know how much thermal power is generated during processes in order to understand the behaviour of the system and, as a consequence, to find an efficient and cost-effective cooling system studying specific controllable parameters.

Generally, BTMS is composed by cooling, heating and insulation components with the following purposes:

- Cooling is required during charge/discharge since heat is generated because of the Joule effect due to the internal resistance of battery;
- Heating is useful to extend low-temperature operability in severe environment or after cold start-up when batteries must be heated quickly;
- Insulation is suggested in summertime and in winter also to prevent discharge capacity fade [37]

Moreover, a BTMS is also responsible of safety because it has to safeguard against explosion, fire and the corrosive nature of electrolyte [38]; for this reason, BTMS comprise protective equipment against electrical hazards like short-circuit, protective measures and specific components to fight electrolyte leakage and thermal runaway. Finally, the BTMS has to regulate the electrical distribution and prevents from over/under voltage, excessive currents and elevated temperatures [39].

A battery thermal management system should satisfy a series of requirement for a good functioning of the system. The desired attributes can be listed as follows:

- Average temperatures of each cell composing the module have to be minimized in order to keep battery within the optimal range.
- Temperature changes should be minimized in each cell.
- Heat has to be removed quickly and efficiently.
- The battery pack should have as little load as possible.
- If temperature management requires the use of refrigerant, leak proofing must be provided [40].
- The materials to be used in the thermal management system must be electrically isolated [41].
- The thermal management system should be easy to set up and the service cost should be cheap [40].

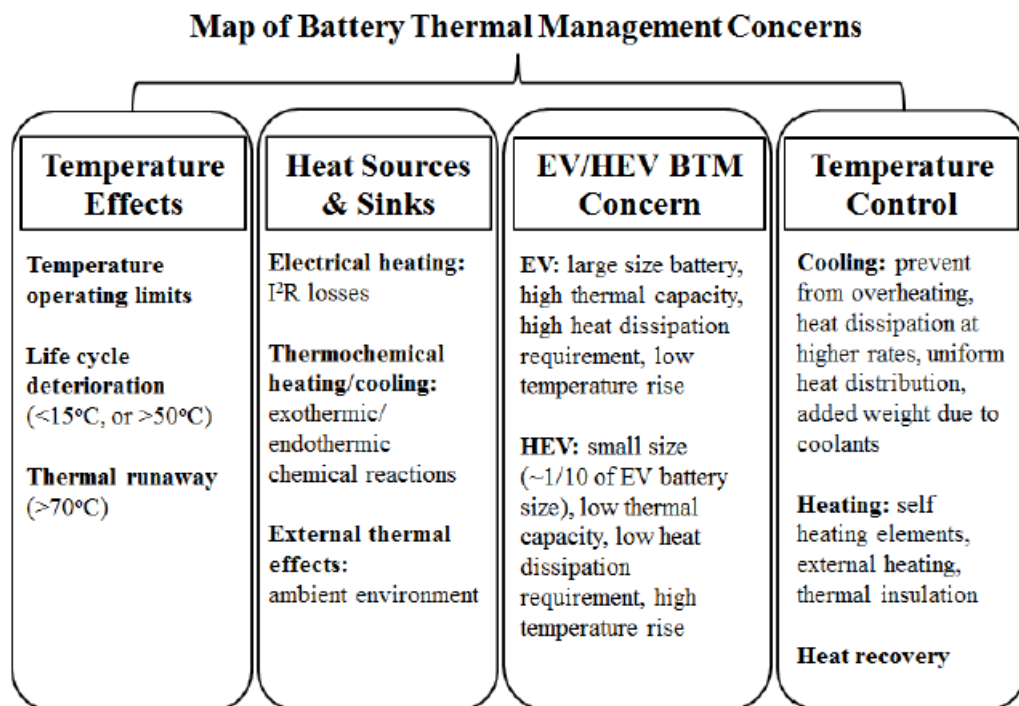


FIGURE 39. MAP OF BATTERY THERMAL MANAGEMENT CONCERNS

## 5.4 Types of cooling systems

A first distinction categorises a BTMS into *passive*, in which there is no ventilation and only the ambient environment (to which heat is released) is exploited, *active*, characterised to have a built-in source that provides heating and/or cooling (through an active ventilation), and *based on medium*. The choice of an adequate cooling system is taken to suit the specific application criteria under consideration, which include: being lightweight, easily packaged in the desired application, being compact, reliable, easy to assembly and placed in an appropriate position [42]. A traditional BTMS includes air as the medium, with an electric blower or fan to move it; on the other hand, liquid BTMS includes water, glycol, oil, acetone, refrigerants and PCM (Phase Change Material) thermal management systems [43]. The following table shows a comparison among air, liquid and refrigerant cooling systems:

Cooling Scheme	Description	Application	Nominal Temperature Difference Allowed Between the Cells
Air	<ul style="list-style-type: none"> <li>-Both cooling and heating is feasible;</li> <li>-Good performance;</li> <li>-Normally large space needed;</li> <li>-Cheapest;</li> <li>-Lower development effort is needed.</li> </ul>	Application is limited but in most cases sufficient for HEV/48V/12V applications	Temperature difference between air and cells can be > than 15 °C limitation
Liquid	<ul style="list-style-type: none"> <li>-Lowest temperature gradients;</li> <li>-Cooling and heating is feasible;</li> <li>-Best performance.</li> </ul>	Liquid cooling can be found in EV, PHEV, HEV, 48V batteries	Cooling plate 1–3 °C
Refrigerant	-“Aggressive” cooling due to very low cooler temperatures. Intelligent thermal management and specific pack design needed to avoid a too-aggressive cooling and condensation of humidity.	HEV, 48V batteries	Cooling plate 3–8 °C

FIGURE 40. COMPARISON BETWEEN COOLANTS

Then, a second classification is based on the fluid/material used:

- 1) Air for cooling/heating;
- 2) Liquid for cooling/heating;
- 3) PCM;
- 4) Heat pipe for cooling/heating;
- 5) Combinations of the previous ones;



### 5.4.1 Air cooling/heating

Air cooling and heating is widely used as thermal management system; either natural or forced air convection can be used for air BTMS. The air can be introduced into the system from the outside or from the vehicle cabin. The simplest strategy is passive air system, even if various research demonstrated that both active and passive air-based thermal management are not so effective in high-energy density and large-scale battery [44], while Pesaran et al. [45] claimed that passive air cooling is possible for batteries of low energy density, but for batteries of high energy density (such as Li-ion batteries) an active air system is required. The risk would be a large thermal gradient between internal cell and the battery pack boundary, resulting in an unequal charge or discharge capacity of the battery cell. Increasing the heat transfer coefficient of the surrounding air by forced air cooling is fundamental, in spite of design complexity and additional power requirements [46].

The next figure shows air cooling processes including passive air cooling, passive cooling heating and active air cooling/heating:

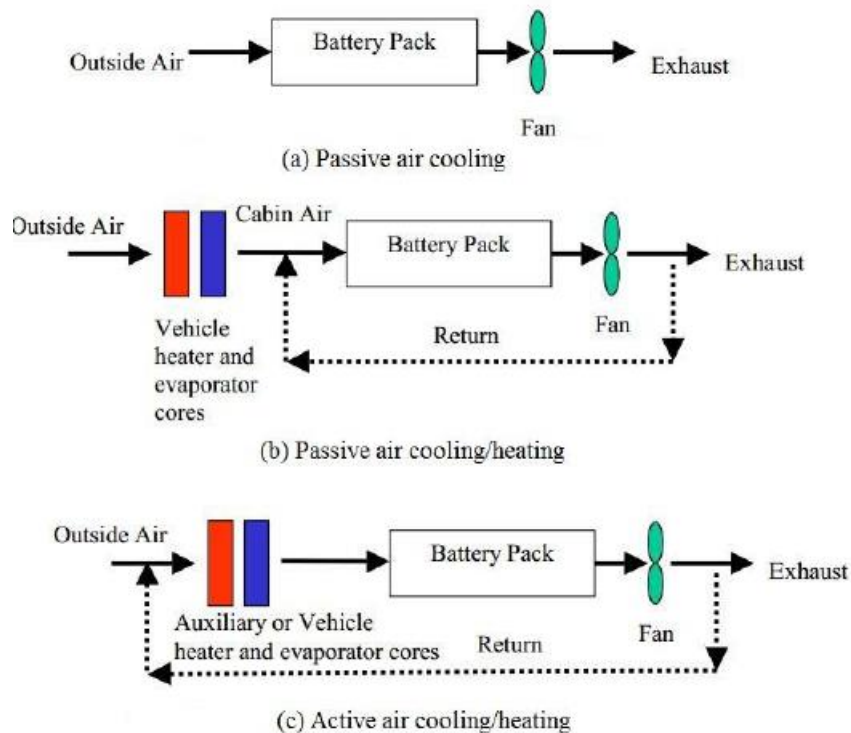


FIGURE 41. PASSIVE AND ACTIVE AIR COOLING SYSTEMS

Concerning an active air BTM, either taking the air directly from vehicle cabin or using the treated air from a secondary loop consume relatively large space for air ducts, blower adding a significant weight to the whole system [47].

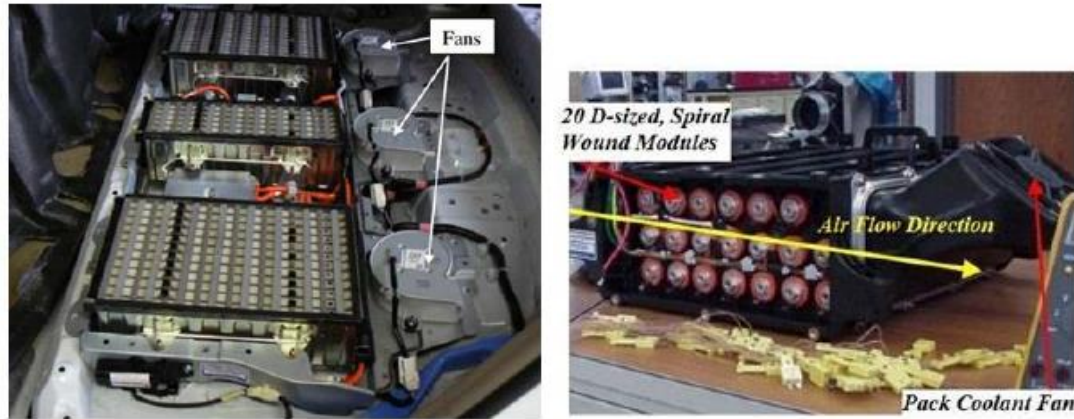


FIGURE 42. AIR COOLING BATTERY PACK ASSEMBLING

Concluding, the simplicity of an air battery cooling system is an advantage over a liquid coolant system, but, in addition to lower heat transfer coefficient, the disadvantage of using air is that the small heat capacity makes it difficult to accomplish temperature uniformity between cells in a module.

### 5.4.2 Liquid cooling/heating

In opposition to air, liquid has higher thermal conductivity and heat capacity; as consequence, more uniform temperature distribution among cells is achieved. On the other hand, liquid cooling systems have a more complex design. Two groups of fluids are used in fluid temperature management [48]: non-electrically conductive fluids directly in contact with the battery (ex. Mineral oils or silicon-based) and electrically conductive ones, coming into indirect contact with the battery thanks to the mixture of ethylene glycol or water. When in direct contact, battery module is immersed in the liquid, while indirect heating or cooling can be carried out through a pipe system around each module. In other studies, temperature stabilization was provided by flow of liquid across small channels in plates placed among cells [49].

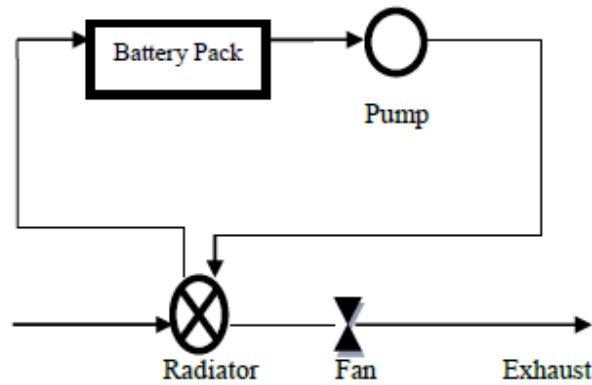


FIGURE 43. PASSIVE LIQUID BTMS [48]

The indirect contact thermal management is more preferred because it ensures a better isolation with environment of the battery module and better safety conditions. In passive systems, the vehicle radiator acts like a cooling fin device: while the fluid is running, the heat which takes from the battery pack removes from the radiator to outside.

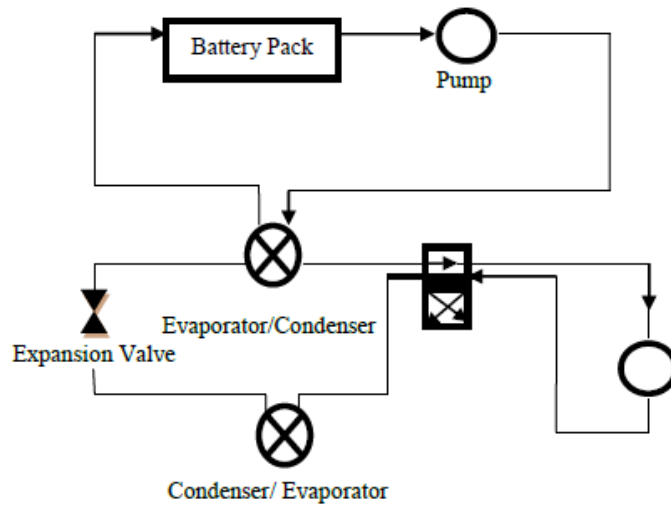
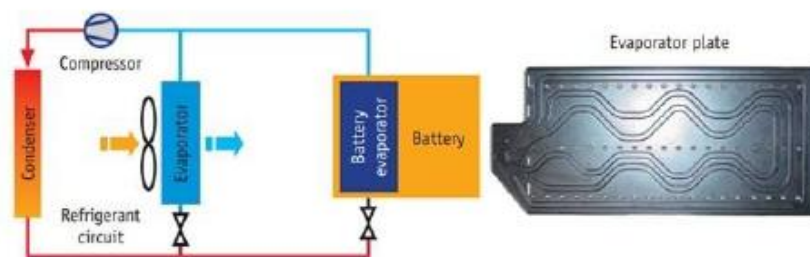


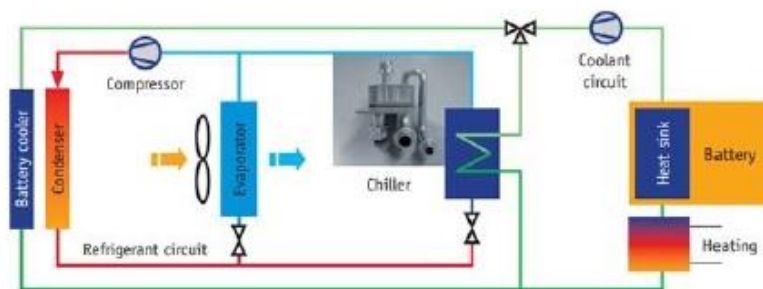
FIGURE 44. ACTIVE LIQUID BTMS [48]

In active thermal management system with liquid there are 2 cycles: the first is warming/cooling the battery, the second one is the cycle of the car's air conditioning system [50].

Liquid BTMS can be divided by the transfer medium: refrigerants or coolants (e.g. water, glycol, oil, acetone). With respect to air, using oil achieved the heat transfer coefficient 1.5 to 3 times and water or water/glycol mixture more than 3 times [51].



(a) Direct refrigerant-based cooling



(b) Secondary circuit with chiller and heat sink in battery

FIGURE 45. REFRIGERANT BASED BTMS

### 5.4.3 Phase Change Material (PCM)

The main feature of a Phase Change Material (PCM) is to store/release a large quantity of heat during its phase transition occurring at “almost-constant” temperature. More precisely, when this kind of material absorbs thermal energy (called latent heat of fusion), its state of aggregation modifies due to the breakdown of intermolecular and molecular bonds. In many applications, the most exploited phase transition is solid-liquid and liquid-solid, since this thermodynamic process doesn't cause considerable volume increases like a liquid-vapour transition, even if the storable energy is certainly lower.

The thermal capacity supplied by traditional materials derives only from the specific heat and it is proportional to the element mass; on the other hand, in PCMs sensible heat is added to the thermal capacity given by the latent heat of fusion. When the temperature is lower than the melting point, PCM absorbs heat as sensible heat with a temperature rise; if the temperature rises up to the melting point, heat is absorbed and stored as latent heat. Then, PCM becomes liquid and heat is absorbed as sensible one.

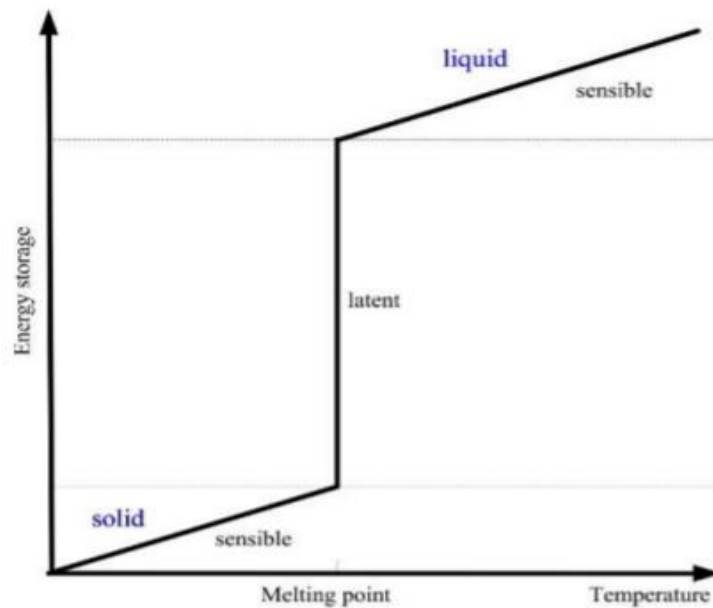


FIGURE 45. RELATION BETWEEN PCM ENERGY STORAGE AND TEMPERATURE

Phase transition begins as the temperature rises to the melting point: during phase transition, which requires a high amount of energy, the material is kept at a temperature close to the melting point. In the solidification, the inverse process takes place, with the release of the thermal energy and the transition to the solid state. Each type of PCM is characterized by a melting temperature and a latent melting heat value.

The following figure shows the working mechanism of PCM on battery cells:

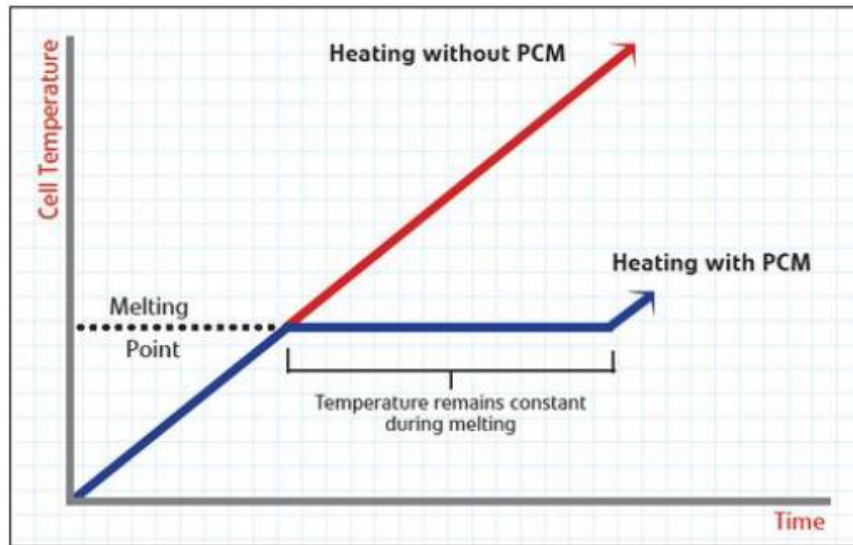


FIGURE 46. CELL TEMPERATURE WITH AND WITHOUT PCM

Rhao et al. [52] pointed out that melting point is the main criteria to select the proper PCM for battery thermal management systems: this value should be chosen in relation to the optimal range of cells working temperature. They stated that it is preferable have a PCM with melting temperature below 45°C to reach a desirable heat dissipation and efficient temperature uniformity across the entire battery unit. Other parameters of critical interest are: high latent heat and specific heat, small volume during phase transition, not being irregular, toxic and flammable, being lost costly while it is in high quantities [53]. Usually, to improve the thermomechanical properties of devices that exploit PCM, it is inserted into metal grids (such as aluminium) because such materials have a poor thermal conductivity (i.e. paraffin wax has  $0.25 \left[ \frac{W}{mK} \right]$ ). For this reason, to solve the conflict between high heat storage capacity and low thermal conductivity, a series of expedients towards making composite PCMs have been conducted:

- Embedding a metal matrix (such as graphite) into PCM;
- Impregnating porous materials [54]
- Adding high thermal conductivity substances in paraffin [55]
- Developing systems with finned structures [56]

However, the thermal conductivity increases correspond to lower heat capacity values and a proper ratio between the two parameters should be considered in order to achieve good

performances. Moreover, if the PCM completely melts, it creates additional thermal resistance provoking a further increase of the pack temperature and a higher risk of thermal runaway. Here, there is an illustration of the assembly of cylindrical Li-ion cells in PCM enhanced battery pack:

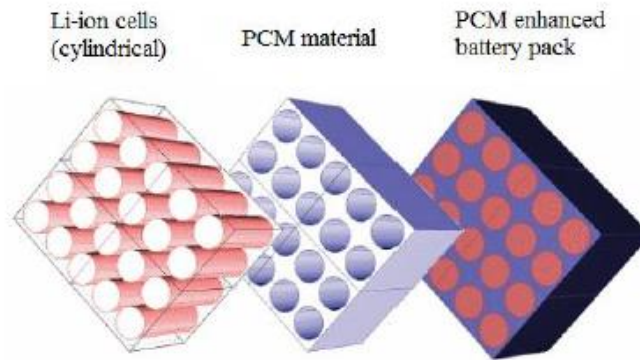


**FIGURE 47. PCM-CELLS ARRANGEMENT**

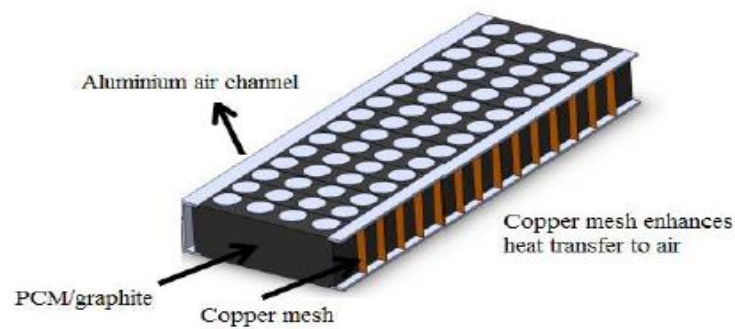


**FIGURE 48. PCM-AIR CHANNELS COUPLING**

Finally, a further important aspect to consider in PCM applications is the type of container system used to not disperse such materials. The need to guarantee watertight and avoid spills or to avoid air comes into contact with the PCM is not to be underestimated. In fact, the phase transition and the presence of liquid material in some moments involve the need for a packaging system that does not allow material dispersion. This problem is solved through the use of different technologies such as the encapsulation in spheres, the use of containers of different shapes and dimensions and the insertion into matrices of solid materials [57]. A summary table of advantages and drawback of PCM use for a battery thermal management system is shown below:



<i>type of system</i>	<i>Medium</i>	<i>System Configuration</i>	<i>Advantages</i>	<i>Disadvantages</i>
PCM	<ul style="list-style-type: none"> <li>• Paraffin Wax;</li> <li>• PCM/Aluminium foam;</li> <li>• PCM/Graphite foam</li> <li>• PCM/Copper metal foam</li> </ul>	DIRECT: cell are hosted into a PCM matrix that exchanges heat with the surface of the battery pack exposed to external environment;	<ul style="list-style-type: none"> <li>• Lightweight and flexible material;</li> <li>• High capacity to accept/release great amount of heat;</li> <li>• Allow heating and cooling;</li> <li>• Smooth external temperature variations because of its large thermal inertia;</li> </ul>	<ul style="list-style-type: none"> <li>• Increase risk of thermal runaway if PCM totally melts;</li> <li>• Not useful in cold start-up pre-heating;</li> <li>• Not uniform melting, especially in high charge/discharge cycles;</li> <li>• Leak-proof battery case is mandatory;</li> <li>• Additional volume between cells is required because of PCM volume expansion is not negligible.</li> </ul>

FIGURE 49. PROS&CONS OF PCM

#### 5.4.4 Heat Pipe

They are considered versatile and efficient passive thermal management systems in many industrial applications and especially in electronic cooling systems [58]. Heat pipe operating principle is similar to PCM, allowing heating and/or cooling with low power consumption. In fact, the fluid inside undergoes a phase change: the heat can be transferred through latent heat of vaporisation from evaporator to the condenser, whereas the working fluid can be passively transported back to the evaporator section by capillary pressure developed within a porous wick [59].

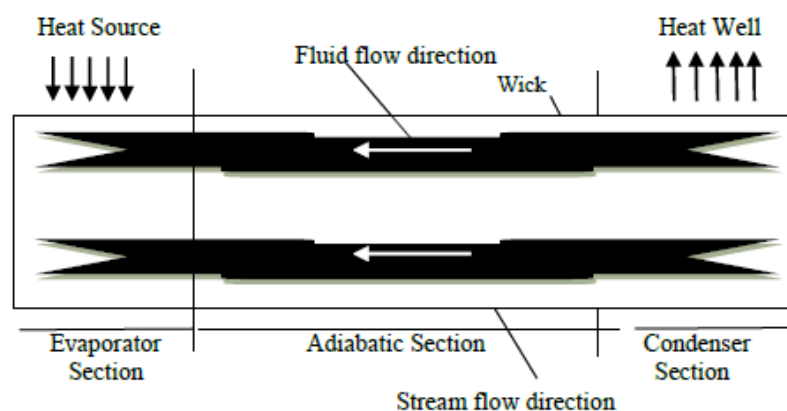


FIGURE 50. HEAT PIPE MECHANISM



The combination of heat pipe and air cooling was adopted in early studies; Tran et al. [60] offered a flat heat pipe for cooling HEV Li-ion batteries with natural and forced convection:

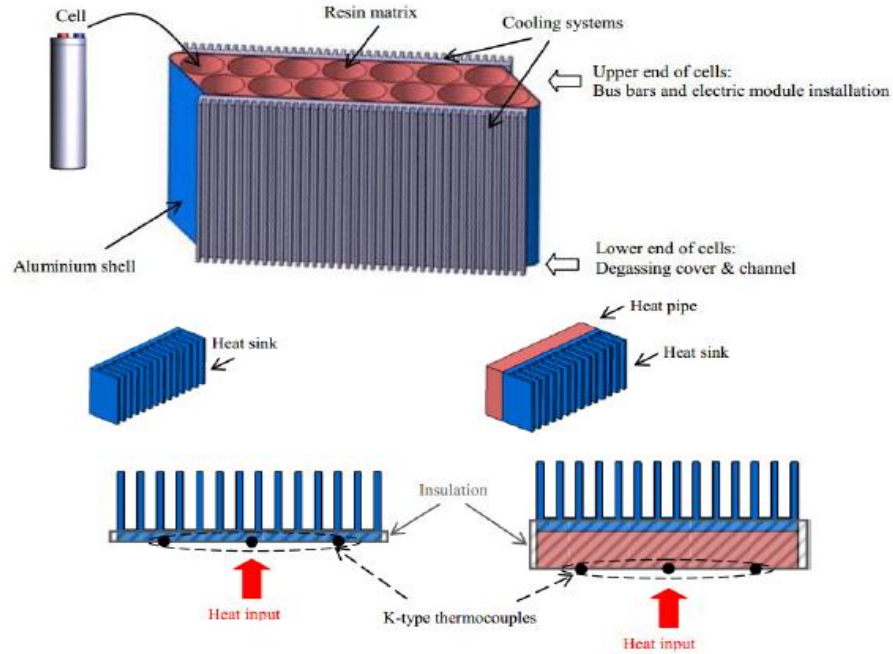


FIGURE 51. COMBINATION OF HEAT PIPE AND AIR COOLING

On the contrary, the use of heat pipe coupled to liquid cooling is scarce: even if this system seems to present the potential of handling increased heat flux efficiently, factors like costs, weight, material compatibility, transient behaviour under high frequency input power etc. should be examined. However, heat pipe is still under development.

#### 5.4.5 Heat pipe assisted PCM

Combinations of PCM and heat pipe could represent very performant battery thermal management systems. Coupling a phase change material with air/liquid heat pipe ensures excellent heat transport effect and an optimal temperature balance for battery module under higher C-rates. Figures below show the schematic production process of battery module (45), a PCM/HP-Air cooling system (in which air passes through the capillary tube to increase heat dissipation coming from the phase change material, and a PCM/HP-Liquid cooling system with the evaporation section (in contact with PCM) and the condensation section (exposed to the air) (46a and 46b) [61].



## 6. Case Study

After a large and exhaustive premise regarding HEVs and Li-ions batteries functioning, their main characteristics and optimal working conditions, a time-dependent analysis and a subsequent optimization have been executed in order to study the thermal behaviour of a Li-ion battery pack model applied on a specific hybrid railway. First of all, a description of the locomotive technology features is made, focusing not only on the overall operation and layout but also on its onboard ESS coupled with diesel engine; then, a portion of the battery pack module composed by prismatic cells coupled with a specific cooling system has been tested under specific operations using ‘COMSOL Multiphysics’, simulating a discharge process to obtain the temperature trend; finally, the effects of using different liquids for that particular cooling system have been studied, varying control parameters in order to reach the optimal thermal range of working.

### 6.1 Hybrid railway description

A prismatic cells Li-ion battery pack has been installed in an existing Diesel Multiple Unit (DMU) railway vehicle, developed by *Blue-Group Engineering and Design*, and then modified through the replacement of one DMU with an ESS in the thesis work of my colleague *Giuseppe Boccardo*. More specifically, he started by a configuration of 4 DMUs to realize a hybrid system substituting one of the diesel units with a Li-ion battery that will recover braking energy, thanks to a regenerative braking strategy, otherwise wasted in form of heat. Here, there is a scheme of the hybridization process studied on the Blue-Group existing train:

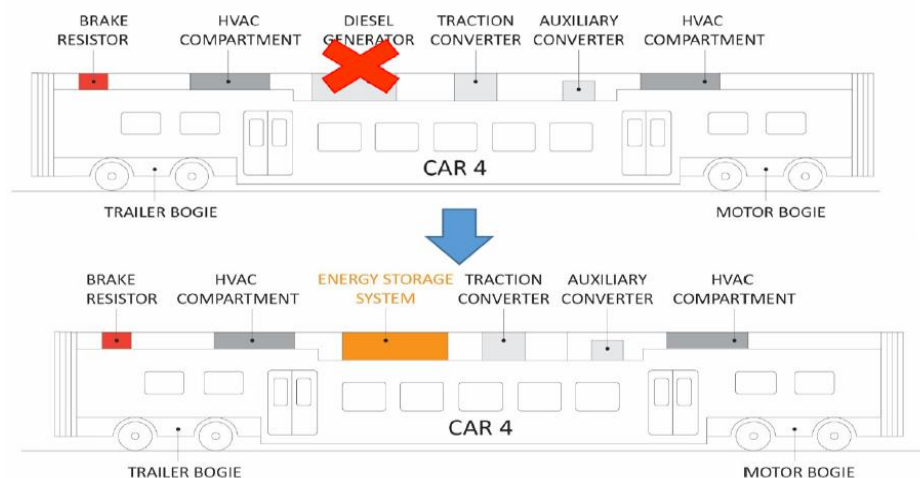
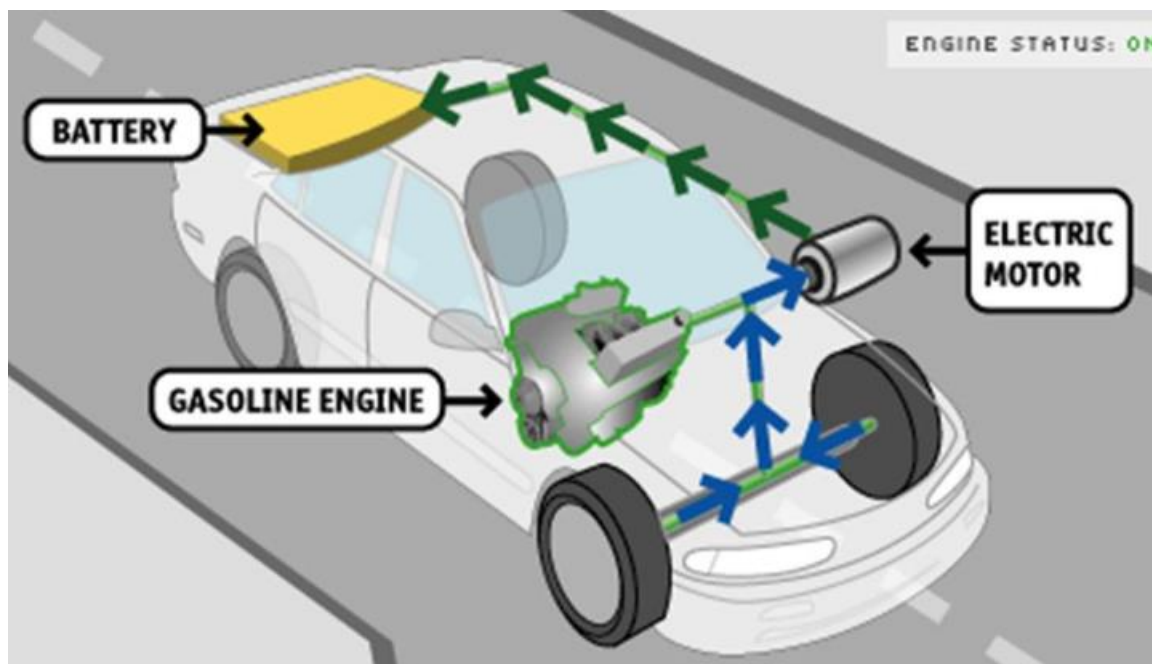


FIGURE 54. HYBRIDIZATION OF THE RAILWAY

Regenerative braking is an energy recovery mechanism which slows a vehicle or object by converting its kinetic energy into a form which can be either used immediately or stored. The most common form of regenerative brake involves an electric motor as a generator; in hybrid electric vehicles, the energy is stored chemically in a battery. Electric motors, when used in reverse function as generators, convert mechanical energy into electrical one, so vehicles propelled also by electric motors use them as generators when using regenerative braking. In dynamic braking systems, traction converter regulates voltage and frequency of the power supply system according to with the tractive/braking effort required, even if they cannot totally replace mechanical braking, especially in high-speed trains [62].



**FIGURE 55. REGENERATIVE BRAKING CONCEPT**

The inception of the onboard battery allows the railway to store energy recovered and, consequently, to save a significant amount of energy reducing the overall vehicle consumption. Moreover, battery permits to operate in a wider range of tracks reaching underground sections and non-electrified urban stations, resulting in lower pollutant emissions in demographic areas.

Thanks to Giuseppe's work, data regarding railway requirements that will be used in this thesis to size the battery pack are shown below:

<b>INPUT DATA</b>		
<i>Total energy demand [kWh]</i>	<u>196</u>	Including auxiliary equipment
<i>Maximum Tractive Power [kW]</i>	1614	Electrical power
<i>Maximum ED Braking Power [kW]</i>	1584	Electrical power
<i>Desired Voltage [V]</i>	<u>950</u>	
<i>Minimum Voltage [V]</i>	850	
<i>Diesel Generator Power [kW]</i>	560	One diesel-generator each car

In particular, the sizing will be estimated satisfying the total energy and voltage requested from the entire system to tow the railway itself. A 18650 cylindrical unit cell constituted by graphite ( $\text{Li}_x\text{C}_6$ ) anode,  $\text{LiPF}_6$  in 1:1 EC:DEC (Ethylene carbonate/Diethylene carbonate) liquid electrolyte and Lithium Nickel Manganese Cobalt Oxide in  $\text{LiNi}_{1/3}\text{Mn}_{1/3}\text{Co}_{1/3}\text{O}_2$  (NMC) cathode has been chosen for the study, thanks to experimental data provided by the co-relator *Arpit Maheswari* reported below:

<b>UNIT CELL</b>		
<i>Voltage [V] <math>V_{cell}</math></i>	3.7	Nominal voltage unit cell
<i>Capacity [Ah] <math>Q_{cell}</math></i>	2.1	Nominal capacity unit cell

It is necessary to clarify that my study will be carried out on prismatic geometry cells instead of cylindrical one, assuming that the other characteristics will remain unchanged, in particular anode-separator-cathode materials and thicknesses (80,25,65 [ $\mu\text{m}$ ] respectively).

In general, knowing that:

$$\text{Energy} = V * Q \quad [\text{Wh}]$$

where  $V$  is the voltage and  $Q$  the capacity, a single battery module has been supposed to have  $N_{series\_cells} = 12$  and  $N_{parallel\_cells} = 10$ . Then, the voltage of a single module will be:

$$V_{single\_module} = N_{series\_cells} * V_{cell} = 12 * 3.7 [\text{V}] = 44 [\text{V}]$$

and, consequently, the number of modules arranged in series will result:

$$N_{series\_modules} = \frac{V_{requested}}{V_{single\_module}} = \frac{950 [V]}{44 [V]} = 22$$

Now, regarding the estimation of the parallel modules number  $N_{parallel\_modules}$ , battery pack capacity has been oversized because Li-ion batteries suffer deep charge/discharge cycles; for this reason, a DOD (depth of discharge) equal to 80% has been considered:

$$E_{battery\_pack} = \frac{E_{requested}}{DOD} = \frac{196}{80\%} [kWh] = 245 [kWh]$$

And finally:

$$E_{battery\_pack} = V_{requested} * Q_{cell} * N_{parallel\_cells} * N_{parallel\_modules}$$

$$N_{parallel\_modules} = \frac{E_{battery\_pack}}{V_{requested} * Q_{cell} * N_{parallel\_cells}} = \frac{245}{950 * 2.1 * 10} = 13$$

Summarizing, the final battery pack configuration taking into account assumptions mentioned above has resulted:

<b>MODULE</b>	
$N_{series\_cells}$	12
$N_{parallel\_cells}$	10
<b>PACK</b>	
$N_{series\_modules}$	22
$N_{parallel\_modules}$	13

## 6.2 The model: A Liquid-Cooled Lithium-ion Battery Pack

As previously mentioned, the battery pack has been modelled and subsequently studied by using the ‘COMSOL Multiphysics’ software, a powerful mean for multiphysics simulations. Before starting with the description of the steps, it is necessary to specify that this project work about the battery cooling system is coupled with a validated electro-chemical and thermal model conducted by my colleague *Laura Scandura* on the 18650 cylindrical cell described in “6.1 Hybrid railway description”.

Now, it is possible to outline the steps of the created liquid-cooled battery pack; the temperature profile in a number of cell and cooling fins has been simulated through a time-dependent analysis. The average heat generated by each cell at a discharge load set to *1C-rate* derives from 1D electrochemical model developed by Scandura.

### 6.2.1 Geometry

Prismatic batteries are more suitable to form modules, thanks to their structure that promotes the heat dispersion having a greater heat exchange surface at the same volume [63].

The first step on COMSOL has been to build the 3D geometry of the system: it has been simplified due to the symmetries along x-y axes and because of the elevated computational costs requested for such kind of simulations software.

The repetitive unit cell of the battery pack consists of two prismatic cells and a cooling fin plate with five channels of square section; the two batteries and the cooling plate are arranged according to the alternation battery-cooling plate-battery (in other words, there is a battery on each side of the cooling fin). Cooling fins and batteries are 2 [mm] thick for a total unit cell thickness of 6 [mm] [64].



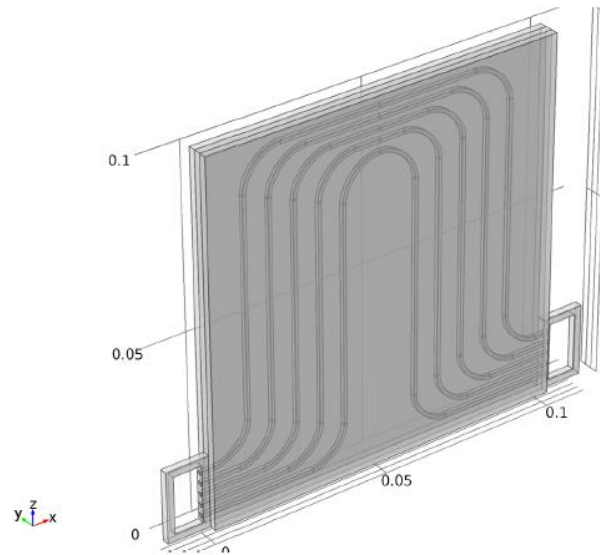


**FIGURE 56. PRISMATIC UNIT CELL OF BATTERY PACK**

These unit cells have been stacked to compose the modelled battery pack geometry. More precisely, three stacked unit cells and two flow connector channels: one on the inlet and one on the outlet of the cooling fins. As anticipated before, the geometry represents the last cells towards the end of the battery pack; the previous cells are not visible in the built geometry, even if their interaction on the overall pack has been taken clearly into account through the imposition of a series of boundary conditions which will be explained soon. The next image shows the final configuration of the pack:

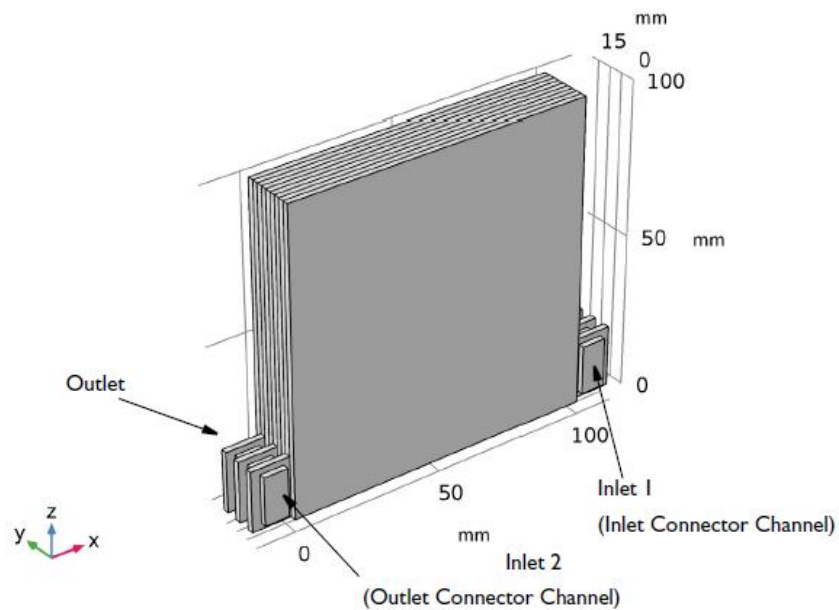


**FIGURE 57. BATTERY PACK GEOMETRY**



## 6.2.2 Materials

After having built the geometry, domains and relative materials have been defined. Domains are:

- Batteries;
- Cooling fins;
- Flow compartment: it consists of the two connectors and the channels crossing the cooling fins.

Batteries materials have been not explicitly defined, being made of a lot of internal materials and substances. The way used to define their characteristics has been to set density, heat capacity, heat source and thermal conductivity properties.

L_neg	80e-6[m]	8E-5 m
L_sep	25e-6[m]	2.5E-5 m
L_pos	65e-6[m]	6.5E-5 m
L_negCC	7.5e-6[m]	7.5E-6 m
L_posCC	10e-6[m]	1E-5 m
L_batt	L_neg+L_sep+L_pos+L_negCC+L_posCC	1.875E-4 m
rho_pos	2451.88[kg/m <sup>3</sup> ]	2451.9 kg/m <sup>3</sup>
rho_neg	1891.99[kg/m <sup>3</sup> ]	1892 kg/m <sup>3</sup>
rho_pos_cc	2700[kg/m <sup>3</sup> ]	2700 kg/m <sup>3</sup>
rho_neg_cc	8960[kg/m <sup>3</sup> ]	8960 kg/m <sup>3</sup>
rho_sep	1008.98[kg/m <sup>3</sup> ]	1009 kg/m <sup>3</sup>
Cp_pos	800[J/(kg*K)]	800 J/(kg·K)
Cp_neg	600[J/(kg*K)]	600 J/(kg·K)
Cp_pos_cc	900[J/(kg*K)]	900 J/(kg·K)
Cp_neg_cc	385[J/(kg*K)]	385 J/(kg·K)
Cp_sep	1978.16[J/(kg*K)]	1978.2 J/(kg·K)
rho_batt	(rho_pos*L_pos+rho_neg*L_neg+rho_pos_cc*L_posCC+rho_neg_cc*L_negCC+rho_sep*L_sep)/L_batt	2294.2 kg/m <sup>3</sup>
Cp_batt	(Cp_pos*L_pos+Cp_neg*L_neg+Cp_pos_cc*L_posCC+Cp_neg_cc*L_negCC+Cp_sep*L_sep)/L_batt	860.49 J/(kg·K)

**FIGURE 58. CALCULATION OF BATTERY HEAT CAPACITY**

Densities and specific heat capacities values are data taken from both literature and validation. Same procedure has been set for the calculation of batteries thermal conductivity:

kT_pos	0.3[W/(m*K)]	0.3 W/(m·K)
kT_neg	1.04[W/(m*K)]	1.04 W/(m·K)
kT_pos_cc	238[W/(m*K)]	238 W/(m·K)
kT_neg_cc	400[W/(m*K)]	400 W/(m·K)
kT_sep	1.21[W/(m*K)]	1.21 W/(m·K)
kT_batt_x	(kT_pos*L_pos+kT_neg*L_neg+kT_pos_cc*L_posCC+kT_neg_cc*L_negCC+kT_sep*L_sep)/L_batt	29.402 W/(m·K)
kT_batt_y	L_batt/(L_pos/kT_pos+L_neg/kT_neg+L_posCC/kT_pos_cc+L_negCC/kT_neg_cc+L_sep/kT_sep)	0.59654 W/(m·K)
kT_batt_z	kT_batt_x	29.402 W/(m·K)

**FIGURE 59. CALCULATION OF BATTERY THERMAL CONDUCTIVITY**

Finally, the following graphic shows the heat generated (from now  $Q_h$ ) from each battery during the discharge process: it is the sum of the entropic contribution and the irreversible heat. As said before, this trend comes from Scandura's study:

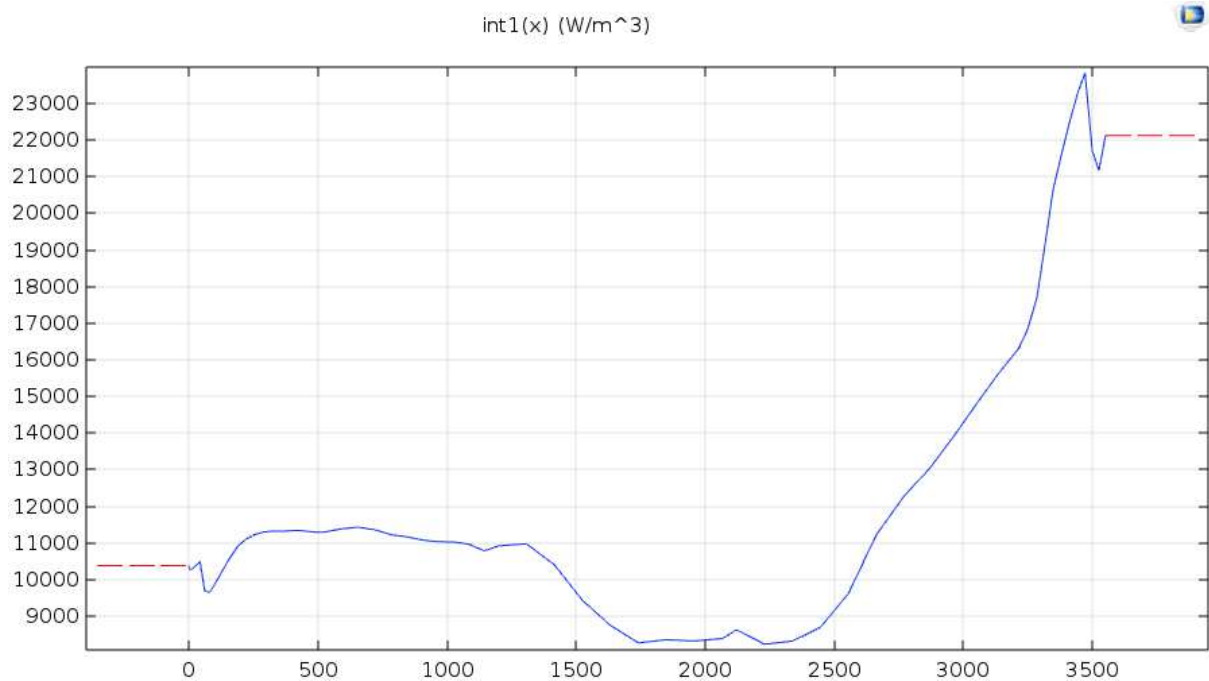


**FIGURE 60. HEAT GENERATED BY BATTERIES**

Cooling fins are made of aluminium, whereas a cooling fluid (such as water, water/glycol mixture, oil...) for the flow compartment has been imposed with its thermodynamic properties depending on a temperature variation range. The temperature field has been solved for the three domains.

### 6.2.3 Physics of the problem

Once the thermo-physical parameters of the materials have been defined, the physics of the problem are set. The model uses *Laminar Flow* interface (applied to flow compartment domain) to solve for the velocity and pressure in the cooling channels, the *Heat Transfer* interface (set for all the domains) for the temperature field and a coupling both of them through a *Non-isothermal flux* Multiphysics.

Laminar flow has been considered because there are not so elevated velocities such that to choose a turbulent model; moreover, even if turbulence has a strong impact on the heat exchange, it significantly affects also hydraulic pressure losses requiring more pump/blower power. For an incompressible viscous fluid, the Navier-Stokes equations system governs a time-dependent fluid dynamic analysis:

$$\begin{cases} \rho \frac{\partial \mathbf{u}}{\partial t} + \rho(\mathbf{u} * \nabla)\mathbf{u} = \nabla * [-p\mathbf{I} + \mu(\nabla\mathbf{u} + (\nabla\mathbf{u})^T)] + \mathbf{F} \\ \rho \nabla * (\mathbf{u}) = 0 \end{cases}$$

The first equation involves the change of velocity with time, a convective term, a pressure term (fluid flow in the direction of largest change in pressure), a viscosity-controlled velocity diffusion term, a body force term (external forces acting on the fluid such as gravity, electromagnetic, etc.); while the second one is the continuity equation.

Concerning heat exchange between solids and fluids, diffusion equation for a time-dependent problem and Fourier law (the heat flux calculated in a certain position and time is proportional to temperature gradient through the thermal conductivity) are set:

$$\begin{cases} \frac{\partial T}{\partial t} = \alpha \nabla^2 T + \frac{q}{\rho c_p} \\ Q = -k \nabla T \end{cases}$$

When the fluid is characterized by laminar motion, the heat exchange in the direction perpendicular to the motion of the fluid takes place only by conduction. So, in the thermal boundary layer, the heat exchange relationship, which equals the heat flux exchanged by convection between the wall and the fluid to the one transmitted by conduction through the first layer in contact with the wall (calculated with the Fourier law), can be applied. The heat diffusion equation takes into account the thermal diffusivity of the solid and a term of internal generation of thermal energy (presence of heat source).

### 6.2.4 Boundary Conditions (BCs)

One of the most important step to conduct a Finite Element Analysis (FEA) correctly is the exact imposition of the BCs.

#### - Flow Boundary Conditions

Since the model cells are the last ones in a large battery pack (the created geometry doesn't represent the complete pack), the flow compartment has two inlets as show in figure 51: the liquid flow that will cross through the modelled geometry will enter at *Inlet 1*, while the fluid flow that has passed the previous cooling fins of the part of battery pack not included in the model will enter at *Inlet 2*.

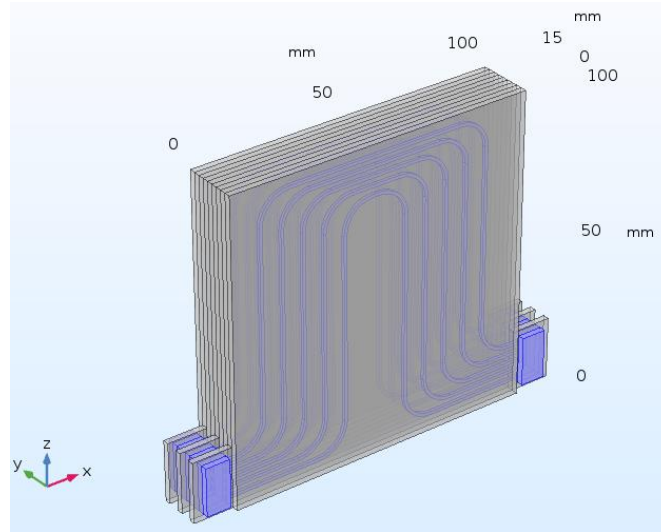


FIGURE 61. FLOW COMPARTMENT

At the initial stage, it has been considered the fluid already present in the flow compartment has a null motion field and pressure, excluding initial values at *Inlet 2*. At *Inlet 1* a laminar influx boundary condition is imposed specifying the incoming volumetric flow rate for each fin of the model; then, defining the number of modelled cooling fins as  $N_{\text{fins,model}} = 3$ , and the total number of cooling fins in the pack as  $N_{\text{fins,pack}} = 6$  (because  $N_{\text{series\_cells}} = 12$  from the sizing), the inflow conditions are set to:

- $\dot{V}_{\text{fin}} = 0.5 \left[ \frac{\text{cm}^3}{\text{s}} \right]$  (example value, this parameter will be changed for optimization)

- $\dot{V}_{inlet1} = N_{fins,model} * \dot{V}_{fin}$
- $\dot{V}_{inlet2} = (N_{fins,pack} - N_{fins,model}) * \dot{V}_{fin}$

As anticipated before, the fluid velocity value along y-direction has been imposed only at *Inlet 2* since the flow coming from previous cooling fins has its own velocity:

$$(N_{fins\_pack} - N_{fins\_model}) * \dot{V}_{fin} / (8[mm] * 16[mm])$$

where 8[mm] and 16[mm] are the dimension of the flow connector channels section at *Inlet 2*. At the outlet, atmospheric pressure is applied and the possibility of reflux of liquid is avoided to not create a reintroduction of liquid into the equipment and therefore motions that are difficult to control.

All other boundaries have been set to condition that on the walls of the solid the tangential velocity is zero, no-slip conditions.

#### - *Heat Transfer Boundary Conditions*

All domains have been set to an initial temperature of 303[K] (*Dirichlet* condition). As concerns batteries blocks, the thermo-dynamics properties calculated above (thermal conductivity, density and specific heat capacity) have been fixed. Same speech has been made for the heat generated, imposed as a ‘heat source’ condition.

At *Inlet 1* an inlet temperature of 303[K] for the cooling fluid has been specified (in the optimization study,  $T_{inlet}$  will be a control parameter and so it will assume many values).

At *Inlet 2* a boundary heat flux (*Neumann* condition) has been applied to take into account the heat produced by the batteries not included in the model geometry. So, considering the average heat source from the battery  $Q_h$  and the battery volume  $V_{batt}$ , the total heat flux is:

$$Q_0 = 2 Q_h (N_{fins\_pack} - N_{fins\_model}) V_{batt} * 0.99$$

where the factor 2 stems from the number of batteries per cooling fin and the factor 0.99 accounts for an assumption if 1% of the heat lost to the surroundings before entering the connector channel [65].

An outflow condition is applied at the outlet of the entire model; symmetry conditions are applied to the surface of the model facing the part of battery pack not included in the geometry. On all other boundaries heat flux conditions (*Robin* condition) have been applied with heat

transfer coefficient  $h = I \left[ \frac{W}{m^2 K} \right]$  in order to account for some heat being lost to the surroundings due to poor insulation.

### 6.2.5 Mesh

A FEM (Finite Element Method) can be applied to bodies capable of being subdivided into a certain large number of elements having defined shape and dimensions. In the continuum, every single finite element is considered a field of numerical integration of homogeneous characteristics. Through this method, a discretization of the domain thanks to the creation of a grid (mesh) constituted by finite elements (triangles, quadrilaterals for 2D domains, tetrahedral for 3D domains) is applied. On each element, the solution of the problem can be expressed by the linear combinations of shape functions. Set up a suitable mesh in order to solve numerically the problem under investigation in efficient way is very important.

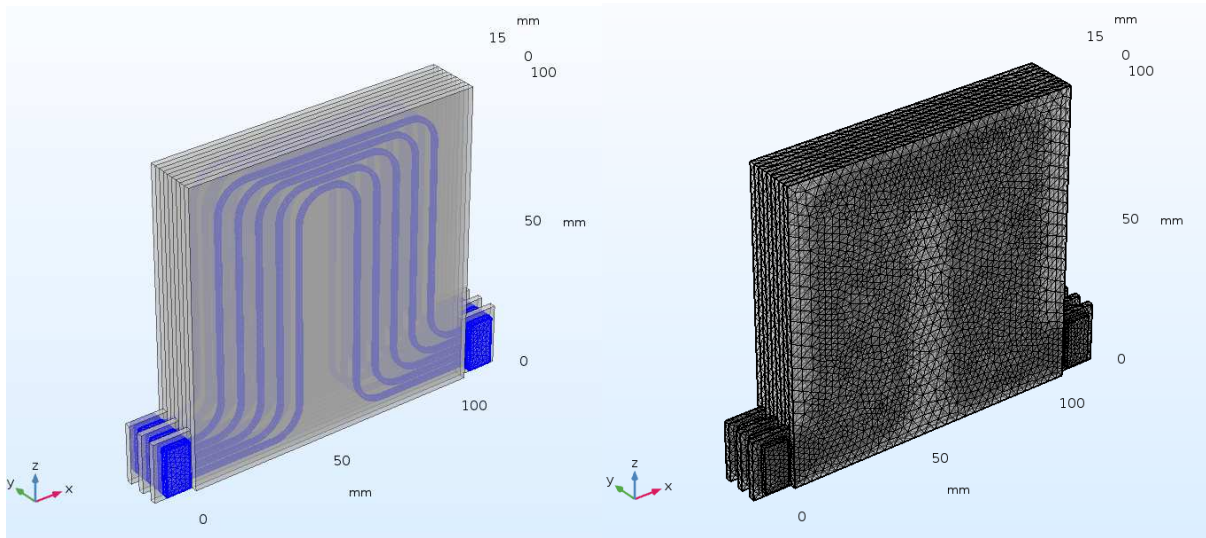


**FIGURE 62. MESH OF THE MODEL**

A distinct mesh is defined for each domain; in particular, the grids for the flow compartment channels and boundaries have been calibrated for the fluid-dynamic with precise minimum and maximum dimension values. For the other domains, a free tetrahedral mesh has been used.

### 6.2.6 Simulation results and Optimization

The objective is to analyse the thermal performances of the created model considering different cooling fluids at various coolant volumetric flow rates ( $\dot{V}_{fin}$ ), coolant inlet temperatures ( $T_{inlet}$ ) and square section channel edge ( $l_l$ ) to find the optimal values for:

- the minimization of the battery average temperature;
- the reduction of the temperature coolant difference between inlet and outlet section (it is a parameter indicating cell temperature uniformity possible achieved);
- the minimization of the pressure drops into the channels (to determine the required pump power).

First of all, a simulation with test values of the three control parameters (i.e.  $\dot{V}_{fin} = 0.03 \left[ \frac{cm^3}{s} \right]$ ,  $T_{inlet} = 303[K]$ ,  $l_l = 1 [mm]$ ) has been made to show the comparison of the battery average temperature evolution of the model without cooling system and using different coolant fluids:

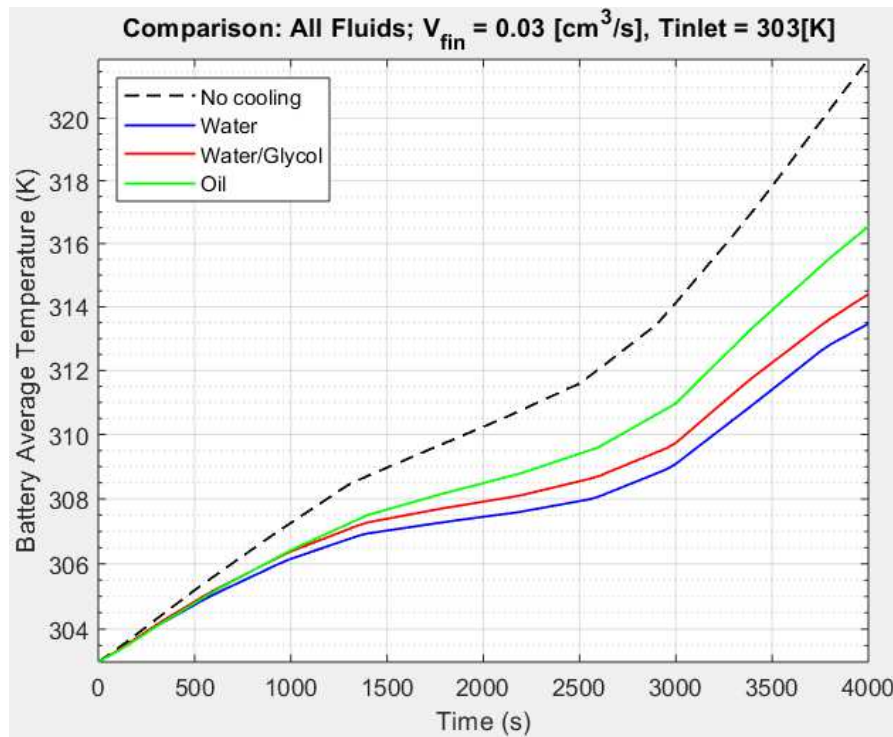


FIGURE 63. COMPARISON OF BATTERY AVERAGE TEMPERATURE COOLED BY DIFFERENT FLUIDS

As predictable, batteries cannot operate without thermal management: in fact, the dashed line reaches a too much high temperature (up to  $\sim 323[K]$ ) at the end of discharge, ‘exiting’ out of optimal working thermal range. So, it is necessary to cool down the system. It is then clear from

the plot that adopting a thermal management system reduces final temperatures (in particular, 7[K] less with oil and about 9-10[K] with water).

It is noticeable that water acts better than water/glycol (50:50 volume fractions) mixture and oil liquids because of higher thermal conductivity: at 303[K],  $k_{\text{water}} = 0.605 \left[ \frac{\text{W}}{\text{mK}} \right]$ ,  $k_{\text{water/glycol}} = 0.525 \left[ \frac{\text{W}}{\text{mK}} \right]$  while  $k_{\text{oil}} = 0.144 \left[ \frac{\text{W}}{\text{mK}} \right]$ . In fact, water/glycol mix works a little bit worse than water due to the addition of ethylene glycol which confers an antifreeze function (useful when batteries work in extreme environmental conditions), but it slightly gets worse thermal performances of pure water; oil has the lowest thermal conductivity among the three fluids and, consequently, batteries reach higher temperatures. Moreover, the latter has also a worse heat specific capacity ( $c_{p\_oil} = 1.925 \left[ \frac{\text{kJ}}{\text{kgK}} \right]$ ) with respect to water/glycol ( $c_{p\_water/glycol} = 3.280 \left[ \frac{\text{kJ}}{\text{kgK}} \right]$ ) and pure water ( $c_{p\_water} = 4.186 \left[ \frac{\text{kJ}}{\text{kgK}} \right]$ ) ones: the following graph shows that oil temperature difference between outlet and inlet sections ( $\Delta T_{\text{coolant}} = T_{\text{outlet}} - T_{\text{inlet}}$ ) is higher than that of other two fluids due to lower  $c_p$  (in other words, oil is rapidly heated compared to pure water and water/glycol mixture because of the smallest heat capacity among three).

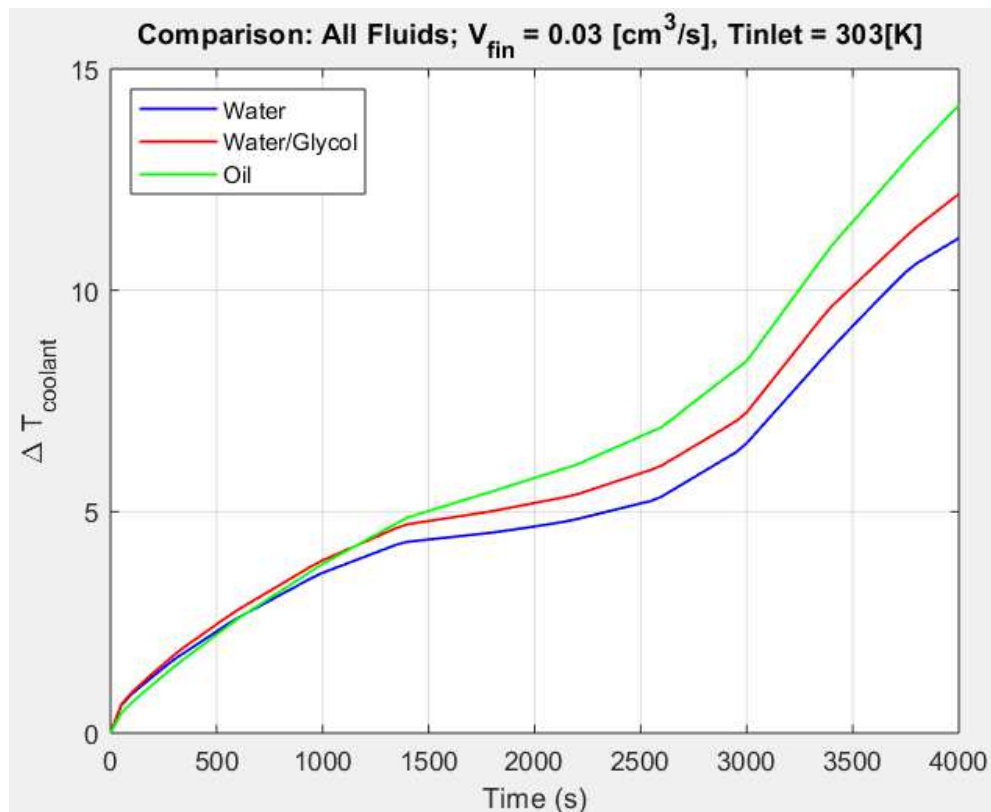


FIGURE 64. COOLANT TEMPERATURE DIFFERENCE

However, none of the three fluids keeps batteries within the optimal thermal range using these control parameters values, because cells temperatures increase over 314[K] and all  $\Delta T_{\text{coolant}}$



exceed 5[K] limit over which there would be a not uniform temperature distribution of each cell. The next group of figures show the 3D temperature evolution at (0,500,1500,2500,3000,3400) seconds (times in which there is a significant change in the heat generated curve) using pure water as coolant.

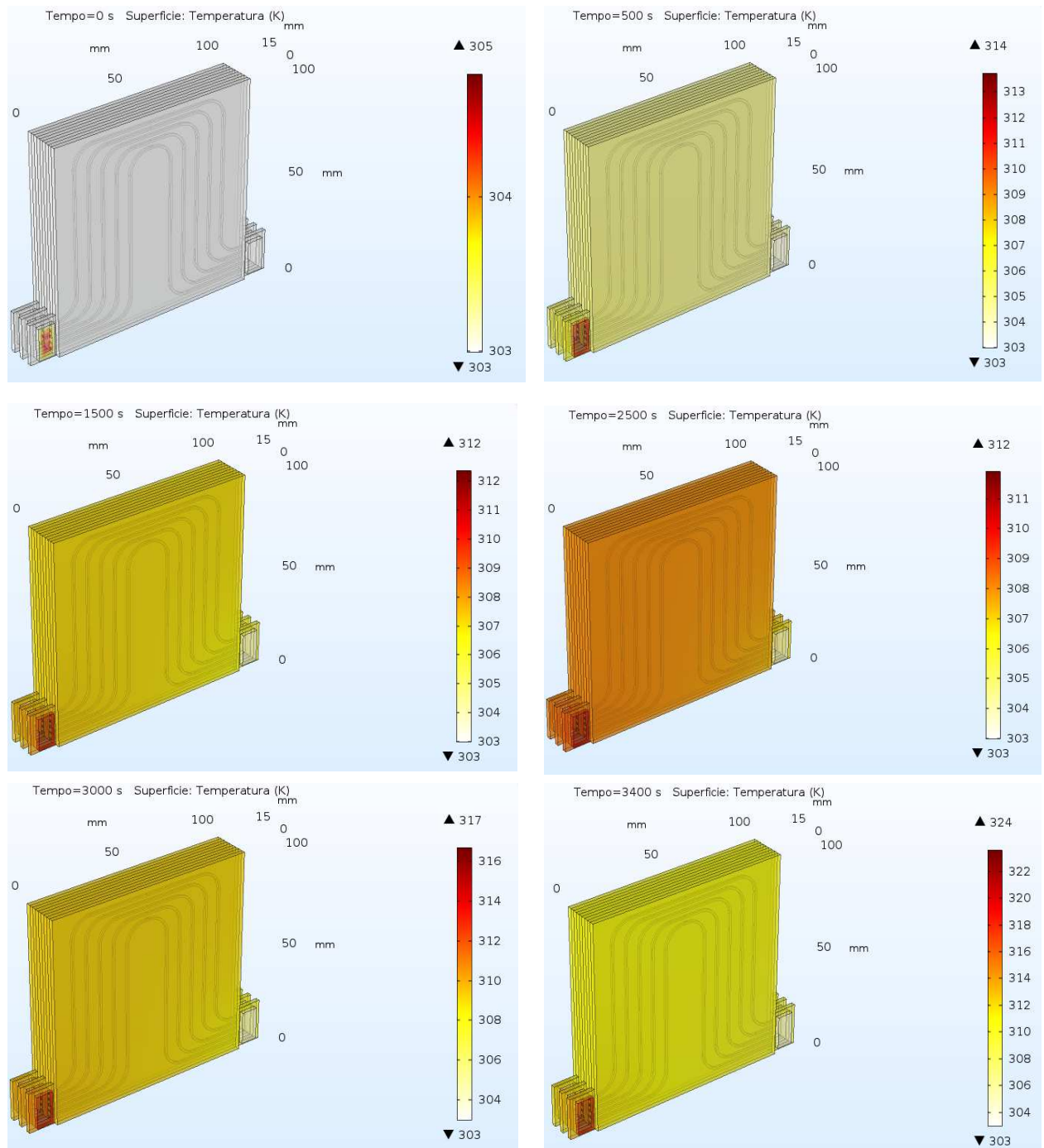
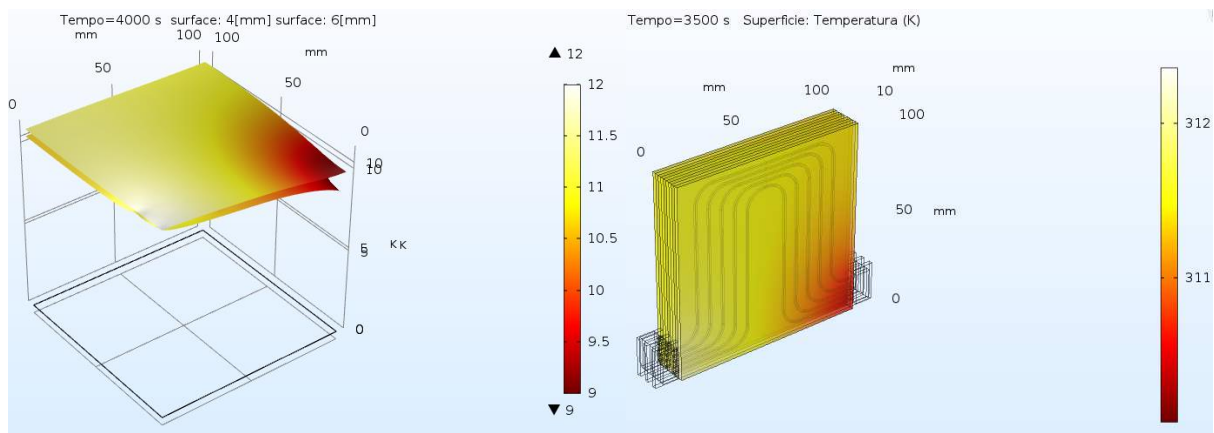


FIGURE 65. SYSTEM TEMPERATURE EVOLUTION DURING DISCHARGE

Using the values set above for the three control parameters, it is possible to notice that the overall system is at 303[K] (initial temperature fixed for the case study) at ‘time = 0’, except the ‘red area’ visible in the Inlet 2 flow connector (because of the imposition of the heat boundary condition taking into account the warmer fluid coming from the previous cells); then, temperatures reach elevated values (up to  $\sim 314$  [K] in batteries domain) with respect to the optimal working range. Moreover, there is a little temperature gradient (there are portions colder than others) starting from the lower-right corner of the battery moving towards *Inlet 2* flow connector because in that corner the cooling fluid is entering the system at 303[K], but then it warms up going through the battery within the channels, removing less heat as the discharge process goes on.



**FIGURE 66. (LEFT) T-T<sub>INLET</sub> OF SECOND AND THIRD BATTERIES. (RIGHT) BATTERY TEMPERATURE PROFILE AT 3500(s)**

The 3D graphs show also the temperature increase (in relation to the inlet fluid temperature) of the second battery at the surface facing the cooling plate ( $y = 4$  [mm]) and at the surface in contact with the third battery ( $y = 6$  [mm]). It is noticeable that the latter has a higher temperature gradient because it is not cooled directly from the cooling fin but it is affected by the heat generated from the third battery.

The following pictures plot the coolant temperature: at the end of the process, the fluid temperatures are slightly lower than in the batteries; with the progress of the discharge, fluid temperatures increase due to a very low volumetric flow rate so that heat coming from batteries warms up fluid channels resulting in a cooling system not so efficient.

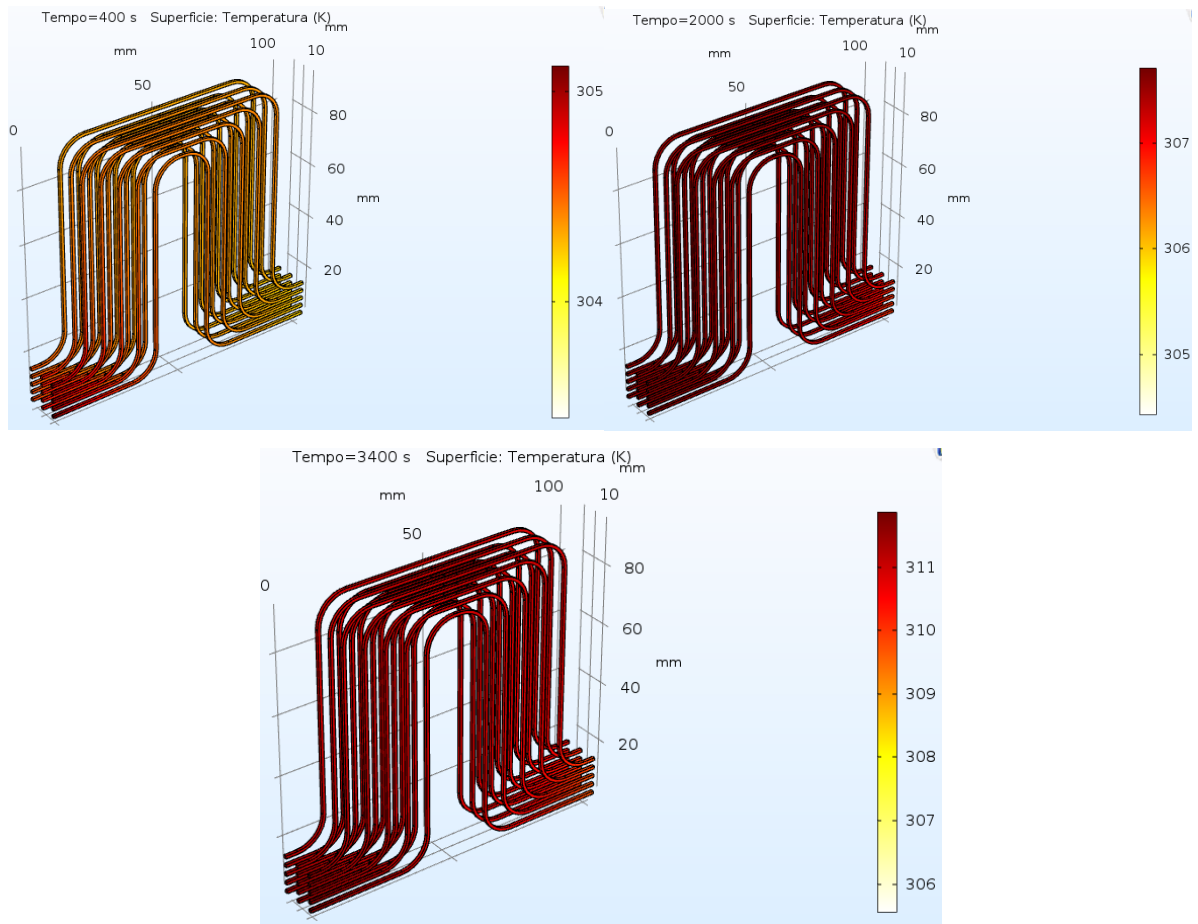


**FIGURE 67. 3D COOLANT TEMPERATURE EVOLUTION**

The next plot represents maximum, average and minimum batteries temperatures and coolant mean temperature trends. Mean temperatures of batteries and coolant are practically coincident; the difference between Max and Min temperatures seems to rise over time. For this reason, it is strictly necessary a BTMS using temperature sensors that communicate directly with the thermal management system to decide the amount of the coolant flow rate.

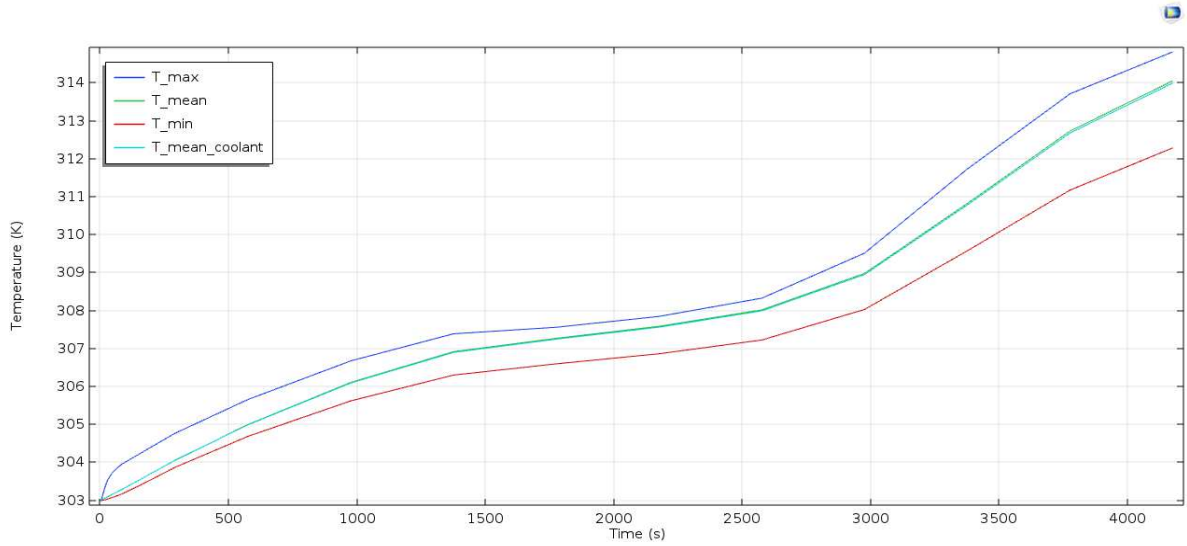


**FIGURE 68. MAX, MEAN AND MIN BATTERY AVERAGE TEMPERATURE TREND**

The optimization process has been executed monitoring batteries behaviour varying the three control parameters one by one, maintaining initial temperature equal to 303[K].

#### 6.2.6.1 Volumetric Flow Rate ( $\dot{V}_{fin}$ )

As seen below, pure water has been used for simulations because of its better thermo-dynamic properties with respect to water/glycol mix and oil ones, even if comparisons among the three will be still made. The thermal power (in terms of sensible heat) carried by channels is proportional to the flow rate of the heat transfer fluid, to its specific heat and to  $\Delta T_{coolant}$ :

$$Q = \dot{m}_{fin} c_p \Delta T_c \quad [W]$$

where mass and volumetric flow rates are linked by fluid density. So, higher  $\dot{V}_{fin}$  values correspond to significant lower batteries average temperatures; moreover, it is evident also that curves become flatter, meaning that cells temperature uniformity is enhanced over the discharge time.

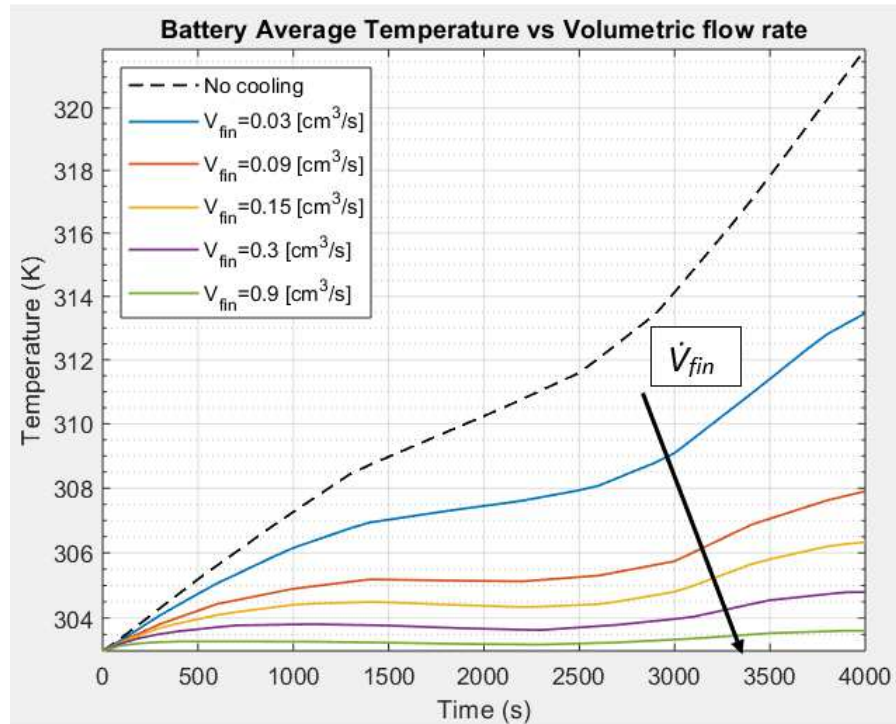


**FIGURE 69. BATTERY AVERAGE TEMPERATURE VS TIME AT DIFFERENT VOLUMETRIC FLOW RATES WATER**

Water/glycol and oil trend are shown, noticing that they operate worse than pure water (battery average temperatures are higher).

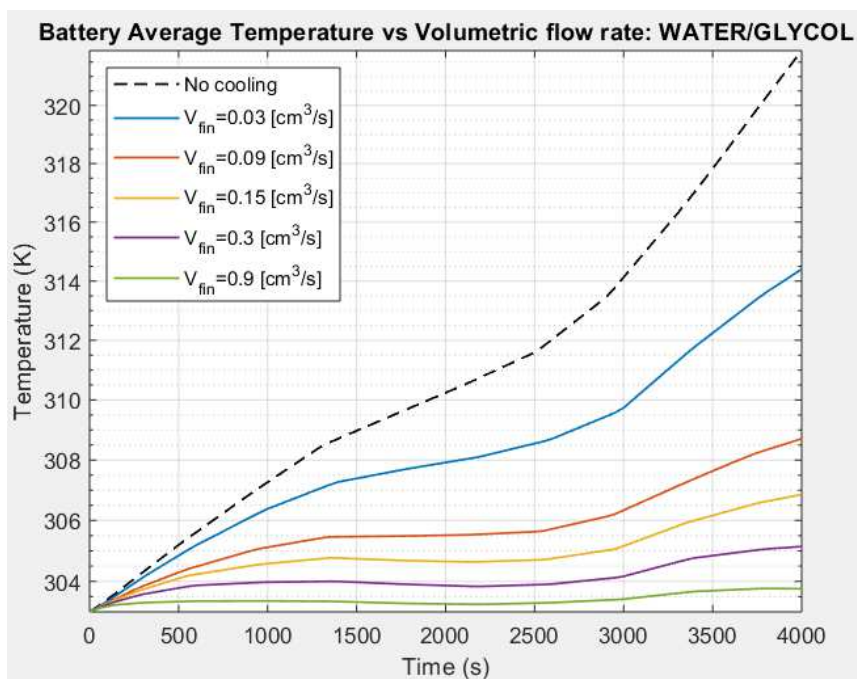


**FIGURE 70. BATTERY AVERAGE TEMPERATURE VS TIME AT DIFFERENT VOLUMETRIC FLOW RATES WATER/GLYCOL**

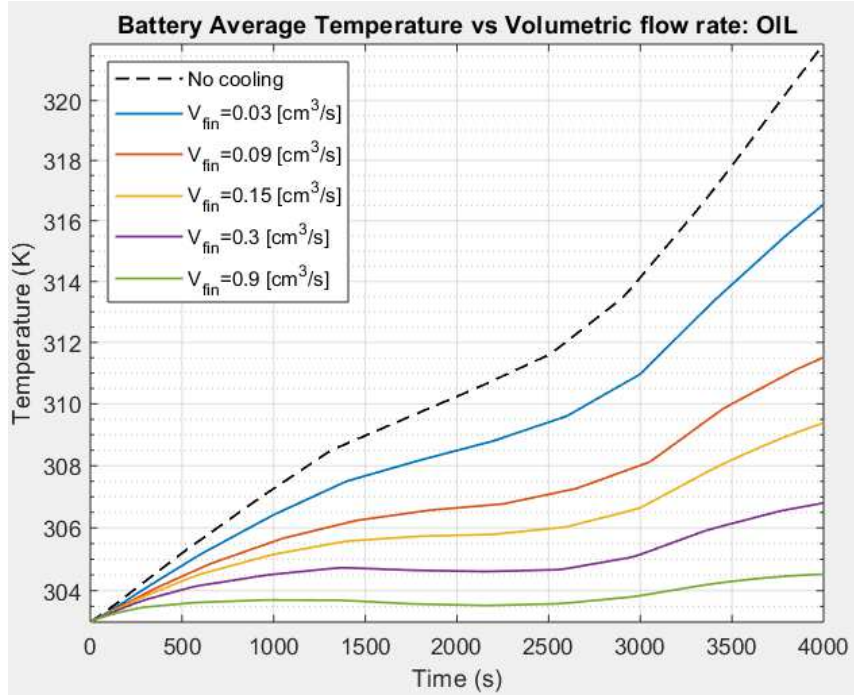


FIGURE 71. BATTERY AVERAGE TEMPERATURE VS TIME AT DIFFERENT VOLUMETRIC FLOW RATES OIL

The improvement of the uniformity is confirmed by plotting also  $\Delta T_{coolant}$  evolution during discharge process at various volumetric flow rates: the trend become more gradual. Considering that the scope is to keep coolant temperature change within the channels as small as possible, little flow rate changes can significantly affect the coolant temperature change and consequently cell temperatures.  $\Delta T_{coolant}$  is inversely proportional to coolant heat capacity flow rate ( $\sim \frac{1}{\dot{m}_c c_p}$ ).

Therefore, in small flow rate range, a little variation in  $\dot{V}_{fin}$  can greatly affect the coolant temperature change and consequently cell temperatures, while in large flow rate cooling an increase in flow rate is not so effective [66] (as shown in the next figures).



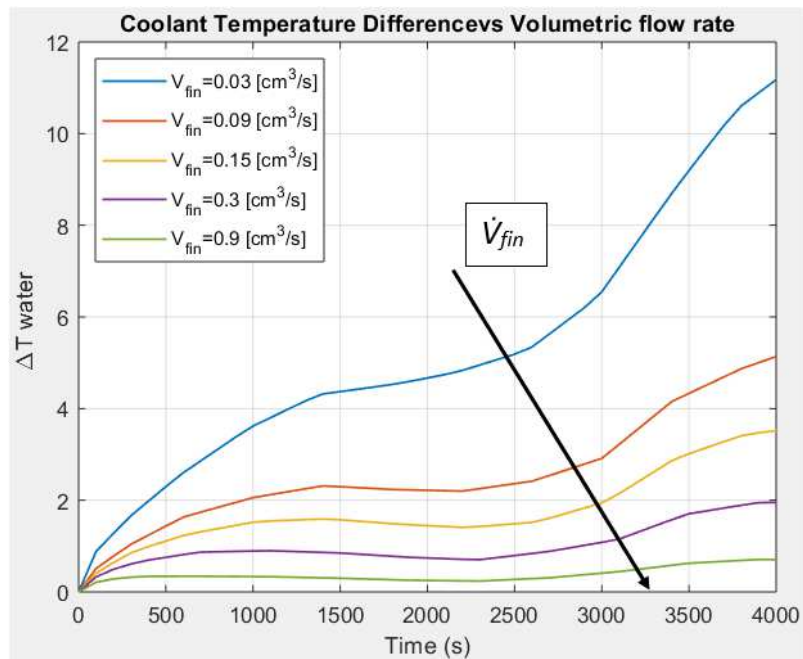


FIGURE 72. WATER TEMPERATURE DIFFERENCE VS TIME AT VARIOUS VOLUMETRIC FLOW RATE

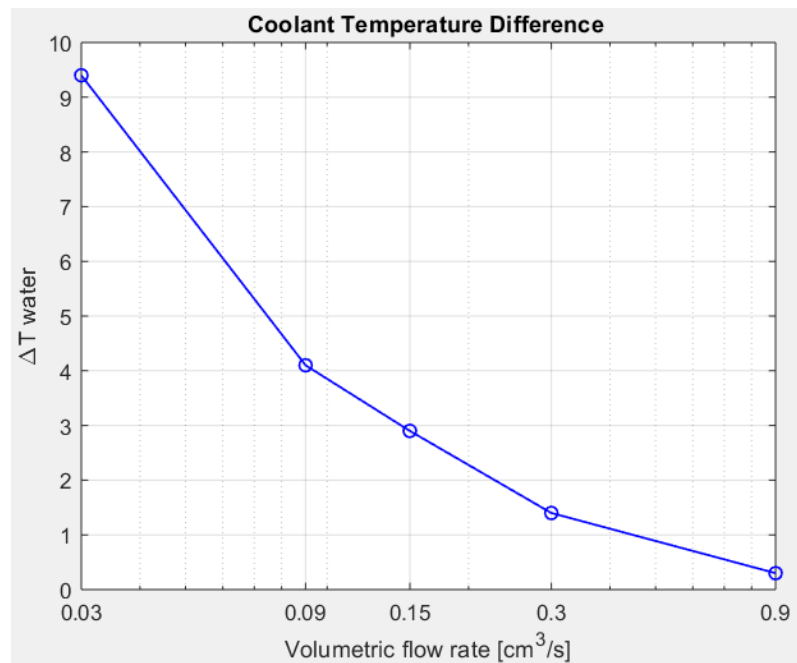


FIGURE 73. WATER TEMPERATURE DIFFERENCE AT THE END OF DISCHARGE

Here, a comparison among the tested coolants regarding the temperature difference at the end of discharge is represented. Pure water is the most performing fluid for achieving the best

temperature distribution of the pack due to its large heat capacity with respect to water/glycol and oil ones.

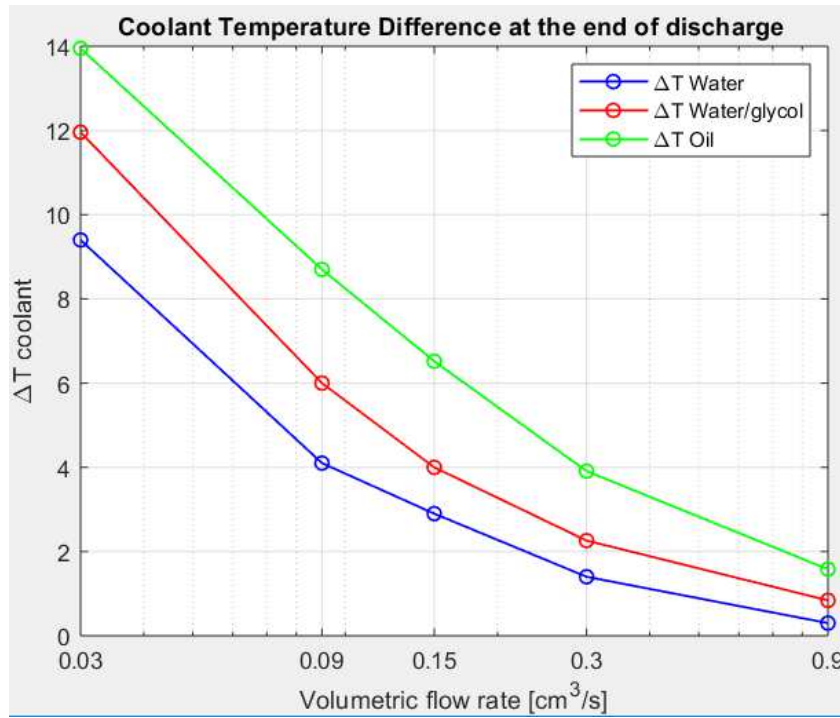


FIGURE 74. COMPARISON OF COOLANT TEMPERATURE DIFFERENCE AT THE END OF DISCHARGE

The operating volumetric flow rate should be carefully decided to control both batteries temperature rise and coolant temperature difference under a set value and, at the same time, to spend minimum pump power. The control target of these two quantities has been specified to be less than 5 (K or °C): from simulations,  $\dot{V}_{fin}$  minimum value satisfying both requirements of  $\Delta T_{water}$  and  $\Delta T_{ave\_battery}$  and minimum power required is resulted to be  $0.09 \left[ \frac{cm^3}{s} \right]$ , as shown the following plot. At this volumetric flow rate correspond a maximum battery temperature achieved of 308[K] (see figure 63); thus, the system works in safety remaining in the optimal thermal range for the entire discharge phase.



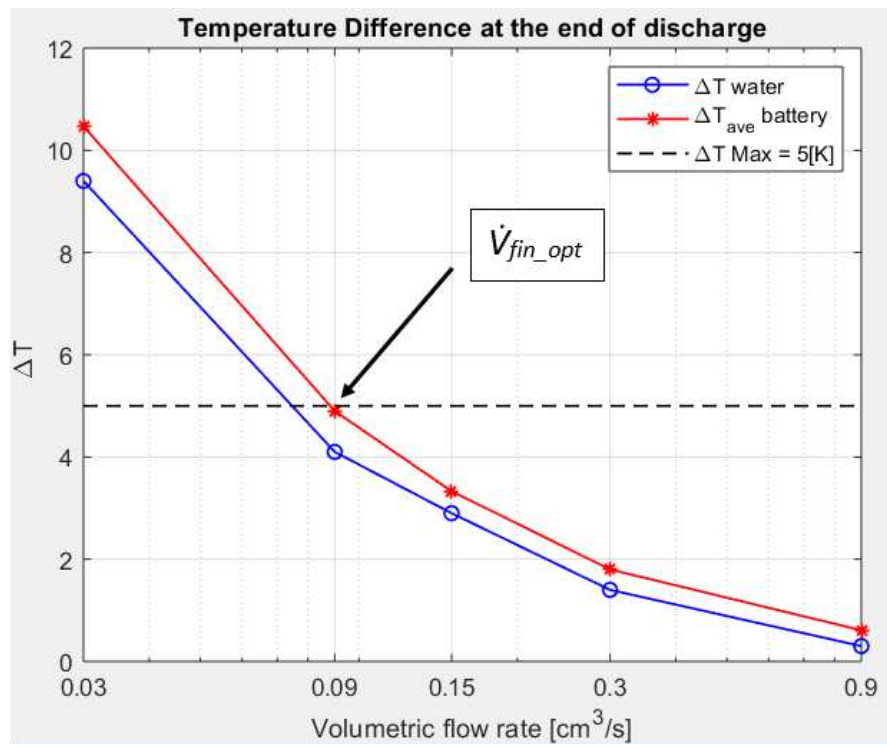


FIGURE 75. OPTIMAL VALUE OF THE VOLUMETRIC FLOW RATE

### 6.2.6.2 Coolant Inlet Temperature ( $T_{inlet}$ )

Starting from the worst volumetric flow rate ( $\dot{V}_{fin} = 0.03 \left[ \frac{cm^3}{s} \right]$ ) configuration, coolant inlet temperature  $T_{inlet}$  variation has been then analysed. Other environmental and system conditions have remained unchanged (remembering that initial temperature of the entire model has been set to 303[K]).

Clearly, heat removed by channels increases as the inlet coolant temperature decreases because of its direct proportionality with  $\Delta T_{water}$ . Consequently, battery average temperature reaches lower values over the time. Then, looking at the diagram, a  $T_{inlet} = 295[K]$  ensures  $\Delta T_{ave\_battery} < 5[K]$  (if inlet temperature is the parameter chosen in order to reach the desired temperatures).

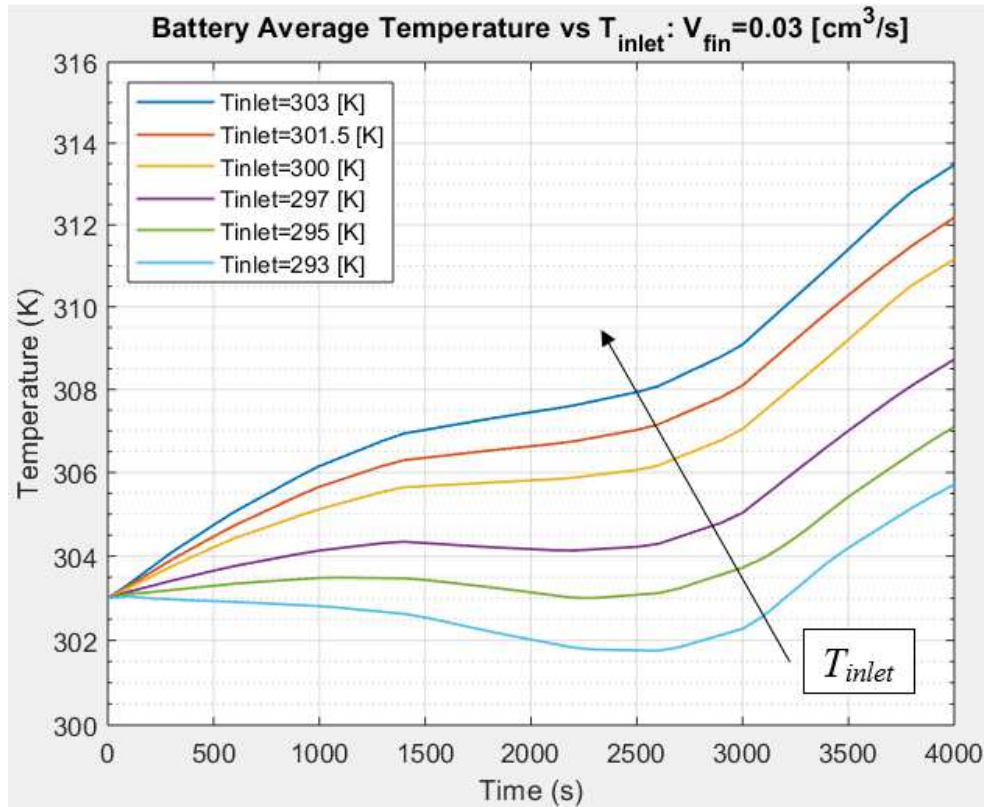
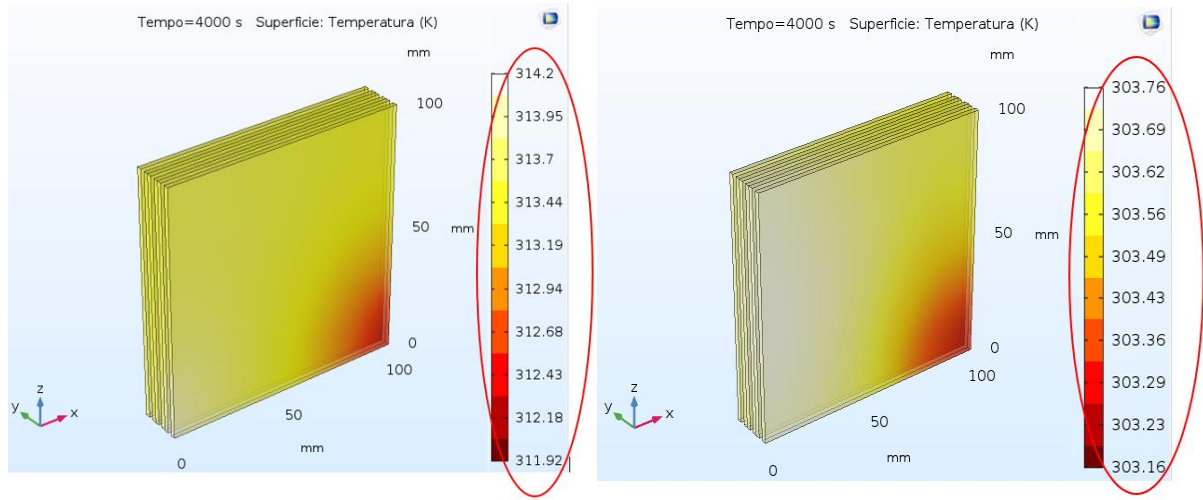


FIGURE 76. BATTERY AVERAGE TEMPERATURE VS TIME AT DIFFERENT COOLANT INLET TEMPERATURE

As concerns the temperature distribution over the cell, its uniformity has been resulted to be independent from coolant inlet temperature. In fact, it can be observed that changing volumetric flow rate at the same  $T_{inlet} = 303 [K]$  reduces temperature difference over the single cell: higher

volumetric flow rates decrease the difference between minimum and maximum battery temperatures improving the uniformity. The following figures show this result:



**FIGURE 77. (LEFT) BATTERY TEMPERATURE DISTRIBUTION WITH  $\dot{V}_{FIN} = 0.03 \left[ \frac{cm^3}{s} \right]$  AT DISCHARGE END. (RIGHT) BATTERY TEMPERATURE DISTRIBUTION WITH  $\dot{V}_{FIN} = 0.9 \left[ \frac{cm^3}{s} \right]$  AT DISCHARGE END.  $T_{INLET} = 303 \text{ [K]}$**

By contrast, varying  $T_{inlet}$  from 303[K] to 293[K] maintaining the same volumetric flow rate  $\dot{V}_{fin} = 0.09 \left[ \frac{cm^3}{s} \right]$ , the temperature difference on the single cell remains more or less unchanged.

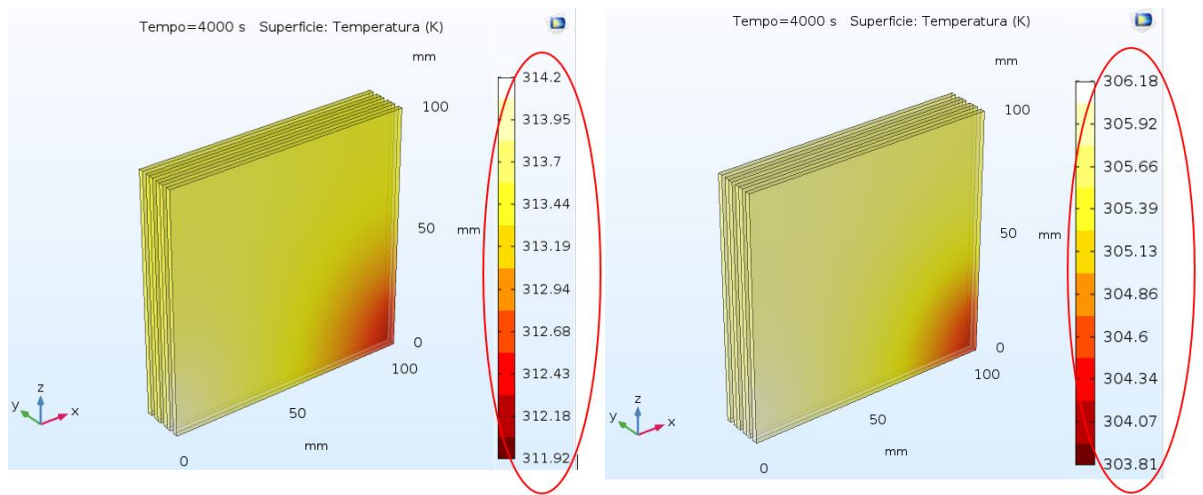


**FIGURE 78. (LEFT) BATTERY TEMPERATURE DISTRIBUTION WITH  $T_{INLET} = 303 \text{ [K]}$  AT DISCHARGE END. (RIGHT) BATTERY TEMPERATURE DISTRIBUTION WITH  $T_{INLET} = 293 \text{ [K]}$  AT DISCHARGE END.  $\dot{V}_{FIN} = 0.03 \left[ \frac{cm^3}{s} \right]$**

So, the battery average temperature profile rises with the increase of inlet coolant temperature and reducing it can be an effective method to cool batteries with a specific flow rate. Instead, the inlet temperature of the coolant has little influence on temperature distribution over the cells. Especially at high C-rate, it should be more convenient to intervene on volumetric flow rate to improve also battery uniformity.

#### 6.2.6.3 Square section channel edge ( $l_1$ )

After determining the optimal volumetric flow rate for the case study, section channels variation has been varied to understand the effects not only on temperatures but also on working pressures.

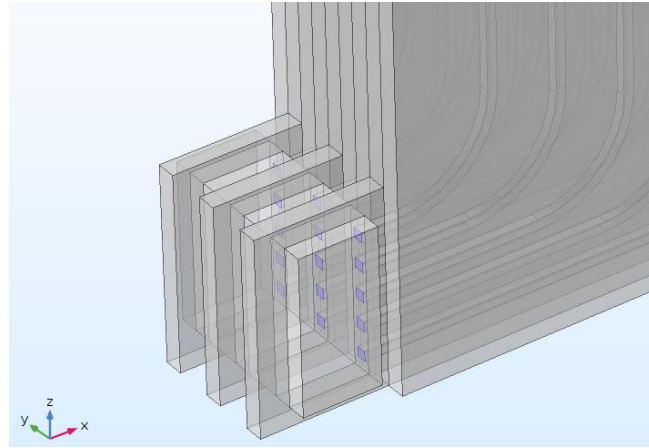


**FIGURE 79. CHANNEL SECTION**

As an example, batteries average temperatures have been evaluated considering a constant  $\dot{V}_{fin} = 0.03 \left[ \frac{cm^3}{s} \right]$  and changing section channel side from  $l_1 = 0.2$  [mm] (very narrow section) to  $l_1 = 1.9$  [mm] (maximum allowable value respecting construction constraint of the model).

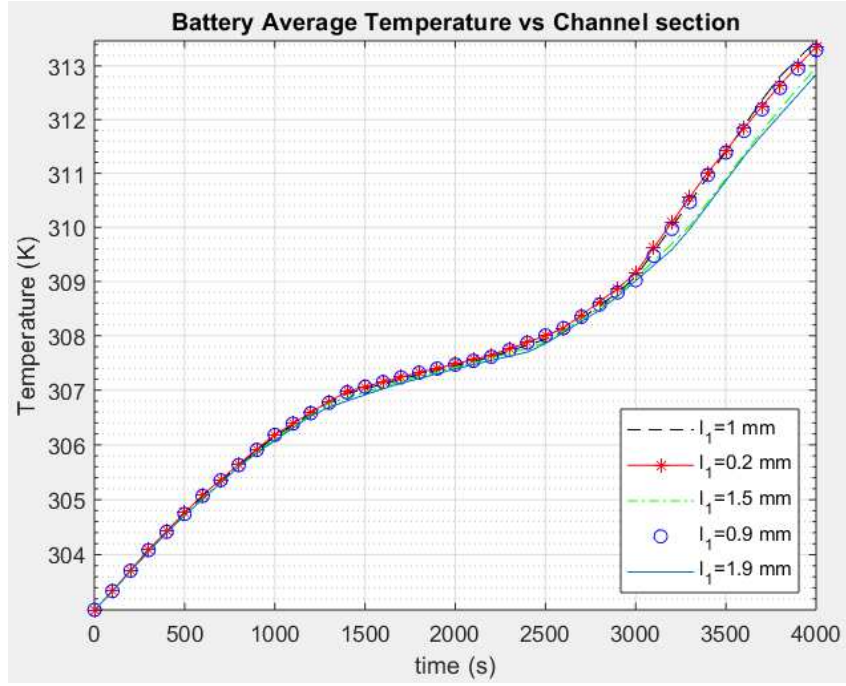


FIGURE 80. BATTERY AVERAGE TEMPERATURE VS TIME AT DIFFERENT CHANNEL SECTIONS

As shown by the figure above, changing channels section is not so affecting because volumetric flow rate is fixed (so, coolant flows faster within channels): the battery average temperature is not the dominant design point for the optimal channel side determination.

On the contrary, this control parameter could be very influencing on the channels pressure losses and, consequently, on the estimation of the required pump power that pushes coolant into channels themselves. From *Poiseuille* law:

$$\Delta p \sim \frac{V_{fin} * \mu}{l_1^3}$$

where  $\mu$  is the fluid dynamic viscosity [Pa\*s]; pressure drop is directly proportional to both volumetric flow rate and viscosity, and inversely proportional to the fourth power of channel side: great  $\Delta p$  variations for each coolant fluid are expected (this time  $l_1 = 0.2$  [mm] case has not been evaluated because of its extremely high pressure drop).

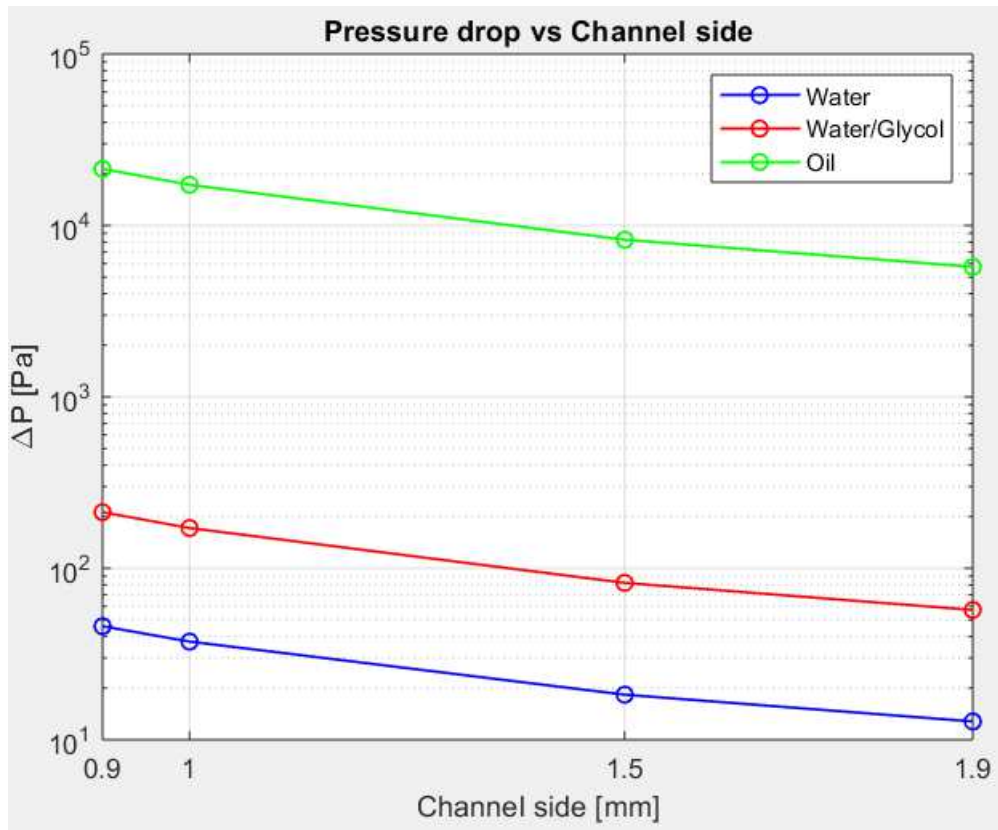


FIGURE 81. PRESSURE DROP VS CHANNEL SIDE

Maximum  $\Delta p$  over the time between inlet and outlet channels section have been calculated. As visible from the graph, an enlargement of channels section corresponds to a decrease of pressure drops; however, at the same volumetric flow rate and coolant inlet temperature (equal to 303[K]), oil pressure losses are so much higher than water and water-glycol mixture, because its dynamic viscosity is bigger of two and three orders of magnitude, respectively ( $\mu_{oil} = 0.4$  [Pa\*s] while  $\mu_{water/glycol} = 0.0041$  [Pa\*s] and  $\mu_{water} = 0.00085$  [Pa\*s]).

Power pump is strictly linked to pressure drop over the circuit and volumetric flow rate; the theoretical hydraulic work ( $P$ ) is calculated as an indication of energy consumption of a thermal management system [67]:

$$P = \dot{V} \Delta p \quad [W]$$

This equation considers both the contribution of the BTMS flow channel layout and the required operating condition to the energy consumption.

The sensitivity of pressure drop versus thermal performance has shown that a larger channel cross section area reduces losses and consequently power pump required by the system, but it has a little effect on the module average temperature. Adopting larger channels is surely

convenient regarding the energy consumption saving, even if they constitute major obstacles and weight addition for the system. Therefore, a good tradeoff value could be  $l_l = 1.5$  [mm].

Concluding, the system behaviour has been analysed in detail at different values of the control parameters chosen for this study. It came out that pure water is the most suitable coolant among the three thanks to its better thermal properties: it has higher thermal conductivity and heat capacity and lower viscosity, thus allowing greater performances. If the railway travels in extreme environmental conditions, water-glycol mixture should be a good solution due to its efficacy (similar to that of water, even if a little worse) and anti-freeze action. Starting from the optimization of the volumetric flow rate, the final optimal configuration has resulted in:

- $\dot{V}_{fin} = 0.09 \left[ \frac{cm^3}{s} \right]$
- $T_{inlet} = 303$  [K]
- $l_l = 1.5$  [mm]

Of course, these values have been obtained relatively to a small portion of the sized battery pack (because of the critical computational costs to simulate a 3D geometry like the pack resulted from sizing process); however, it could be a qualitative analysis to understand the overall behaviour and possible design parameters on which to act for the improvement of the battery pack.



### 6.2.7 Water-cooling coupled with Phase Change Material (PCM)

After analysing that pure water is the most efficient coolant among the three studied fluids, an integrated system coupling water-based fluid channels with PCM has been tested. A pure RUBITHERM phase change material has been chosen with the criteria that its melting temperature range should be relative to the optimal thermal range of the batteries. Here, RT35HC PCM properties are shown:


	<b>The most important data:</b>		
	<b>Melting area</b>	<b>34-36</b>	<b>[°C]</b>
		main peak: 35	
	<b>Congeeing area</b>	<b>36-34</b>	<b>[°C]</b>
		main peak: 35	
	<b>Heat storage capacity ± 7,5%</b>	<b>240</b>	<b>[kJ/kg]*</b>
	Combination of latent and sensible heat in a temperatur range of 27°C to 42°C.	<b>67</b>	<b>[Wh/kg]*</b>
	<b>Specific heat capacity</b>	<b>2</b>	<b>[kJ/kg·K]</b>
	<b>Density solid</b> at 25 °C	<b>0,88</b>	<b>[kg/l]</b>
	<b>Density liquid</b> at 40 °C	<b>0,77</b>	<b>[kg/l]</b>
	<b>Heat conductivity (both phases)</b>	<b>0,2</b>	<b>[W/(m·K)]</b>
	<b>Volume expansion</b>	<b>12</b>	<b>[%]</b>
	<b>Flash point (PCM)</b>	<b>177</b>	<b>[°C]</b>
	<b>Max. operation temperature</b>	<b>70</b>	<b>[°C]</b>

FIGURE 82. RT35HC PROPERTIES

The system has been modified placing PCM matrices on each side of the cooling fin and near to batteries. PCM plates have been coated with aluminium to enhance the heat exchange with batteries themselves, since generally a phase change material has a poor thermal conductivity.

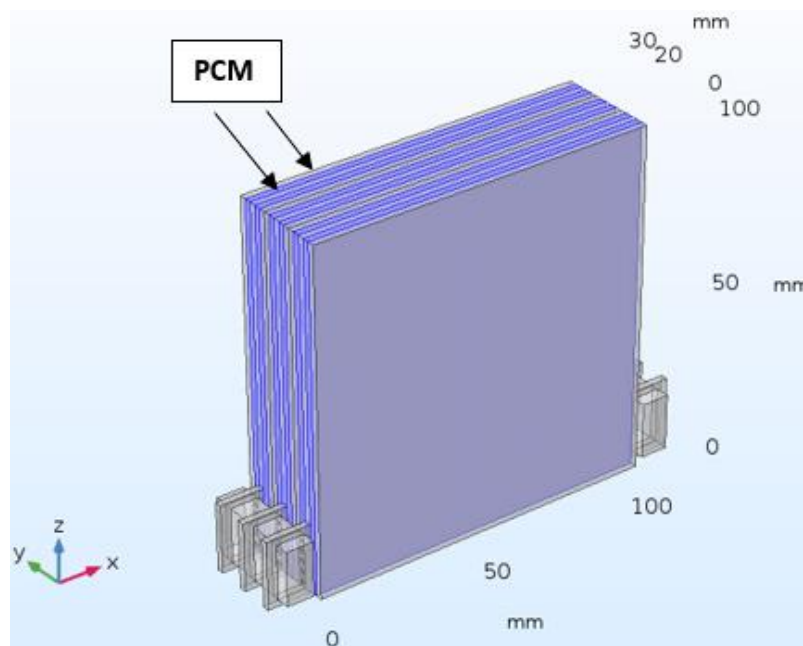


FIGURE 83. MODEL WITH PCM



To simulate a phase change on COMSOL, the specific heat of the PCM has been modified so that to include the latent heat contribution inside the phase changing temperature range, thus taking into account the amount of heat absorbed/released from the melting/condensation process.

Therefore, a Gaussian expression for the specific heat has been added to the material properties of the PCM:

$$c_p(T) = c_{p_s} + \frac{L}{\Delta T_{sl}\sqrt{\pi}} \exp\left(\frac{-(T - T_{av})^2}{\Delta T_{sl}^2}\right)$$

where:

- $L$ : latent heat of fusion;
- $T_{av}$ : melting average temperature;
- $\Delta T_{sl}$ : half of melting range.

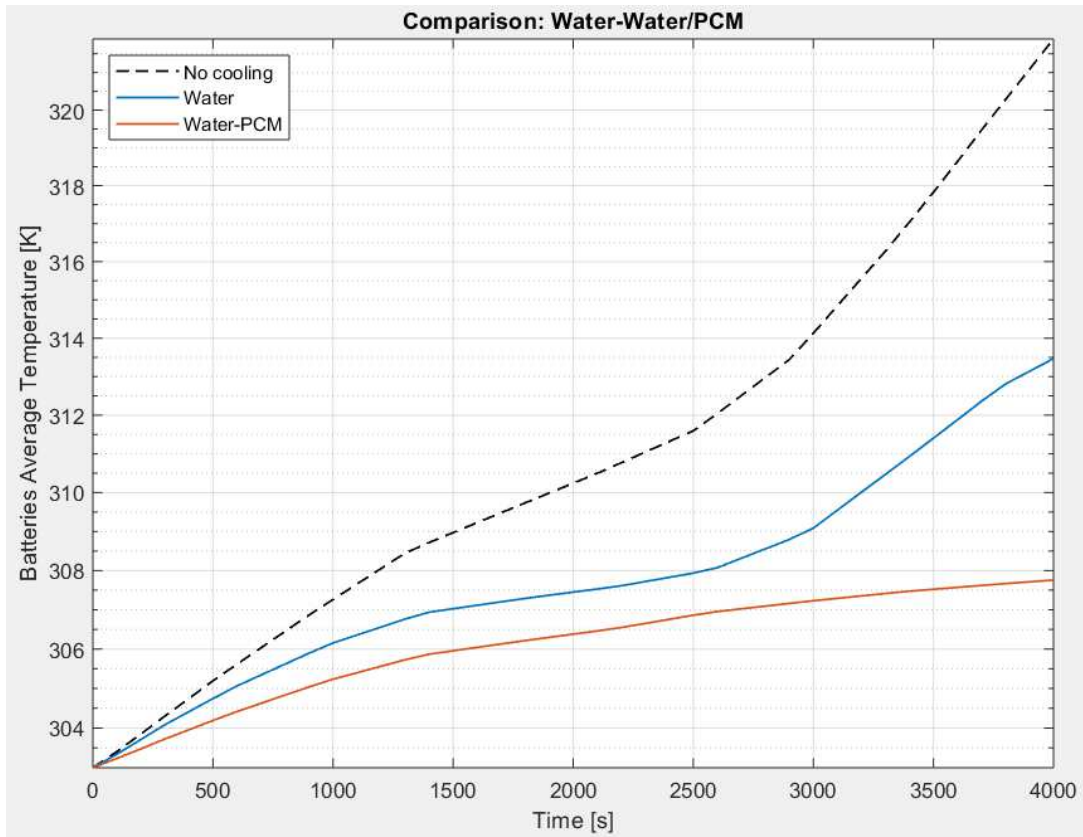


FIGURE 84. COMPARISON OF BATTERY AVERAGE TEMPERATURE WITH AND WITHOUT PCM

The figure shows the comparison between batteries average temperatures of water-cooled and water-cooled assisted with PCM systems, at the same  $\dot{V}_{fin} = 0.03 \left[ \frac{cm^3}{s} \right]$ ,  $T_{inlet} = 303[K]$ . It is evident that PCM assisted cooling system enhances strongly batteries thermal performances, reaching a temperature difference over time of 5[K]. Thus, the criteria to keep pack temperature during the process under the limit considered so far is satisfied despite the worst volumetric flow rate previously analysed. So, the use of PCM allows a lower volumetric flow rate and, consequently, an energy saving in terms of pump. Moreover, the increase in temperature is more gradual, especially from 2500s to the end of the process (in this range heat generated curve has a significant slope). The following diagram shows the trends of the two systems including also water temperature for the two systems and PCM temperature.

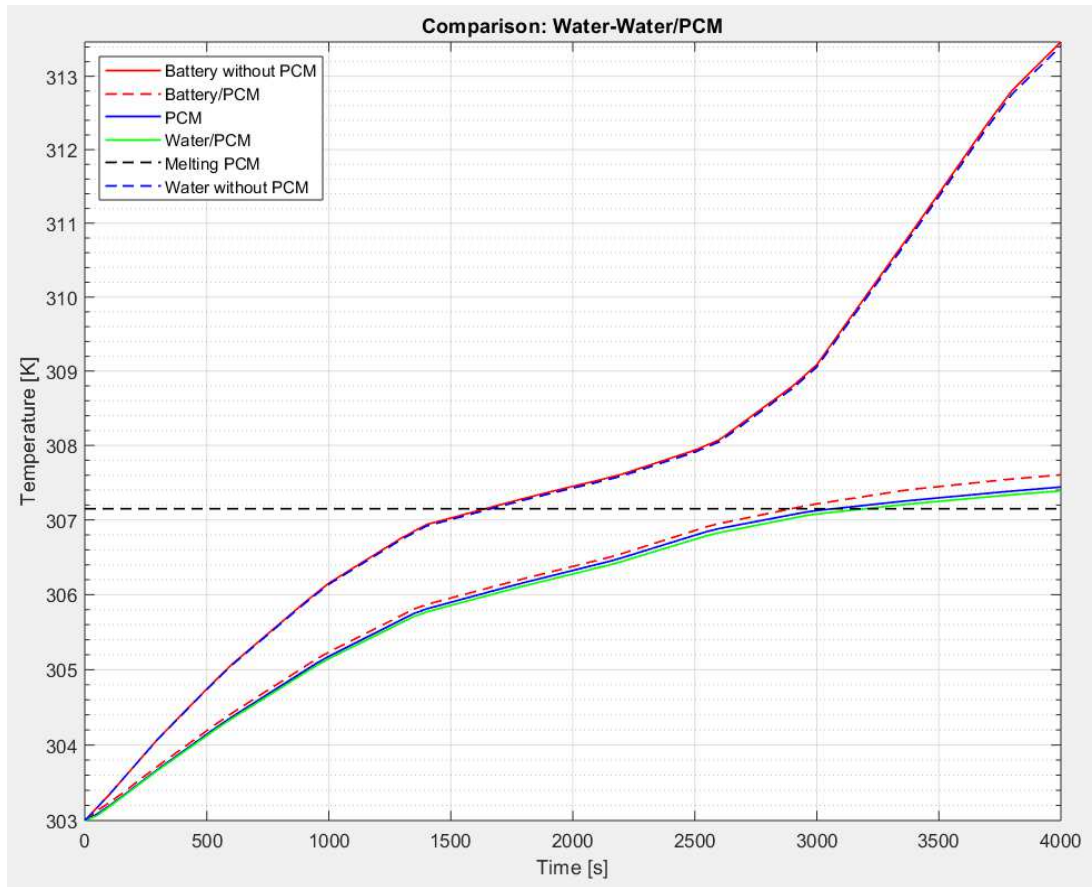


FIGURE 85. BATTERY, COOLANT AND PCM TEMPERATURES

It can be noticed that PCM reaches its melting point starting to liquefy; so, it uses the latent heat changing phase and delaying the increase of battery temperature. Also water follows battery and PCM temperatures trends, staying below battery curve and reaching temperatures much lower than to the standard configuration.

When batteries are not requested to work, their temperatures lower and PCM returns to be solid. The initial battery temperature does not exceed the PCM melting point, because PCM doesn't use the latent heat increasing the overall heat capacity and energy consumption. A disadvantage of the PCM use is the mass addition to the system, causing an increase in vehicle weight and a decrease of the overall railway performances; the mass of the PCM required could be evaluated as:

$$M_{PCM} = \frac{Q_{dis}}{c_p(T_m - T_i) + H}$$

where  $Q_{dis}$  (J) is the heat released from battery,  $c_p$  ( $\text{J kg}^{-1} \text{K}^{-1}$ ) is the specific heat of PCM,  $(T_m - T_i)$  is the difference between the melting temperature and initial temperature of PCM,  $H$  ( $\text{J kg}^{-1}$ ) is the latent heat of PCM. Anyway, mass should be chosen in relation to an estimation of the energy savings, because its addition increases the overall cost. PCM needs a packaging so that to contain the material at liquid phase.

Finally, PCM confers an important advantage for systems working under cold conditions: because of the heat stored as latent one, just a smaller part of it is transferred to the surroundings and when the battery temperature drops below the PCM melting point, this heat will be released to the module.

### 6.2.8 The development of nanofluids

Over the past decade, many scientists have been attracted by “traditional” heat transfer fluids (like water, engine oil, ethylene glycol, etc.) modified by the addition of nanomaterials, obtaining the so-called “nanofluids”. They are still conducting studies because of the expected superior thermal properties of these nanofluids, going towards important improvements concerning the conductive and convective heat transfer.

Nanoparticles are typically spherical or cylindrical in shape; they are composed by a solid core (defining thermal, electric, magnetic and optical properties) and a coating (defining the stability of the particle suspension as well as the hydrophilic or hydrophobic behaviour and the interfacial Kapitza resistance [68]). Nanofluids are suspensions of nanoparticles (diameter less or equal to 100 nm) immersed in a base fluid: these predominantly include ceramic (copper, copper oxide, aluminium, aluminium oxide, zinc oxide, titanium oxide etc [69]), metal (gold, silver) or carbon (carbon nanotube or graphene).

Thermo-physical properties of nanofluids depend strongly on the particle volume fraction ( $\Phi$ ), particle shape and size, base fluid material and temperature; generally, a nanofluid has a thermal conductivity larger than that of the base fluid, but this is accompanied by a higher viscosity and a smaller heat capacity. The following table shows thermal conductivities values obtained by theoretical and experimental models:

<i>Nanofluid</i>	<i>Particle diameter (nm)</i>	<i>Particle length (nm)</i>	$\Phi$ (%)	<i>Temperature (°C)</i>	$K_{nf} \left( \frac{W}{mK} \right)$	<i>References</i>
Al <sub>2</sub> O <sub>3</sub> -water	40	-	10	23	0.734	[70]
Al <sub>2</sub> O <sub>3</sub> -EG	40	-	10	23	0.312	[70]
CuO-water	29	-	12	21-23	0.70	[71]
SWCNT-water	1	100-600	0.2	60	0.756	[72]
SWCNT-EG	1	100-600	0.2	55	0.358	[72]

For this project work, Al<sub>2</sub>O<sub>3</sub>-water nanofluid has been employed considering  $\Phi = 5\%$  and  $\Phi = 10\%$  particle volume fractions. The way used to simulate a nanofluid on COMSOL has been to create a fluid “ad hoc” writing thermal conductivity, viscosity, density and heat capacity functions deriving from literature and different scientist studies. The models used in this case are reported below:

- *Thermal conductivity ( $k_{nf}$ )*

$k_{r\_max} = 1 + 3\Phi$  maximum thermal conduction enhancement within the macroscopic theory [73], valid for  $k_p \gg k_{bf}$  (where  $k_p$  and  $k_{bf}$  are particle and base fluid conductivities respectively).

Then, knowing  $k_{bf}$ , through Maxwell-Garnett (MG) model [74]:

$$k_{nf} = k_{r\_max} * k_{bf}$$

- *Viscosity ( $\mu_{nf}$ )*

$$\mu_r = \frac{1}{1-2.5\Phi} \quad \text{from Lundgren [75] generalized Brinkman's method.}$$

$$\mu_{nf} = \mu_r * \mu_{bf}$$

- *Density ( $\rho_{nf}$ )*

the effective nanofluid density is usually calculated by a mixing rule [76, 77]:

$$\rho_{nf} = (1 - \Phi) \rho_{bf} + \Phi \rho_p$$

- *Specific Heat capacity ( $c_{p,nf}$ )*

Pak and Cho model [64]:

$$c_{p,nf} = (1 - \Phi) c_{p,bf} + \Phi c_{p,p}$$

After evaluating the main thermal properties, battery average temperatures have been calculated considering the volumetric flow rate ( $\dot{V}_{fin} = 0.03 \left[ \frac{cm^3}{s} \right]$ ) in order to see the improvement using nanofluid as coolant. From the following plot, it is clear that temperatures reached at the end of discharge process are lower increasing the particle volume fraction. Nanofluids composed by carbon nanotubes (single or multiple wall carbon nanotubes SWCNT- MWCNT) should show better thermal properties.

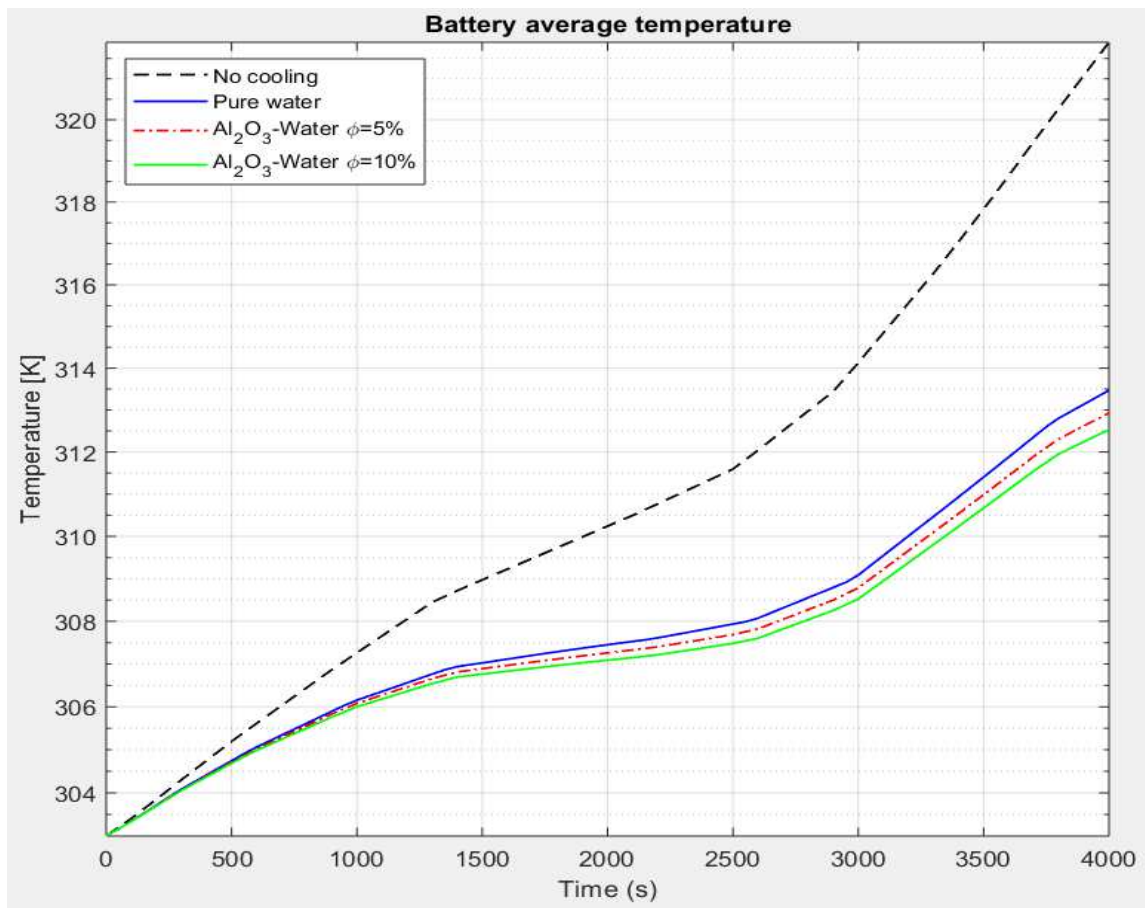


FIGURE 86. BATTERY AVERAGE TEMPERATURE USING  $\text{Al}_2\text{O}_3$ -WATER NANOFLUID

## 7. Conclusions

A detailed comparison among different liquid coolants has been made in this project work to obtain the best solution in achieving optimal battery pack temperatures. More specifically, oil, water-glycol mixture (50:50 volume percent) and pure water have been compared at the same operating and environmental conditions. From this first analysis, pure water has shown better performances than other two liquids because of its higher thermal conductivity and heat capacity. Alternatively, even if water-glycol mix has slightly worse thermal performances than pure water, it guarantees good cooling and allows battery functioning also in extreme environmental conditions because glycol addition confers resistance to very low temperatures acting as anti-freeze. In contrast, oil has not only the worst thermal conductivity and heat capacity, but also the highest viscosity; this drawback causes significant pressure losses within channels and, consequently, oil requires more pump power increasing energy consumptions.

Then, other simulations have been performed varying volumetric flow rate, inlet coolant temperature and channels section control parameters to minimize battery average temperature and to achieve a uniform temperature distribution over the cells. In particular, optimal values of these control parameters have been determined fixing a constraint on both battery temperature difference (between start and end discharge process) and coolant temperature difference (between outlet and inlet channel at discharge end) equal to 5(K). Channels section has been varied too in order to determine a trade-off value between less pressure drop and major obstacles.

A new solution for battery thermal management has been proposed inserting PCM layers on each side of the cooling fin, facing cells. The obtained thermal enhancement has been evident because PCM addition has satisfied the battery temperature constraint of 5(K) using a lower volumetric flow rate of the water. Consequently, PCM use permits energy saving in terms of pump, even if its mass should be chosen properly because it increases the overall weight lowering vehicle performance.

Finally, the temperature profile using a  $\text{Al}_2\text{O}_3$ -Water nanofluid has been briefly studied for future developments. Two cases of particle volume fraction have been compared with respect to pure water and slight improvements have been obtained, arising interest for further researches.





# Bibliography

- [1] «Global Carbon Atlas,» [Online]. Available: <http://www.globalcarbonatlas.org/?q=en/content/welcome-carbon-atlas>.
- [2] M. Zambrini, «Il peso del settore dei trasporti sui cambiamenti climatici e le prospettive di contenimento delle emissioni: gli scenari internazionali ed europei».
- [3] E. Commission, «EU Transport in Figures, Statistical Pocketbook 2014».
- [4] J. P. L. Kirill Murashko, «Modelling of the battery pack thermal management system for Hybrid Electric Vehicle».
- [5] [Online]. Available: [https://it.wikipedia.org/wiki/Veicolo\\_ibrido](https://it.wikipedia.org/wiki/Veicolo_ibrido).
- [6] K. Prajapati, «Hybrid Vehicle: a study on Technology».
- [7] Indraneelbhandari, «Off peak power storage: Advanced adiabatic Compressed Air Energy Storage - Introduction».
- [8] H. Pei-Hsing, K. Jenn-Kun e H. Chun-Yen, «A new application of the UltraBattery to Hybrid fuel cell vehicles».
- [9] I. E. C. (IEC), *Electrical Energy Storage* .
- [10] [Online]. Available: <https://www.comsol.com/blogs/advancing-vanadium-redox-flow-batteries-with-modeling/>.
- [11] K. Janis, F. V.V., M. Vanags e V. Solovey, «Energy storage solutions for small and medium-sized self-sufficient alternative energy objects».
- [12] [Online]. Available: [https://www.mdpi.com/journal/materials/special\\_issues/Biomass\\_Derived\\_Carbon\\_Materials](https://www.mdpi.com/journal/materials/special_issues/Biomass_Derived_Carbon_Materials).
- [13] B. University.
- [14] [Online]. Available: <http://www.global-tanpo.com/?t=view&id=68>.
- [15] <https://batteryuniversity.com/>.
- [16] [Online]. Available: <http://www.awbatt.com/prismatic-lifepo4-battery/lifepo4-prismatic-battery-cell-3.2v-60ah-for-12v-24v-48v-72v-battery-packs.html>.
- [17] [Online]. Available: [https://uacj-automobile.com/sheets\\_and\\_plates07.html](https://uacj-automobile.com/sheets_and_plates07.html).
- [18] EPEC, pp. <https://www.epectec.com/batteries/prismatic-pouch-packs.html>.
- [19] [Online]. Available: <https://www.electriccarpartscompany.com/>.
- [20] TARGRAY, pp. <https://www.targray.com/li-ion-battery/lithium-ion-cells>.
- [21] B.-3. M. L.-i. Safe.
- [22] pp. HowStuffWorks - Hoe Lithium-ion Batteries Work.
- [23] G. P. I. Ltd., «Lithium Ion technical handbook».
- [24] ENEA, «Agenzia nazionale per le nuove tecnologie, l'energia e lo sviluppo economico sostenibile».
- [25] M. M. S. a. S. K. Khan, «Towards an Ultimate Battery Thermal Management System: A Review.».
- [26] R. V. V. Z. J. Williford, «Effects of entropy changes in anodes and cathodes on the thermal behavior of lithium ion batteries, Journal of Power Sources.».
- [27] A. A. Pesaran, «"Battery thermal models for hybrid vehicle simulations," Journal of Power».
- [28] A. Pesaran, « Battery thermal models for hybrid vehicle simulations, Journal of Power Sources. 110:377–382.».
- [29] T. L. M. H. Matthe R., «Battery System for Electric Vehicle with Extended Range».
- [30] F. Ladrech, «"Battery Thermal Management for HEV & EV – Technology overview,"».
- [31] N. Sato, «"Thermal Behaviour analysis of lithium-ion batteries for electric and hybrid"».
- [32] S. A. M. F. J. R. S. a. S. A.-H. S. A. Khateeb, «"Thermal management of Li-ion battery with phase change material for electric scooter: experiment validation"».

- [33] A. D., I. K. e B. Z., «Thermal Management of Li-ion Battery Packs. Comsol Conference.».
- [34] Z. H. R. a. S. F. Wang, «"A review of power battery thermal energy management,"».
- [35] J. A.N., D. D.W., A. D.P., A. K. e H. G.L., «Low-temperature study of lithium-ion cells using a Li y Sn micro-reference electrode. Journal of Power Sources.».
- [36] A. Pesaram e G.-H. Kim, «Battery thermal management design modeling».
- [37] M. M. S. a. S. K. Khan, «Towards an Ultimate Battery Thermal Management System: A Review. MDPI-Batteries, 2017. 3(9): p. 1-18.».
- [38] P. R. R. a. T. K. Balakrishnan, «Safety mechanisms in lithium-ion batteries. Journal of Power Sources».
- [39] Q. e. a. Wang, «A critical review of thermal management models and solutions of lithium-ion batteries for the development of pure electric vehicles.».
- [40] M. Ç. K. Furkan SÖKMEN, «Review of Batteries Thermal Problems and Thermal Management Systems».
- [41] Z. W. S. Rao, «A review of power battery thermal energy management, Renew. Sustain. Energy Rev.».
- [42] G. Kim, K. Smith, K. Lee, S. Santhanagopalan e A. Pesaran, «Multi-domain modeling of lithium-ion batteries encompassing multi-physics in varied length scales».
- [43] M. J. S. a. S. K. K. Mohammad Rezwan Khan, «Towards an Ultimate Battery Thermal Management System: A Review».
- [44] Y. C. a. J. W. Evans, «Heat transfer phenomena in lithium/polymer-electrolyte batteries for electric vehicle application».
- [45] A. A. Pesaran, S. Burch e M. Keyser, «An approach for designing thermal management systems for electric and hybrid vehicle battery packs».
- [46] Q. a. J. B. a. L. B. a. Y. Y. Wang, «A critical review of thermal management models and solutions of lithium-ion batteries for the development of pure electric vehicles».
- [47] BEHR., «Thermal Management for Hybrid Vehicles».
- [48] M. Ç. K. Furkan SÖKMEN, «Review of Batteries Thermal Problems and Thermal Management Systems».
- [49] L. P. K. X. F. Y. C. S. Jin L.W., «Ultra-thin minichannel LCP for EV battery thermal management. Appl. Energy.».
- [50] M. Ç. K. Furkan SÖKMEN, «Review of Batteries Thermal Problems and Thermal Management Systems».
- [51] S. G. a. T. F. F. T. M. Bandhauer, «A Critical Review of Thermal Issues in Lithium-ion Batteries," Journal of Electrochemical Society, vol. 158, pp. R1-R25, 2011.».
- [52] S. F. W. a. G. Q. Z. Z. H. Rao, «Simulation and experiment of thermal energy management with phase change material for ageing LiFePO<sub>4</sub> power battery».
- [53] M. Ç. K. Furkan SÖKMEN, «Review of Batteries Thermal Problems and Thermal Management Systems, pag.44».
- [54] Z. G. Z. a. X. M. Fang, «Study on paraffin/expanded graphite composite phase change thermal energy storage material».
- [55] M. K. Y. K. a. O. M. J. Fukai, «Thermal conductivity enhancement of energy storage media using carbon fibers».
- [56] G. Z. a. R. L. V. Shatikian, «Numerical investigation of a PCM-based heat sink with internal fins».
- [57] R. F. Paolo Principi, «Realizzazione di strutture multistrato contenenti Materiali a Cambiamento di Fase (PCM) per la realizzazione di celle frigorifere».
- [58] Y. Y. M. D. Yang X., «Recent developments of lightweight, high performance heat pipes».
- [59] Q. Wang, B. Jiang, B. Li e Y. Yan, «A critical review of thermal management models and solutions of lithium-ion batteries for the development of pure electric vehicles,» p. pp.39.

- [60] S. H. B. D. a. S. F. T. H. Tran, «Experimental investigation on the feasibility of heat pipe cooling for HEV/EV lithium-ion battery».
- [61] X. L. G. Z. J. Z. F. H. Y. L. Qiqiu Huang, «Experimental investigation of the thermal performance of heat pipe assisted phase change material for battery thermal management system».
- [62] G. Boccardo, «Energy saving strategies in diesel railcars».
- [63] T. B. R. David Linden, "Handbook of Batteries - third edition" - McGraw Hill.
- [64] C. Multiphysics. [Online]. Available: <https://www.comsol.it/>.
- [65] «models.bfc.li\_battery\_pack\_3d.pdf».
- [66] A. Pesaran e G. Kim, «Battery Thermal Management System Design Modeling, Conference Paper NREL/CP\_540\_40446 November 2006».
- [67] J. Smith, M. Hinterberger, C. Schneider e J. Koehler, «Energy savings and increased electric vehicle range through improved battery thermal management».
- [68] M. B. Bigdeli, M. Fasano, A. Cardellini, Eliodoro Chiavazzo e P. Asinari, «A review on the heat and mass transfer phenomena in nanofluid coolants with special focus on automotive applications».
- [69] S. Harish, K. Ishikawa, E. Einarsson, S. Aikawa, T. Inoue, P. Zhao, M. Watanabe, S. Chiashi, J. Shiomi e S. Maruyama, «Temperature Dependent Thermal Conductivity Increase of Aqueous Nanofluid with Single Walled Carbon Nanotube Inclusion».
- [70] TimofeevaEV, GavrilovAN, McCloskeyJM, TolmachevYV, SpruntS, L. LM e e. al, «Thermal conductivity and particle agglomeration in alumina nanofluids: experimental and theory».
- [71] M. HA, R. G, N. CT e D. D, «New temperature dependent thermal conductivity data for water-based nanofluids».
- [72] H. S, I. K, E. E, A. S., I. T, ZhaoP e e. al., «Temperature dependent thermal conductivity increase of aqueous nanofluid with single walled carbon nanotube inclusion».
- [73] G. J, P. B, C. M, G. J, M. J, W. J e e. al., «Enhanced thermal conductivity and viscosity of copper nanoparticles in ethylene glycol nanofluid».
- [74] M. JC, A treatise on electricity and magnetism, vol. 1.
- [75] L. TS, Slow flow through stationary random beds and suspensions of spheres.
- [76] P. BC e C. YI, «Hydrodynamic and heat transfer study of dispersed fluids with submicron metallic oxide particles.».
- [77] H. C, L. W, C. Y e L. C, «Natural convection heat transfer of alumina–water nanofluid in vertical square enclosures: an experimental study.».
- [78] M. JC, A treatise on electricity and magnetism, vol. 1. Dover(UK).
- [79] B. A, Q. L, H. J, M. P, H. J, G. W e e. al., «Nanostructured SiC by chemical vapor deposition and nanoparticle impaction.».